# Faculdade de Engenharia da Universidade do Porto

FEUP

# Chitosan microspheres to remove *Helicobacter pylori* adhesion in human gastric mucosa

Ana Patrícia Carvalho Henriques

Porto, 23 rd June 2014

# Resumo

*Helicobacter pylori* (*H. pylori*), uma bactéria gram-negativa espiralada, é um dos agentes infeciosos mais comuns em todo o mundo, colonizando a mucosa gástrica de mais de 50% da população mundial e cerca de 80-90% da população Portuguesa.

Devido à sua motilidade flagelar e capacidade para criar um microambiente favorável, a *H. pylori* é capaz de persistir no ambiente acídico do estômago e aderir ao epitélio gástrico, estabelecendo com sucesso a infeção. A adesão é mediada por moléculas na superfície bacteriana, denominadas adesinas, capazes de reconhecer glicanos expressos na superfície de células epiteliais gástricas e na camada de muco que reveste a mucosa gástrica. A longo prazo, a presença da bactéria aumenta significativamente o risco de desenvolver várias complicações gástricas, sendo uma delas o cancro gástrico.

Atualmente, as terapias convencionais contra a infeção causada pela *H. pylori* baseiam-se na administração combinada de dois antibióticos e um inibidor da bomba de protões. No entanto, o tratamento é ineficaz em 20% dos casos, deixando cerca de 140 milhões de doentes em todo o mundo sem tratamentos alternativos. As taxas de cura têm vindo a diminuir ao longo dos anos, principalmente devido à resistência bacteriana aos antibióticos e à baixa adesão dos pacientes.

Neste contexto, várias terapias alternativas estão sob investigação. O quitosano, um polímero catiónico natural e não tóxico, tem sido bastante investigado como uma ferramenta contra infeções gástricas, principalmente devido à sua biocompatibilidade e biodegradabilidade, juntamente com as suas propriedades anti- bacterianas e mucoadesivas. Apesar da crescente aplicação de sistemas de encapsulação baseados em quitosano, a utilização de microesferas de quitosano como um sistema de ligação à *H. pylori* foi também proposta, onde, após administração oral, as microesferas são capazes de capturar e remover bactérias do estômago, tirando partido da sua capacidade mucoadesiva/anti-bacteriana.

Embora encontradas livremente na camada de muco, as bactérias são também encontradas aderidas ao muco e à superfície de células epiteliais nas fovéolas gástricas (invaginações do estômago). A estabilidade das microesferas de quitosano em meio ácido, quando reticuladas com genipina, foi já demonstrada, bem como a sua capacidade para se ligar e remover a *H. pylori* aderente às células gástricas. Estudos em secções 2D de mucosa gástrica humana mostraram que as fovéolas gástricas têm aproximadamente 70 µm de largura, o que pode dificultar a penetração das microesferas anteriormente desenvolvidas, com diâmetro de cerca de 170 µm, e a remoção das bactérias instaladas no interior das fovéolas. É então sugerido que, de modo a alcançar as bactérias e removê-las do estômago, as microesferas devem apresentar um tamanho menor do que o descrito anteriormente.

Assim, o objetivo deste projeto consiste no desenvolvimento de microesferas com cerca de 50 µm, pequenas o suficiente para penetrar as fovéolas da mucosa gástrica. Microesferas de quitosano foram produzidas e caracterizadas, e a sua penetração nas fovéolas gástricas de ratinho e humanas foi avaliada, bem como a sua capacidade de adesão à *H. pylori*.

Para esse propósito, microesferas de quitosano foram produzidas através de três sistemas diferentes, nomeadamente o sistema eletrostático, de pressão co-axial e aerodinâmico. Técnicas baseadas em microscopia ótica (Microscópio Ótico e IN Cell Analyzer) e na difração de laser (Mastersizer) foram usadas para caracterizar as microesferas de quitosano relativamente ao seu tamanho e morfologia.

Um modelo ex-vivo de estômagos frescos de ratinho foi utilizado para otimizar a marcação com fluorescência da mucosa gástrica. Diferentes marcadores foram testados, revelando DAPI (amostra fixa) e o marcador de membrana CellMask™ Deep Red (fresco) com bons marcadores para a visualização da mucosa gástrica. As microesferas de quitosano com um diâmetro médio de 20 µm foram produzidas com sucesso e incubadas com as mucosas gástricas de ratinhos e humana. Microscopia de confocal revelou a presença de microesferas em diferentes planos da mucosa, confirmando assim a sua capacidade de penetrar as fovéolas gástricas.

Além disso, a incubação da *H. pylori* com as microesferas revelou a sua capacidade de aderir à superfície das partículas.

Em conclusão, os resultados sugerem as microesferas de quitosano desenvolvidas como uma ferramenta promissora para explorar o tratamento de infeções causadas por *H. pylori*.

# Abstract

*Helicobacter pylori (H. pylori), a spiral-shaped gram-negative bacterium, is one of the most common infectious agents in the world, colonizing human gastric mucosa of over 50% of the world's population and 80-90% of the Portuguese population.*

*Due to its flagellar motility and ability to create a favourable microenvironment, H. pylori is able to persist in the stomach acidic environment and attach to the gastric epithelium, establishing the infection. Its adherence is mediated by molecules (adhesins) on the bacterial surface able to recognize glycans expressed on the surface of gastric epithelial cells and mucus layer lining the gastric mucosa. Long-term carriage significantly increases the risk of developing several gastric-specific complications, going from gastritis to gastric cancer.*

*Current H. pylori infection conventional therapies rely on a concomitant administration of two antibiotics and proton pump inhibitor. However, the treatment is inefficient in 20% of the cases, leaving nearly 140 million patients worldwide without any alternative treatment option. The cure rates have been declining over the years, mostly due to bacterial resistance to antibiotics and poor patient compliance.*

*In this context, several alternative therapies are under investigation. Chitosan, a natural-nontoxic cationic polymer, has been thoroughly investigated as a tool against gastric infections, mainly due to its biocompatibility and biodegradability coupled with its anti-bacterial and mucoadhesive properties. Despite the growing application of chitosan-based encapsulation systems, the use of chitosan microspheres as a H. pylori binding system has also been proposed, where, after oral administration, microspheres are able to capture and remove bacteria from the stomach, taking advantage of their muco/bacterial adhesive capacity.*

*Although found free-swimming in the mucus layer, bacteria are also found adherent to the mucus layer and the surface of epithelial cells in gastric foveolae (stomach invaginations). The stability of chitosan microspheres in acidic environment, when crosslinked with genipin, has been demonstrated as well as their ability to bind and remove adherent H. pylori from gastric cells. Studies using 2D sections of human gastric mucosae have shown that human stomach foveolae are ~70 μm wide, which might hamper the penetration of previously developed chitosan microspheres, with a diameter around 170 μm, and the removal of the bacteria living within the foveolae. Therefore, it is suggested that the microspheres should be smaller than the previously developed in order to reach bacteria and remove them from the stomach.*

*The aim of this project is to develop chitosan microspheres with a diameter around 50 μm, small enough to penetrate gastric foveolae and remove bacteria adhered inside. The microspheres were produced and characterised, and their penetration into mice and human gastric foveolae as well as their ability to adhere onto H. pylori evaluated.*

*For this purpose, chitosan microspheres were produced by three different systems, namely high voltage electrostatic, co-axial air stream and aerodynamically driven systems. Techniques based on optical microscopy (Optical Microscopy, IN Cell Analyzer) and laser diffraction (Mastersizer) were used to characterize chitosan microspheres regarding size and morphology.*

*An ex-vivo model using fresh mice stomach samples was used to optimize the fluorescence labelling of gastric mucosa. Different dyes were explored, revealing DAPI (fixed sample) and CellMask$^{TM}$ Deep Red plasma membrane (fresh) stain as good gastric mucosa markers. Chitosan microspheres with an average diameter of 20 μm were successfully produced and incubated with mice and human gastric mucosa. Confocal microscopy revealed their presence in different plans of the mucosa, thus confirming their ability to penetrate the gastric foveolae.*

*Moreover, H. pylori incubation with chitosan microspheres has revealed their ability to adhere to the surface of the particles.*

*In conclusion, results suggest chitosan microspheres developed as a promising tool to explore as H. pylori infection treatment.*

# Acknowledgements

My supervisor, Inês C. Gonçalves, for the constant trust, encouragement and support. For the guidance and knowledge shared throughout these last few months.

Cristina Martins and Bioengineered Surfaces Team for the support and shared ideas at the laboratory.

Paula Sampaio and Maria Lázaro for all the precious help on the confocal images acquisition and analysis.

Prof. Paulo Costa for the assistance with VarJ30 production system and Mastersizer equipment and for allowing their utilization throughout the project.

Cátia Lopes for the help with the cryostat and André Maia for the assistance with the IN Cell Analyzer acquisition and data analysis. Catarina Leitão regarding her help in the FACS equipment.

Last but not least, my family as well as my friends for all the support and encouragement during these five years.

# Table of Contents

# Figure List

# Table List

# Abbreviations and Symbols

| | |
|---|---|
| BabA | Blood group antigen binding adhesin |
| CagA | Cytotoxin-associated gene A |
| DA | Degree of Acetylation |
| DD | Degree of Deacetylation |
| DNA | Deoxyribonucleic acid |
| FEUP | Faculdade de Engenharia da Universidade do Porto |
| FITC | Fluorescein isothiocyanate |
| *H. pylori* | *Helicobacter pylori* |
| INEB | Institute of Biomedical Engineering |
| MW | Molecular Weight |
| mics | Microspheres |
| $OD_{600}$ | Optical density at 600 nm |
| OM | Optical Microscopy |
| PPI | Proton Pump Inhibitor |
| SabA | Sialic acid binding adhesin |
| TPP | Sodium Tripolyphosphate |
| VacA | Vacuolating cytotoxin A |

# Chapter 1

# Introduction

## 1.1 Stomach and its mucosal surface

The digestive tube is a musculomembranous tube, with about 9 metres long, extending from the mouth to the anus, and lined throughout its entire extent by mucus membrane [1]. The stomach is the first intra-abdominal and the most dilated part of the gastrointestinal tract, and is situated between the end of the esophagus and the beginning of the small intestine, the duodenum [1].

It is a muscular, highly vascular, distensible bag-shaped organ, divided in four main different regions [1]: cardia, fundus, body and pylorus. The cardia, where the contents from the oesophagus are deposited, is the acute angle between the abdominal esophagus and the fundus of the stomach, the upper curvature. The body (corpus) corresponds to the bigger region of the stomach leading to the pyloric antrum, which is the lower section narrowing toward the pylorus, which occupies the distal one quart of the stomach, surrounded by the smooth muscle pyloric sphincter [2].

The wall of the stomach consists of four layers: serosa, muscularis, submucosa and mucosa, together with vessels and nerves (Figure 1) [1]. The outermost layer of the stomach is the serosa, a thin serous membrane made of simple squamous epithelial tissue and areolar connective tissue. The muscularis layer is composed by 3 layers of smooth muscle tissue arranged with its fibers running in 3 different directions: longitudinal external, circular media and oblique internal. The submucosa is made of various connective tissues, blood vessels, and nerves, and surrounds the mucosa, the innermost layer of the stomach. The stomach mucosa contains simple columnar epithelium tissue, a layer of loose connective tissue of lamina propria, and thin layer of smooth muscle, the muscularis mucosae. The surface of the epithelium is connected via the foveolae (gastric pits) and neck region to the deeper gastric glands [3]. These foveolae contain exocrine cells able to produce mucus and secrete digestive

enzymes and hydrochloric acid into the lumen of the stomach, creating an environment with an acidic pH, able to kill many of the bacteria present in the stomach [4].
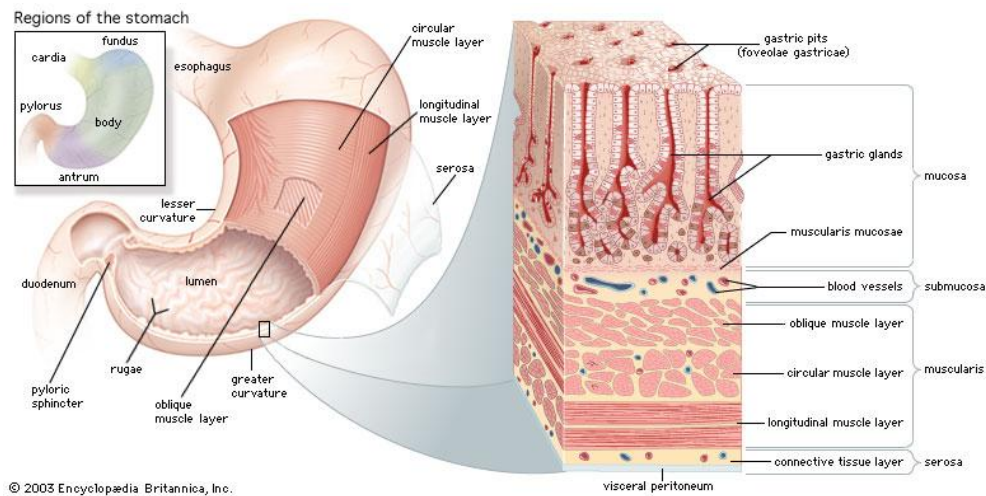


**Figure 1 -** Structures of human stomach and gastric mucosa [5].

The mucus layer is a biochemically complex medium, highly hydrated and rich in high molecular weight and heavily glycosylated glycoproteins known as mucins, antimicrobial peptides, immunoglobulins and other intestinal proteins [6]. The alkaline and viscous mucus is continuously secreted by the mucous superficial cells and neck cells, being its function to protect gastric epithelial cells against chemical, enzymatic, microbial and mechanical harm [7]. Mucins act as diffusion barrier to acidic HCl instilled into the lumen of the stomach and alkaline bicarbonate ions secreted by the gastric epithelium, causing the stomach pH to vary between pH 1.2–2.5 in the gastric lumen and pH ~7.4 near the epithelial surface [8].

## 1.2 *Helicobacter pylori* colonization

*Helicobacter pylori* (*H. pylori*), spiral-shaped gram-negative bacteria, is one of the most common infectious agents, colonizing the gastric mucosa of over 50% of the human population [1]. *H. pylori* infection is the strongest known risk factor for gastroduodenal ulcer development, present in 60–80% of gastric ulcers and being as well causally (1-3%) related to gastric adenocarcinoma [2]. Infection induces an inflammatory response that does not eradicate the bacterial colonization, but which instead persists for the lifetime of the individual [3]. However, less than 20% of infected individuals have clinical symptoms [4].

The risk of serious clinical outcomes is related to interactions between the host, bacteria and environment [2]. In general, the host is able to eliminate the bacteria through gastric acidity, peristaltic movements and mucus continuously secreted from glands of the epithelial cell, which pushes bacteria toward the luminal surface, inhibiting the adhesion and colonization of the bacteria in the gastric mucus layer [5]. However, *H. pylori* have evolved intricate mechanisms to avoid the bactericidal acid in the gastric lumen and to survive near to, to attach to, and to subvert the human gastric epithelium and immune system [2]. The hostile environment features are overcome by virulence factors that create a micro

environment favourable to its survival. The bacteria is then able to escape the acidic pH of the stomach (pH 1.2–2.5) crossing the mucus layer that covers and protects the gastric cells, reaching the gastric epithelium where the pH is more neutral (pH ~7.4). This is achieved due to its flagellar motility and secretion of urease, which converts endogenous urea into ammonia and carbon dioxide, thereby buffering gastric acid in the immediate vicinity of the organism [6].

Most *H. pylori* are frequently found moving in the mucus layer, but some bacteria actually adhere to the surface of gastric epithelial cells. Schreiber et al. [7] revealed that *H. pylori* colonizes mainly a thin mucus layer located 0-25 µm above the tissue surface, being the majority of *H. pylori* (88%) found within the first 15 µm, with 30% either swimming in the layer immediately adjacent to the epithelial cells (0-5 µm) or adhering to them.

Non-adherent *H. pylori* are able to cause a direct injurious effect on gastric epithelial cells, which is amplified by production and release of a vacuolating cytotoxin, VacA (Figure 2) [8]. This secreted protein is able to induce multiple structural and functional alterations in cells, such as the formation of large intracellular vacuoles [9,10] and the increase in membrane permeability [11]. This event occurs through its insertion in cell membranes, which in turn leads to the formation of anion selective channels [12]. In addition, VacA stimulates apoptosis in gastric epithelial cells [13], by inducing the release of cytochrome *c* from the mitochondria, therefore activating caspase 3. The inhibition of the expansion of T cells, thereby allowing *H. pylori* to evade the adaptive immune response, is also attributed to VacA protein action [14].

Nevertheless, attachment is a prerequisite for a successful microbial colonization of epithelial surfaces. Interaction between the bacteria and the cells is mediated by molecules on the bacterial surface, adhesins, which recognize proteins or glycoconjugates expressed on the surface of gastric epithelial cells and also in the mucus layer lining the gastric mucosa [6]. *H. pylori* express adhesins that confer intimate adherence to the gastric epithelium where the bacteria can gain easy access to nutrients from host tissues [15]. These adherence properties protect the bacteria from the extreme acidity of the gastric lumen and displacement from the stomach by forces such as those generated by peristalsis and gastric emptying [16]. Two carbohydrate structures in surface mucus cells serve as specific ligands for *H. pylori* adhesins: Lewis blood group antigens, such as Lewis b (Le$^b$), mainly distributed in the epithelium surface, and Lewis x (Le$^X$), located deeper in the mucus [5]. The blood group antigen-binding adhesin (BabA) was shown to recognize the Le$^b$ while sialic acid-binding adhesin (SabA) mediates the adherence of *H. pylori* to inflamed gastric mucosa by binding sialylated carbohydrate structures such as sialyl Lewis x (sLe$^x$) [5,6].

Apart from adhesins and VacA protein, the cytotoxin-associated gene (cagA) is another genetic determinant involved in *H. pylori* virulence [17]. CagA antigen, gene inserted in the *H. pylori cag* pathogenicity island (PAI), is an *H. pylori* strain-specific factor, which increases the risk for development of distal gastric cancer [18], by inducing strong gastric inflammation [19]. Subsequent to epithelial cells adherence, *H. pylori* is able to assemble a type IV secretion system, encoded by the cag pathogenicity island (PAI), which translocates the CagA protein into gastric epithelial cells [19,20]. Once inside the former epithelial cells, CagA is tyrosine-phosphorylated, however both phosphorylated and nonphosphorylated CagA can cause numerous cellular alterations [20].
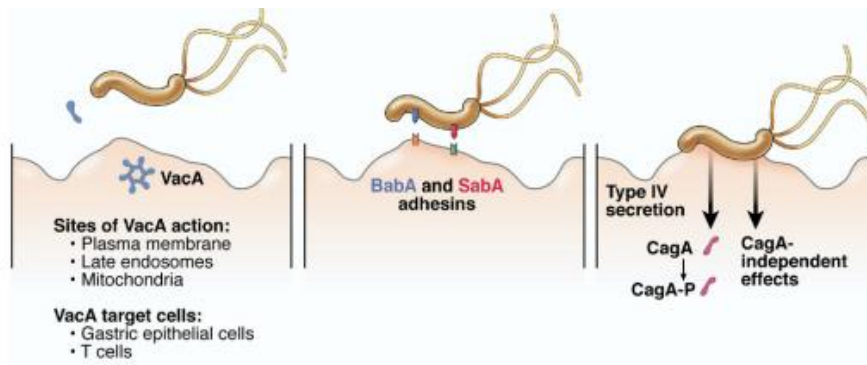
**Figure 2 -** Factors that influence the interactions of H pylori with human gastric mucosa [21]. The secretion of VacA protein by nonadherent bacteria can affect several cell types, including gastric epithelial cells and T cells [22]. Adhesins, namely BabA and SabA, mediate the binding of H. pylori to the gastric epithelial cells and mucus [16]. The adherent bacteria are able of assemble a type IV secretion system that allows the entrance of CagA protein into the gastric cells conducting to cellular alterations [20].

*H. pylori* capability of expressing these aforementioned factors will conduct to strains with different levels of pathogenicity, which will be determinant for the interaction between the bacteria and the human host [23].

## 1.3   Current treatments

*H. pylori* eradication treatments require not only antibiotics to kill the bacteria, such as amoxicillin, clarithromycin or metronidazole, but also anti-acid medications, particularly proton pump inhibitors (PPI) such as omeprazole, rabeprazole, lansoprazole,  to increase the environmental pH, therefore ensuring antibiotics stability  within stomach [2].

Current available regimens to treat *H. pylori* infection rely on a triple treatment, which includes PPI-clarithromycin and amoxicillin or metronidazole [24-26]. Nevertheless, the most recent data have recognized lack of efficiency on the former treatment, often allowing the cure of only a maximum of 70% of the patients, which is less than the 80% rate aimed [26] and expected for an infectious disease [27]. The administration of the three antibiotics together with a PPI (non-bismuth quadruple therapy) has also been considered [28] as well as the bismuth-containing quadruple therapy following the development of a gallenic formulation including bismuth salts, tetracycline and metronidazole in the same pill [29].

The Maastricht IV/Florence Consensus Report [24] has stated that PPI-clarithromycin-containing triple therapy without prior susceptibility testing should be abandoned when the clarithromycin resistance rate in the region is more than 15-20%. Moreover, recommended regimens vary slightly between areas with low or high clarithromycin resistance. Regarding the former case, clarithromycin-containing treatments are recommended for first-line empirical treatment, with bismuth-containing quadruple therapy being also an alternative. In order to increase the efficacy of triple therapy, some modifications may be implemented:  a higher dose (twice a day) of PPI can be used and extending the duration of PPI-clarithromycin-containing triple therapies from 7 to 10-14 days improves the eradication success by about 5% and therefore may be considered as well. PPI-clarithromycin-metronidazole (PCM) and PPI-clarithromycin-amoxicillin (PCA) regimens are equivalent, and therefore metronidazole can be used instead of amoxicillin as the second antibiotic. After failure of a PPI-clarithromycin-containing treatment, either a bismuth-containing quadruple

therapy or levofloxacin-containing triple therapy is recommended. Concerning areas of high clarithromycin resistance, bismuth-containing quadruple therapies are recommended for first-line empirical treatment. If this regimen is not available, sequential treatment or a non-bismuth quadruple therapy is recommended. In case first line regimen fails, levofloxacin containing triple therapy is recommended. In both areas, after failure of second-line therapy and whenever possible, the treatment should be guided by antimicrobial susceptibility testing.

Particularly, for patients with penicillin allergy, in areas of low clarithromycin resistance, for a first-line treatment, a PPI-clarithromycin-metronidazole combination may be prescribed while in areas of high clarithromycin resistance, the bismuth- containing quadruple therapy should be advised [24].

## 1.4    Reasons for unsuccessful treatments

The low rate of success in *H. pylori* is manly related to: (a), poor penetration and (b) antibiotic degradation, (c) *H. pylori* resistance to the antibiotics, (d) recurrence of infection and (c) poor compliance.

The mucus membrane and *H. pylori* ability to survive in the deep gastric mucosa and in the intercellular space between epithelial cells have been proved to limit the access of the drugs to the site of action [5,30], causing poor penetration of the antibiotics [5], therefore reducing the concentration of antibiotics at the site of action.

Antibiotic degradation is also a problem leading to unsuccessful treatments, since to act effectively against *H. pylori*, the released antibacterial agents must remain stable in the acidic environment of the gastric lumen [31], in order to reach the site of infection in their active form [32]. Their proved instability in stomach environment [31–35], reduces the bioavailability of the antibiotics reducing their effect on *H. pylori*, therefore preventing the complete eradication of the bacteria [5,30], even in the presence of PPIs [33,36].

The difficulty of establishing a standard treatment regimen worldwide has also been referred as an obstacle to the successful treatment of *H. pylori*. A significant variation in the resistance to antibiotics in *H. pylori* has been reported [37], especially to clarithromycin, which global resistance rate has increased in Europe from 9% in 1998 [38] to 17.6% in 2008-9 [39]. Therefore, knowledge of previously prescribed antibiotics in the population and information about the presence of resistance in the region or other similar areas provides a basis for the prescription of the treatment, suggesting the use of some antibiotics over others. As *H. pylori* often becomes resistant when single antibiotics are used for other infections, discussion with the patient and identification of which antibiotics have been used in the past may be useful to gather information about possible resistance. Their prior use might exclude them from specific *H. pylori* therapy [2].

In addition, *H. pylori* treatment raises some concerns due to the possible recurrence of infection [37]. In fact, despite the fact that re-infection after eradication is rare in developed countries, in developing countries is still relatively high, around 13% [40].

Poor patient compliance due to the dosage regime [41] and due to adverse effects such as diarrhea, nausea, and retching [36] have also been considered as limited factors [24].

Overall, it has been estimated that eradication therapy is unsuccessful in nearly one in five patients [42], leaving potentially around 140 million people without an alternative

treatment [43]. Despite the large number of studies, an optimal therapeutic regimen for the treatment of *H. pylori* has not yet been defined, and therefore, alternative therapies are required.

## 1.5   Alternative therapies

Alternative therapeutic approaches able to overcome the aforementioned problems have been considered. Special attention has been given to the antimicrobial activity of certain non-antibiotic compounds, such as polyunsaturated fatty acids [44], vaccines developed against *H. pylori* [45], inhibitors of virulence factors [17,46] and other molecules, such as polyphenols [47], able to reduce the activity of the bacteria, therefore maximizing the success of the treatment. Some of the strategies may be applied as co-adjuvants of the current available therapies [48], leading to an improved outcome. Encapsulation of drugs for local delivery has been another extensively studied approach seeking to improve antibiotics effect against *H. pylori*[49].

Certain polyunsaturated fatty acids (PUFA) have been considered due to their inhibitory effect on bacterial growth [50]. Particularly, docosahexaenoic acid (DHA), an n-3 polyunsaturated fatty acid (n-3 PUFA), has been identified as an antibacterial agent, due to its ability to inhibit *H. pylori* growth *in vitro* and *in vivo* by reducing gastric mucosa colonization [48], by altering the bacterial membrane protein composition [44]. The recurrence of *H. pylori* infection in the mouse model was shown to decrease as a result of the combination of DHA with standard treatments.

Given the worldwide variation of *H pylori* infection prevalence, which in 2010 ranged between 7% and 87% [51], a vaccination strategy would be a valuable option to fight *H. pylori* infection [45,52,53]. However, despite several attempts to develop an *H. pylori* vaccine for humans, progress has been slow. Patent WO 2008/105740 A1 (*A New immunoglobulin against Helicobacter pylori)* describes the preparation of antibodies against the *H. pylori* BabA adhesin and suggests their application in the development of *H. pylori* passive vaccination. However, its action remains unproven.

Virulence factors inhibitors have also been considered in this sense. For instance, being urease essential for the survival of *H. pylori* [54], drugs such as acetohydroxamic acid (AHA), a specific urease inhibitor able to inhibit ammonia production [46], may also be valuable alternatives to fight *H. pylori*.

Several studies have shown that phenolic compounds found in cranberries, green tea, apple and wine, affect *H. pylori* [55,56]. A recent study showed that both gallic acid and catechin, two abundant phenolic compounds widely distributed among plants [57], display growth inhibitory effects in *H. pylori* [47].

The encapsulation process appears as a solution for several problems associated with the administration of the drugs alone. These systems are able to protect the drug from rapid degradation or clearance, extending their half-life and solubility, and reducing its immunogenicity [33,58–60]. Previous studies [61] revealed that local application of antibiotics to gastric mucosa resulted in better eradication compared to systemically available antibiotic. Encapsulation allows not only local drug delivery but also a controlled release of the drug [62], thus increasing the retention and concentration at the site of infection [63,64]. In fact, previous studies have reported that the efficacy in eradicating *H. pylori* infection

may be   improved by delivering the antimicrobial agents from the gastric lumen into the mucus layer [31,32,65].

Different strategies have been tested including floating drug delivery systems, density-based approaches, mucoadhesive/bioadhesive systems and swelling systems for improving the gastric retention time of the system [5]. Several shapes and sizes can be acquired by these systems, including microspheres, nanoparticles, liposomes or other nano systems.

Particularly, micro/nano particle systems made from naturally occurring biodegradable polymers have been developed and applied to *H. pylori* treatment [59,66], seeking to overcome the limits of the conventional application of drugs for *H. pylori* treatment, characterized by limited effectiveness, poor biodistribution and lack of selectivity. These have been preferred over the conventional dosage forms like tablet and capsule because of their increased surface area, which by  increasing the absorption of the drug reduces the dosing frequency, thus improving the patient compliance [5]. Moreover, because these tablets or capsules may fall to the base of the stomach from where they are readily emptied, little, if any, drug is delivered to the body or fundus of the stomach, being the main drug action through systemic effect [67].

In order to enhance the effect of the drug, further improvements on the micro/nano systems can be performed. Mucoadhesive polymers have been extensively used for gastric applications due to their ability to prolong the contact of the drug with the gastric mucosa [68], increasing residence time in the stomach [69] by adhering to the mucus layer [70]. Mucoadhesion is thought to occur due to electrostatic forces between the mucosal surface that is negatively charged and a positively charged polymer, followed by mechanical interlocking of the polymer chains, van der Waal's force, hydrogen bonding and other forces [71,72]. This adherence allow micro/nano systems to more easily penetrate the gastric mucus barrier, which permit drug diffusion to occur without acidic degradation and at the desired local [5,30], therefore enhancing bioavailability and stability of the drug. Controlled release of a drug  may lead to lower administration frequency [69], thus minimizing the resistance problems associated with systemic administration of antibiotics [73].

Mucoadhesive polymer should fulfil some requirements such as strong hydrogen bond–forming group, such as carboxylate or hydroxyl, strong anionic charge, high molecular weight, adequate chain flexibility, surface energy property favouring spreading onto the mucus and low or no toxicity [60]. Several materials have been considered for preparing these systems, including synthetic polymers, such as polylactic acid, copolymers of lactic, glycolic acids, poly(vinyl alcohol), and natural polymers such as chitosan [74].

## 1.6   Chitosan

Chitosan (Figure 3), a naturally occurring polysaccharide composed of D-glucosamine and N-acetyl-D-glucosamine [75], is obtained by alkaline deacetylation of chitin, which is the second most abundant polysaccharide after cellulose [76,77]. Chitin is the principal component of the exoskeleton of crustaceans such as shrimps, crabs, prawns and lobsters, cell walls of some fungi such as *aspergillus* and *mucor* and insects [78]. The conditions used for deacetylation determines the polymer molecular weight and the degree of deacetylation (DD), which will directly affect the chemical and biological properties of the polymer [79].
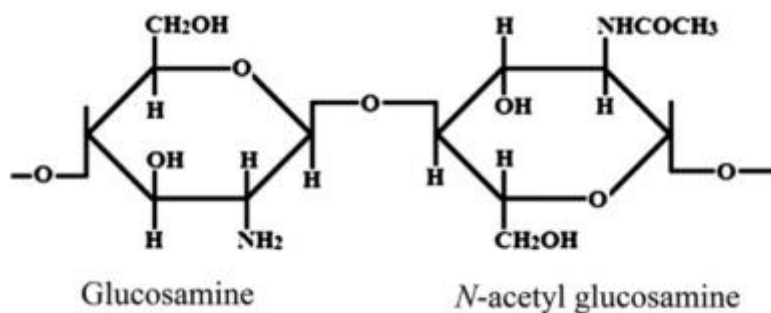
**Figure 3 -** Chemical structure of chitosan [80].

Chitosan is a polycationic, nontoxic, biodegradable and biocompatible polymer, stable in neutral conditions due to the strong inter and intra-molecular hydrogen bonds that the amine and hydroxyl groups on glucosamine unit are able to form [81]. Chitosan is a versatile polymer: its structure can vary considerably in size (average molecular weight; Mw) and DD [82], being this diversity exponentially increased by the numerous chemical modifications that are possible to perform [82].

Its cationic character, along with the presence of reactive functional groups, has demonstrated chitosan as a valuable component in the preparation of mucoadhesive formulations [71,83].

Chitosan mucoadhesive [79] and antimicrobial properties [84–86] are particularly relevant, namely regarding the treatment of *H. pylori* [74].

The mucoadhesive properties of chitosan result from the protonation of D-glucosamine residues at low pH, which leads to strong electrostatic interactions established between these charged free amines and gastric mucins, negatively charged at the acidic stomach pH [71,87,88]. He et al., [83] evaluated and demonstrated the excellent mucoadhesive properties of chitosan solution and chitosan microspheres. Turbidimetric measurement revealed a strong interaction between chitosan in aqueous solution and mucin, while i*n vitro* studies with chitosan microspheres demonstrated similar results. The interaction between mucin and chitosan microspheres was suggested to be dominated by electrostatic attraction, which can be related to the effective surface charge. Mucoadhesion of chitosan microspheres in rat small intestine was also evaluated, revealing that not only chitosan microspheres adhere to mucins, they also can be adsorbed onto mucosal tissue. Factors such as ionic strength, surface charge and pH were found to influence interaction of the microspheres with mucins [83].

Regarding the antibacterial activity of chitosan, it is the consequence of the electrostatic interactions between the same cationic amino groups and the anionic groups on the bacterial wall, which leads to the inhibition of bacterial proliferation [88].

This polymer has been widely used in the pharmaceutical field as well as a carrier for drug delivery and as biomedical material [89], being commercially available in different forms, such as films, fibers, beads, scaffolds and micro/ nano particles [75].

## 1.7    Chitosan as encapsulation system

Chitosan micro [66,90] and nano [91,92] particles have been used to provide controlled release of many drugs and to improve the bioavailability of degradable substances such as proteins or enhance the uptake of hydrophilic substances across the epithelial layers.

- *Chitosan micro/nanoparticles production methods*

The production method selected for chitosan particles preparation is a relevant factor influencing its final features. The selection of the microencapsulation technique is primarily determined by the solubility of the drug and the polymer in various solvents systems [93,94], as well as by the particle size requirement [95]. To date, various methods and approaches have been proposed for the preparation of chitosan particles, such as ionotropic gelation, coacervation technique, spray drying, or emulsification/solvent evaporation (Table 1). Nevertheless, combination between the different methods can occur, depending on the purpose of the study and on the requirements established [96].

It is important to prepare uniform-sized particles, controlling the size for their application in drug delivery system. The reproducibility of microspheres between batches is relevant when selecting the production method since it might lead to poor repeatability of the release behaviour and efficacy of drug among doses [97].

**Table 1 -** Examples of methods for preparation of chitosan micro/nanoparticles [74].

| Particles production method | Particle Size | Advantages (+)/Disadvantages (-) |
|---|---|---|
| **Ionic gelation**<br><br>Drop wise addition of chitosan solution (positively charged) under constant stirring into a polyanionic solution (negatively charged, generally TPP).<br>Complexation between oppositely charged species results in chitosan to precipitate as spherical particles. | Nanoparticles (nm)<br>20-200 [38]<br>550-900 [33]<br>152-376 [40]<br>Microspheres (µm)<br>~170 [41]<br>100-400 [42] | + Processing under mild conditions.<br>+ Organic solvent free.<br>+ Low toxicity impact of reagents.<br>+ No changes in drug chemistry.<br><br>- Difficult entrapment of high molecular weight drugs.<br>- Poor stability in acidic conditions. |
| **Precipitation/Coacervation**<br><br>1. Addition of a solute (generally a salt) to chitosan solution, forming micro/nanoparticles due to a decrease in chitosan solubility.<br><br>2. Chitosan solution might also be blown into an alkali solution using a compressed air nozzle to form coacervate droplets. | Nanoparticles (nm)<br>100-250 [43]<br>Microspheres (µm)<br>1.5-2.5 [44] | + No complex apparatus needed.<br>+ Few purification steps required.<br>+ Organic solvent free.<br>+ High loading capacity combined with a sustained drug release.<br><br>- Poor stability in acidic conditions |
| **Spray drying**<br><br>Preparation of chitosan solution where a suitable cross-linking agent could be added (if desired). This solution or dispersion is then atomized in a stream of hot air. Atomization leads to the formation of small droplets, from which solvent evaporates instantly leading to the formation of free flowing particles.<br>Temperature and humidity might be regulated. | Microspheres (µm)<br>3-12 [45]<br>140-281 [46] | + Simple, reproducible, and easy to scale up.<br>+ Low cost process.<br>+ Fast solvent removal.<br>+ Good sphericity.<br>+ Narrow size distribution.<br>+ Low dependency of the solubility of the drug and polymer.<br><br>- High temperatures required.<br>- Size influenced by several parameters.<br>- Possible difficulty in spraying fluid of high viscosity. |
| **Supercritical anti-solvent precipitation**<br><br>Spraying of the chitosan solution into a precipitation chamber with supercritical $CO_2$ (anti-solvent), causing rapid contact between the two media. A higher super-saturation ratio of the solution is generated, resulting in fast nucleation and growth. | Microparticles (µm)<br>1.0- 2.5 [47] | + Processing under mild conditions.<br>+ Complete anti-solvent removal.<br>+ Non-toxic reagents.<br>+ Narrow size distribution.<br>+ No changes in drug chemistry. |

| | | |
|---|---|---|
| **Emulsion cross-linking**<br><br>Chitosan aqueous solution is extruded into an oil phase, generally liquid paraffin (under intensive stirring), forming and water-in-oil (w/o) emulsion. Aqueous droplets are stabilized by adding a surfactant. The stable emulsion is cross-linked by using an appropriate cross-linking agent such as glutaraldehyde. | Microspheres (µm)<br>60-100 [48]<br>100-330 [49]<br>350-690 [50] | + Control of particle size.<br>+ Good sphericity.<br><br>- Slow process.<br>- Chemical cross-linking agents used, possibly inducing chemical reactions with the drug.<br>- Difficult removal of the unreacted cross-linking agent. |
| **Solvent Evaporation**<br><br>Aqueous chitosan solution is added to an organic phase with vigorous stirring to form the primary water in oil emulsion (w/o). The latter is then added to a large volume of water containing a surfactant, forming a multiple emulsion (w/o/w). The double emulsion is then subjected to stirring until most of the organic solvent evaporates, leaving solid microspheres. | Microspheres (µm)<br>100-200 [51] | + Processing under mild conditions.<br>+ Favorable for encapsulation of thermally sensitive drugs.<br>+ Indicated for delivery of small molecule drugs.<br>+ Good sphericity.<br><br>- Organic solvents usage.<br>- Low drug encapsulation efficiency. |
| **Reverse micellar method**<br><br>The surfactant is dissolved in an organic solvent followed by the addition of chitosan, drug and cross-linking agent, under constant vortexing overnight. The organic solvent is evaporated, obtaining a transparent dry mass. The latter is dispersed in water and then a suitable salt is added to precipitate the surfactant out. | Nanoparticles (nm)<br>~100 [52] | + Narrow size distribution.<br><br>- Organic solvent usage. |

Due to the high solubility of chitosan in the gastric fluids [75,98], it is important to consider mechanisms able to enhance its mechanical and physical properties during the micro/nano particles production, so that a gastric application, such as for the treatment of *H. pylori,* is viable. When associated to drug delivery, the dissolution of the chitosan can be restrictive, since due to the protonation of the glucosamine residues of the chitosan in the acidic pH, an extensive swelling of the microsphere is verified, followed by a faster release of the drug [31], which might not be desirable. As a consequence, low retention time and difficulty in crossing the mucus barrier have been observed as well [43].

- *Chitosan micro/nanoparticles stability under acidic conditions: crosslinking*

In order to overcome this restriction and to preserve the stability and three dimensional structure of chitosan gel under gastric conditions or enzymatic degradation, physical and chemical modifications of chitosan have been used as a reinforcement strategy of the chitosan structure, improving its mechanical resistance and chemical stability in acidic solutions [75,81,95,98].

Tripolyphosphate (TPP), a non-toxic polyanion able to interact with chitosan via electrostatic forces, is conventionally used to form ionic crosslinked networks [98]. However, although TPP has fast gelling ability and higher stability in acid than the chitosan alone [98], it is difficult to accurately control the physical gel pore size, chemical functionalization, dissolution and degradation [79]. As an alternative, chemical crosslinking agents, mainly glutaraldehyde, have been considered [99,100]. Glutaraldehyde reacts with chitosan forming covalent bonds mainly with the amino groups of the polymer. However, glutaraldehyde, as well as other synthetic crosslinking reagents, is cytotoxic, which may impair the biocompatibility and biodegradability of the microspheres [101,102]. Biocompatible natural occurring crosslinking agents have therefore been thoroughly investigated, seeking for a less cytotoxic agent, able to form stable and biocompatible crosslinked products. Genipin is particularly effective for chemically crosslink polymers containing amino groups [79], forming secondary amides and heterocyclic amino linkages [101]. Sung et al. [103] have found that genipin-crosslinked networks are significantly less cytotoxic (about 5000–10000 times) than

those crosslinked by glutaraldehyde [100,104], and also that they degrade slower than glutaraldehyde-crosslinked ones [105].

Conjugation of crosslinking methods [32] is also a valuable possibility in order to improve its usage for biomedical applications. Mi et al. [81] produced chitosan gel beads by the fixation of its amine groups with a co-crosslinking agent composed of TPP (ionic crosslinker) and genipin (chemical crosslinker). Simply, the negative charged TPP ions react with positive charged chitosan through electrostatic interactions, while genipin reacts with chitosan via covalent bonding [75,98]. However, this interaction was found to be dependent on the pH value of the co-crosslinker [81,106]. UV (Ultra Violet Spectroscopy), FTIR (Fourier Transform Infrared Spectroscopy) and EDAX (X- ray energy dispersion) analysis revealed that chemical crosslinking by genipin can be inhibited due to the presence of H$^+$ in the co-crosslinking process, significantly encouraging the ionic crosslinking reaction while diminishing the chemical crosslinking reaction. Depending on the pH, chitosan can bind more easily with TPP ions (low pH) or with genipin (neutral or alkaline pH), fact related to the presence of $OH^-, P_3O_{10}^{5-}, H^+$ and $NH^{3+}$ on the solution. Different pH conditions will alter the concentration of these ions and therefore crosslinkers relation with chitosan: ionic crosslinking will be the dominant reaction at lower pH, while  the chemical crosslinking of chitosan with genipin will dominate the reaction of co-crosslinking at higher pH [81]. Shah et al., [32] developed drug containing microspheres prepared by ionic crosslinking (TPP) and precipitation. Chitosan microspheres were loaded with amoxicillin and metronidazole, capable of adhere to the mucus layer, releasing the contents locally at the site of infection.

Apart from crosslinking, alternative approaches can be considered, such as reacetylation for instance with acetic anhydride, strategy that has been shown to reduce chitosan solubility and improve drug release capacity of the microspheres [107].

- *Influence of crosslinking degree on chitosan particles properties*

Nevertheless, chitosan modifications should be addressed carefully, since chitosan final properties depend on the extent of crosslinking reaction [95,108]. Its swelling ability, and consequently the release rate of the drug, as well as its mucoadhesive properties might be affected [101,109]. As previously said, the latter may be attributed to molecular attractive forces formed by electrostatic interaction between positively charged chitosan and negatively charged mucosal surfaces [106], and therefore by increasing the degree of crosslinking, the number of free primary amines will be reduced. Consequently, the possible ligand density and the polymer reactivity may also decrease as well as the accessibility to internal sites of the material, leading to a loss in the flexibility of the polymer chains [95]. Apart from crosslinking, ionic modification and salt formation can also affect the mucoadhesive properties of chitosan [110,111].

In order to control the crosslinking degree, several factors must be taken into account (Table 2), including not only concentration and volume of crosslinking agent, incubation time, temperature and stirring speed, but also MW and DD of chitosan [90,95]. When designing a particle for a specific application, all these factors should be taken into account during preparation [112], so that an optimized system can be developed.

**Table 2** – Factors influencing chitosan micro/nano particles features.

| Chitosan | Size | | Charge | | Swelling | |
|---|---|---|---|---|---|---|
| Molecular weight | | | ↑ | [113] | | |
| Degree of deacetylation (%) | — | [114] | ↑ | [113] | | |
| Concentration (%w/v) | ↑ | [115] | | | ↑ | [115] |
| Polymer-drug ratio | ↑ | [90] | ↑ | [90] | ↑ | [90] |
| Crosslinking | ↓ | [83,90] | ↓ | [83,90] | ↓ | [75,109] |

Regarding crosslinking, by increasing agent or volume of crosslinker, incubation time or temperature, crosslinking degree is increased. A high degree of deacetylation of chitosan favours crosslinking since it requires mainly deacetylated reactive units. The size of the particle is strongly dependent on the concentration of the solutions [33], and the higher the degree of crosslinking, the less irregular are the microspheres, and the smaller the particle size [83], due to the shrinking of the network observed. The charge of the particle, and therefore its mucoadhesive properties, is evaluated through potential zeta, and is reduced when the crosslinker volume, incubation time or stirring speed is increased [83,90]. The swelling ability influences the drug release profile, which is normally decreased when the incubation time and therefore the degree of crosslinking is increased [75,109]. Prolonged *in vitro* drug release time is also associated with higher degrees of crosslinking [115].

All these parameters represent consequences regarding particles performance *in vitro* and *in vivo*, and therefore should be evaluated carefully. For instance, because the accumulated locations of the microspheres containing drug depend on the size of the particles, if the size distribution of microspheres is broad, the bioavailability of drug will be low and the side-effects of the drug will be increased [97].

## 1.8   Chitosan as a binding agent

Despite the growing application of chitosan particles as drug delivery vehicles, low retention of microspheres in the stomach, resistance to the delivered antibiotics, amongst other factors have prevented the development of efficient therapies against *H. pylori*, therefore persisting the need of alternative options for the treatment of *H. pylori* infection [74].

The antimicrobial activity of chitosan and its derivatives was observed against several bacteria [116,117], fungi [118] and parasites [119]. In liquid medium, chitosan was able to inhibit the growth of some spoilage bacteria such as *Bacillus subtilis* IFO 3025, *Escherichia coli* RB, *Pseudomonas fragi* IFO 3458 and *Staphylococcus aureus* IAM 1011 [120].

Antimicrobial activity of chitosan or chitosan-based films has also been investigated, showing reduced microbial growth [117,121,122]. Leceta et al., [123] evaluated the antimicrobial activity of chitosan-based films and chitosan film forming solutions against *E. coli* 0517H, and *L. plantarum* CECT748, observing that only chitosan film forming solutions presented antibacterial properties, whereas chitosan-based films dried at room temperature only showed bacteriostatic properties. Particularly, chitosan ability to bind and kill *H. pylori*

has been investigated and demonstrated [124], revealing new potential therapies against *H. pylori*.

Nogueira et al. [124] produced chitosan thin films and evaluated its effect on *H. pylori* in a pH range that simulates gastric conditions (2.6, 4.0 and 6.0). Results revealed that chitosan films were able to induce cell death of more than 75% of the adherent bacteria, independently of pH. Therefore, the potential use of chitosan-based biomaterials as adjuvants in the elimination of *H. pylori* gastric infection might be a valuable option.

In fact, Fernandes et al. and Gonçalves et al. [43,108] produced chitosan microspheres that rather than being used as a vehicle for gastric drug delivery, were designed and applied as an *H. pylori*-binder system. The rational of the strategy consists on eliminating *H. pylori* present in the stomach by binding the bacteria and impairing its adhesion to host cells. As binding agent, it is important to prevent dissolution of microspheres while maintaining its mucoadhesive properties, so that binding can happen, followed by removal of the bacteria intact from the stomach, through the intestinal tract, after gastric mucosal turnover. Furthermore, the microsphere should have a size which allows it to effectively bind *H. pylori* bacteria. Bacteria contained in the stomach but not adhered to the gastric mucosa or mucus layer can also be bound by the microspheres [43]. Therefore, a diameter between about 70 $\mu$m and about 200$\mu$m would allow the microspheres not only to adhere to bacteria present on the mucus barrier, but also to bacteria adhered to foveolaes.

This system was further improved by directing the microspheres toward *H. pylori*. Glycosilated receptors that specifically bind to molecules displayed on the surface of *H. pylori* bacteria were incorporated on the system [125], thereby adsorbing the bacteria so that they can be removed from the gastric mucosa and/or mucus layer or prevented from binding to the gastric mucosa and/or mucus layer. The glycan receptors of *H. pylori* include fucosylated blood group antigens, such as Lewis B and/or Sialyl-Lewis X receptors. By removing bacteria from the stomach, colonisation of the gastric mucosa and mucus layer by *H. pylori* bacteria is reduced, and re-colonisation can be reduced or prevented.

## 1.9   Active targeting to improve *H. pylori* treatment

Active targeting can provide the system specificity by directing it towards the mucosal surfaces or bacteria. Complex systems can combine bioadhesive properties, selective targets and delivery of the drugs, resulting in a system with improved ability to effectively kill and eradicate *H. pylori*. Any ligand/drug with a high binding affinity for mucins or for the bacteria can be covalently linked to the microspheres with the appropriate chemistry [5,59]. Depending on the purpose, lectins, bacterial adhesins, amino acid sequences or antibodies can be used, either to increase adhesion of bioadhesive microspheres to specific cell surface glycoproteins, mucins or bacteria wall [126].

Particularly, lectin-conjugated nanoparticle systems, which may bind to the carbohydrate residue present on the bacterial surface, have been proposed and play an effective tool for eradication of *H. pylori*. This may influence its adherence to the membrane of surface mucous cells [127].

A study performed by Ramteke et al. [33] demonstrated the efficacy of a more complex system on the delivery of antibiotics: chitosan-glutamic acid nanoparticles containing triple therapy were produced by ionotropic gelation. With a particle size ranging between 550nm

and 900nm, the nanoparticles showed to inhibit growth of *H. pylori*, however the drug was totally released within the first 5h. In order to improve the selectivity and efficacy of the nanoparticles, the authors functionalized the chitosan nanoparticles with α(L)-fucose, verifying an improvement on the antibacterial effect when comparing to non-conjugated ones. The fucose-conjugated formulations showed strong agglutination with *H. pylori*, confirming the presence of lectin type receptors on the surface of *H. pylori* that can selectively bind with the specific ligand present on nanoparticles. *In vitro* antibacterial studies revealed a higher eradication rate for monotherapy when functionalized nanoparticles were used when comparing to non-functionalized. Triple therapy showed once again to have better effects when applied with functionalized nanoparticles, with an eradication rate of 97.17% against 91.01% for non-conjugated chitosan nanoparticles and  81.32% for plain triple therapy. These results show superior targeting potency toward lectin receptors on *H. pylori* surface. Chitosan nanoparticles without antibiotics, both functionalized and non-functionalized, were shown to possess antimicrobial activity against *H. pylori*, with a maximum % of growth inhibition of 5.13% for non-functionalized nanoparticles and 7.9% for functionalized ones. *In vivo* tests demonstrated the *H. pylori* elimination from the stomach of the mice after administration of the nanoparticles. An eradication of 100% was found for functionalized nanoparticles, confirmed by the negative results of the Gram-staining and urease test. Non-functionalized ones presented an eradication rate of 50% or less, while plain triple therapy presented even lower values.

To notice that functionalization leads to an increase in the particle size [33], which depending on the application, may not be desired.

# Chapter 2

# Aim

The overall aim of this project lies on the production and study of the ability of 50 μm *H. pylori*-binding chitosan microspheres to penetrate the gastric foveolae, using for that ex-vivo models consisting of mice and human fresh stomachs.

So that the global aim could be achieved, the work was subdivided into three major sections:

### 1. Production of chitosan microspheres

Previous studies have demonstrated the ability of chitosan microspheres to interact with *H. pylori* and adhere to the gastric mucosa. However, previously developed chitosan microspheres presented a diameter around 170 μm, which hampered the penetration and removal of the bacteria installed inside the foveolae. For that reason, the development of smaller microspheres is crucial to reach the bacteria adhered to the surface of gastric epithelial cells. Previous studies using 2D sections of human gastric mucosae have shown that human stomach foveolae are ~70 μm wide, therefore microspheres with approximate size of 50 μm should ideally be used.

For this purpose, chitosan microspheres were produced by ionotropic gelation, though recurring to three different equipments, namely high voltage electrostatic system, co-axial air stream system and aerodynamically driven system.

An intensive screening of several parameters was performed before selecting the best condition. Chitosan degree of acetylation (DA) was one of the parameters assessed and its effect was evaluated on the production process. From two DA (6% and 16%), differing in the number of primary amines available to establish other reactions, the lowest one was selected in order to potentiate the mucoadhesive properties of the microspheres.

In order to be stable in the gastric acidic conditions, chitosan microspheres will be crosslinked with genipin. Both genipin crosslinking and chitosan mucoadhesive properties are processes dependent on the amount of active primary amino groups present on the chitosan D-glucosamine units. Therefore, the crosslinking process must be controlled and readjusted to the selected microspheres. Morphology and size distribution of chitosan microspheres were analysed by three different equipments, based on optical microscopy coupled with image acquisition (Optical Microscopy and IN Cell Analyzer high-throughput microscopy) and laser diffraction (Mastersizer equipment).

### 2.  Penetration of chitosan microspheres into the gastric mucosa

Following the production of the aimed chitosan microspheres with size average around 50 µm, the evaluation of their ability to penetrate the gastric foveolae is crucial to accomplish to remove *H. pylori* present within the gastric foveolae. An ex-vivo model was chosen since it allows mimicking the 3D structure of the stomach while preserving its mucus layer, which is enrolled on bacteria adhesion process.

Since mice have been frequently used as an animal model to study *H. pylori* infection, preliminary studies regarding labelling optimization were performed using fresh stomachs from C57BL/6 mice strain. Nucleic acids and plasma membrane stains were tried out in fixed and fresh stomachs.

Adhesion studies relied on the incubation of the fresh stomach with the chitosan microspheres at 37ºC, for a 2h-period, at pH 6.0, followed by the specific labelling. Samples were observed under fluorescence and confocal laser scanning microscopy. Citrate-phosphate buffer was used at pH 6.0 since it allows mimicking the acidic stomach conditions, particularly the ones near the epithelial cells (pH 6.0).

### 3.  Evaluation of the adhesion of chitosan microspheres to *H. pylori*

The ability of the chitosan microspheres to interact with *H. pylori* is also relevant to the whole process. Therefore, J99 *H. pylori* strain, obtained from human isolates and presenting BabA and SabA adhesins on its surface, was selected to conduct the adhesion studies.

The chitosan microspheres prepared were incubated with *H. pylori* for 2h-period. In order to evaluate if being alive would influence the *in vitro* interaction of *H. pylori* with chitosan microspheres, parallel studies were conducted using FITC-fixed J99 strain and live bacteria, using nucleic acid stains. Fluorescence microscopy was used to visualize the samples as well as confocal laser scanning microscopy, the latter to better assess bacteria adhesion and to evaluate whether bacteria only adheres to the surface of the microsphere or if it goes inside.

# Chapter 3

# Materials and Methods

## 3.1 Chitosan Microspheres Preparation

### 3.1.1 Chitosan purification

Squid pen chitosan powder with a DA of 6% (MW> 500,000 Da) and 16% (MW 283,000-472,000 Da) was weighted, separately, and dried for 24 h inside a vacuum oven (60ºC). Afterwards, chitosan was hydrated in Milli-Q water for 24 h at 4ºC and glacial acetic acid was added to achieve a final concentration of 0.2 M, being kept overnight at room temperature. Chitosan should be protected from light all the time as it is sensitive to it. Chitosan solution was then filtered and precipitated by addition of NaOH, until the solution was alkaline. Chitosan suspension was centrifuged, the supernatant was discarded and deionized water was added, followed by pellet resuspension. This process was repeated 3 times. Chitosan suspension was then frozen at -80ºC, and lyophilised for 72 h. Lastly, chitosan was milled until a fine powder was obtained.

### 3.1.2 Preparation of chitosan solution

Purified chitosan powder was dried in a vacuum oven at 60°C for 24 h. Chitosan was previously hydrated using Milli-Q water at 4°C under slow magnetic stirring, and after 24h incubation, glacial acetic acid was added to achieve a final concentration of 0.1 M and left overnight under moderate stirring at room temperature. For each DA, three solutions with different concentrations of 0.5%, 1% and 1.5% (w/v) were prepared. Afterwards, each chitosan solution in acetic acid was filtered using a 5 μm pore size syringe filter (Millipore) followed by a 0.8 μm pore size filter (Millipore).

## 3.2 Chitosan microspheres production

Chitosan microspheres were produced by ionotropic gelation into a sodium triphosphate pentabasic (TPP; Sigma-Aldrich) solution (pH 9.0) using three different methods. The aim was to identify the system able to provide the most suitable microspheres, with adequate size and morphology. Several parameters were varied in order to optimize the microspheres production.

### 3.2.1  High voltage electrostatic system

Chitosan microspheres were produced in a high voltage electrostatic system (Nisco Encapsulation UnitVar 1, NISCO). Briefly, a syringe with chitosan solution was placed on a syringe pump and connected to the nozzle. A voltage of 7.0 kV/cm was applied between the needle feeding the chitosan solution and the 5% (w/v) TPP solution underneath. This voltage forces the droplets to fall off the 0.09 mm diameter needle tip (PE-00515, Nisco) into the TPP eletroconductive solution. The chitosan solution flow rate was adjusted and TPP solution was subjected to slow stirring (35 rpm). Conditions evaluated are specified in Table 3.
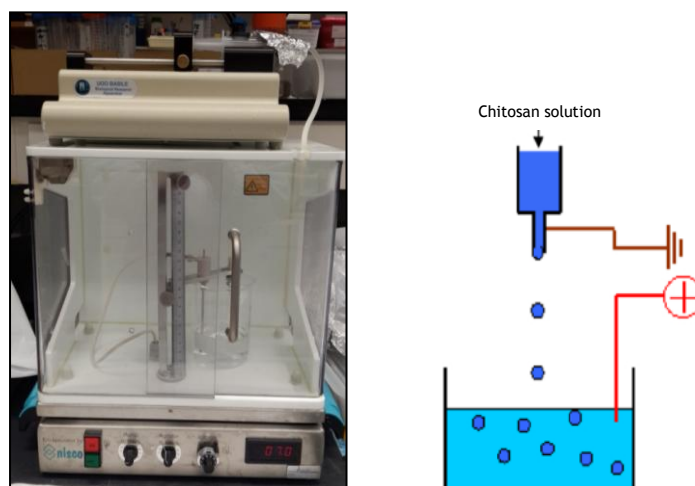


**Figure 4 -** High voltage electrostatic system.

### 3.2.2  Co-axial air stream system

Chitosan microspheres were produced by droplet extrusion under co-axial air stream (Nisco Encapsulation Coaxial Airflow Induced Dripping VAR J1, NISCO). Briefly, a syringe with chitosan solution was placed on a syringe pump and connected to the nozzle. The unit is equipped with two connections, one for the hose which provides the chitosan solution, and the other connection being aimed for an air hose. Chitosan droplets were extruded through a needle (PE-00515, Nisco) into a 5% (w/v) TPP solution, under a co-axial air stream with controlled pressure, which blows the chitosan droplets from the needle tip into the TPP gelling bath before they would fall due to gravity. Syringe pump flow rate was adjusted and the microspheres were formed under slow stirring (35 rpm). A number of parameters were

investigated by changing one parameter while keeping the others constant. Conditions evaluated are specified in Table 3.
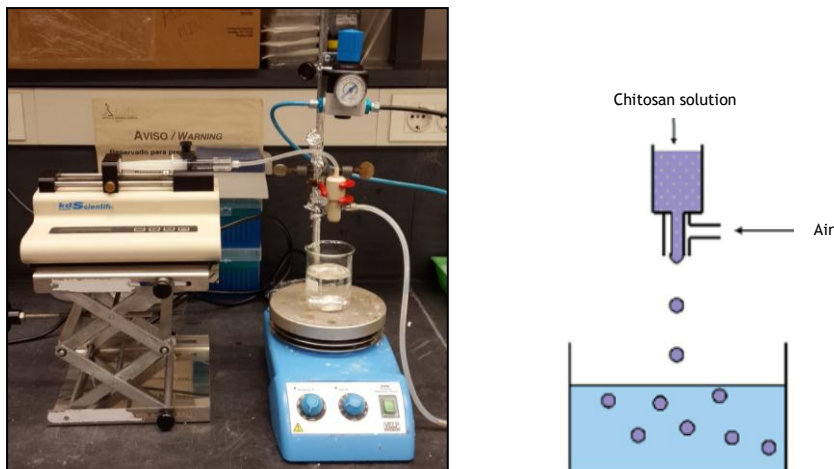


**Figure 5 -** Droplet extrusion under co-axial air stream system.

## 3.2.3 Aerodynamically driven system

Chitosan microspheres were produced by an aerodynamically driven system (Nisco Encapsulation Unit Var J30, NISCO). Briefly, the syringe with the chitosan solution is placed on the syringe pump and connected to the nozzle. The chitosan enters through a central needle, which is enclosed in a pressure chamber with an exit through the orifice. A second orifice allows air to enter the chamber, which pressure can be fixed with a potentiometer. The exit orifice, which is centrally in line with the axis of the needle, has been counter-sunk externally. The counter sunk leads to the aero dynamical effect so that the jet has a smaller diameter when passing the orifice than before at the needle. Since the size of the drops is determined by the chitosan flow rate and the pressure inside the chamber, these parameters were investigated, as well as chitosan solution concentration. Only degree of acetylation of 6% was used in this method.
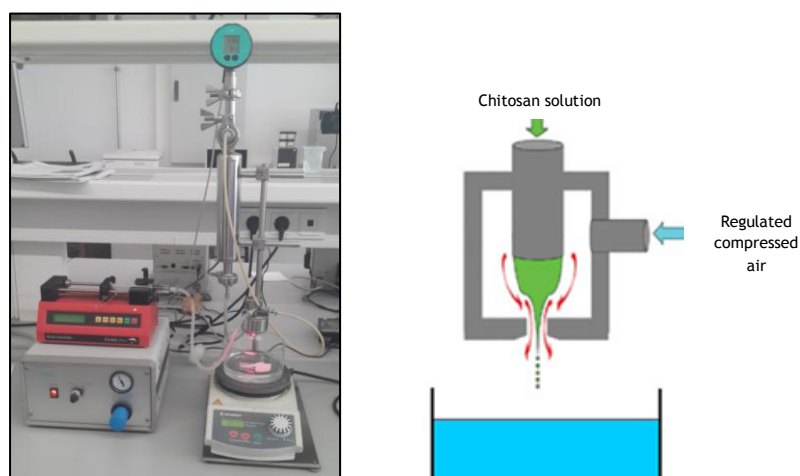


**Figure 6 –** Aerodynamically driven system.

## 3.2.4  Variable conditions

Table 3 shows the parameters varied during microspheres production, regarding the three methods tested.

**Table 3** – Conditions tested during Ch microspheres production.

| | Ch degree of acetylation | Ch solution concentration | Syringe pump flow rate | Air stream pressure | Nozzle diameter |
|---|---|---|---|---|---|
| High voltage electrostatic system | 6% 16% | 0.5 % (w/v) 1 % (w/v) 1.5 % (w/v) | 0.4 mL/h 1 mL/h 10 mL/h 20 mL/h | NA | NA |
| Droplet extrusion under co-axial air stream system | 6% 16% | 0.5 % (w/v) 1 % (w/v) 1.5 % (w/v) | 0.4 mL/h 1 mL/h 10 mL/h 20 mL/h | 0.25 bar 0.4 bar 0.6 bar 1 bar | NA |
| Aerodynamically driven system | 6% | 0.5 % (w/v) 1 % (w/v) | 0.25 mL/min 0.33 mL/min 0.5 mL/min 1 mL/min | 0.205 bar 0.525 bar | 0.25 mm 0.50 mm |

NA – not applicable

# 3.3  Chitosan microspheres characterization

## 3.3.1  Size and morphology

Chitosan microspheres were characterized mainly regarding size and morphology by different techniques, each one providing complementary information. Three equipments were used to perform the analysis of the particles.

## 3.3.2  Optical Microscopy

Optical microscopy was first used to roughly determine the average diameter of the chitosan microspheres. The latter were transferred to 24-well plates and images were acquired in Bright field using the 10x objective. Diameter of manually selected chitosan microspheres was then measured using AxioVision Software (Zeiss), always horizontally in the larger part of the microspheres to avoid bias.

### 3.3.3 IN Cell Analyzer

IN Cell Analyzer 2000 (GE Healthcare) is a super-fast, sensitive, and flexible wide-field cell imaging system, which simultaneously allows the acquisition of high quality images and posteriorly the analysis of morphological parameters.

Chitosan microspheres were transferred preferentially to a 96-well plate, and an automated screening was performed throughout all the specified wells. Images were acquired in 10x objective using Bright field. Afterwards, in the coupled IN Cell Developer Toolbox, a customized protocol was created for chitosan microspheres quantification and analysis. Initially, the target to be located and measured, that is each microsphere, was defined. After that, pre-processing operations were implemented in order to make the microspheres easy to detect, namely operations that erode and dilate image features, reduce noise and correct uneven background intensity. To separate and isolate the microspheres from the remaining image features, a segmentation algorithm was implemented based on particular sizes, shapes and intensities. After defining what is considered a microsphere, specific measurements were selected from a library of pre-defined morphological and densitometric measures: area, length, average diameter, maximum chord and form factor of each microsphere were determined. This protocol was then applied to each image acquired, providing a list of the selected measures for each microsphere identified by the protocol. The associated software Spotfire™ DecisionSite™ allowed an interactive visualization of the obtained data through different graphs. From these graphs, outsiders were eliminated as well as particles smaller than 10 μm, which in most of the cases were debris and artefacts of the image. Only after this analysis, average measures regarding microspheres characteristics were considered.

### 3.3.4 Mastersizer

Mastersizer 3000 (Malvern) is a particle sizing instrument which uses the technique of laser diffraction to measure particle size distributions, from 0.01 μm up to 3.5 mm.

Chitosan particles are drawn into a water container (The Hydro EV, Malvern) until enough sample is recognized. Five measurements are performed for each sample and a sequential combination of measurements with red and blue light sources is used to measure across the entire particle size range. Sonication can be applied to increase separation between chitosan particles. The coupled software gives the information regarding microspheres size. Given that it cannot be assured that all the microspheres are exactly spheres, the particle size is defined using the concept of equivalent spheres. In this case, the microspheres size is reported as a volume equivalent sphere diameter, meaning that the particle size is defined by the diameter of an equivalent sphere having the same volume. A volume weighted distribution is then given where the contribution of each particle in the distribution relates to the volume of that particle. Apart from the histogram regarding the size distribution, parameters based upon the maximum microspheres size for a given percentage volume of the sample, named percentiles, are reported. Percentiles Dv10, Dv50 and Dv90 are given, being D diameter, v volume (specifying the distribution weighting) and 10, 50 and 90 the percentage of sample below this particle size.

Since microspheres produced in aerodynamically driven system VarJ30 under 525 mBar pressure, 0.5 mL/min flow rate with 0.25 mm nozzle and chitosan with DA 6% at 0.5% (w/v)

presented the average diameter of 50 µm aimed, they were selected for all subsequent studies.

## 3.4 Genipin crosslinking kinetics

Chitosan microspheres were rinsed three times with Milli-Q water by centrifugation at 10 000 rpm for 7 min. After that, in order to determine the adequate crosslinking level of chitosan microspheres, the crosslinking kinetics was assessed at various time points. Briefly, 20 µL of rinsed chitosan microspheres suspension were transferred to a 24-well plate and 500 µL of 10 mM genipin (Wako Chemicals GmbH) solution prepared in 0.01 M phosphate buffer saline (PBS) (Sigma, pH 7.4) were added. The crosslinking level of chitosan microspheres was determined using an Inverted Fluorescence Microscope (IFM, AxioVert, Zeiss). Images were taken every 15 min over a 12-h period. Single chitosan microspheres were visualized in the DAPI channel (470 nm) and their densitometric mean fluorescence was followed over time.

From the kinetics study a time point corresponding to an intermediate crosslinking degree was selected and chitosan microspheres were incubated in 10 mM of genipin solution over 45 min under 120 rpm stirring at 25ºC. After crosslinking, the microspheres were rinsed three times by centrifugation with Milli-Q water, frozen in liquid nitrogen and lyophilised at -80ºC for 96 h.
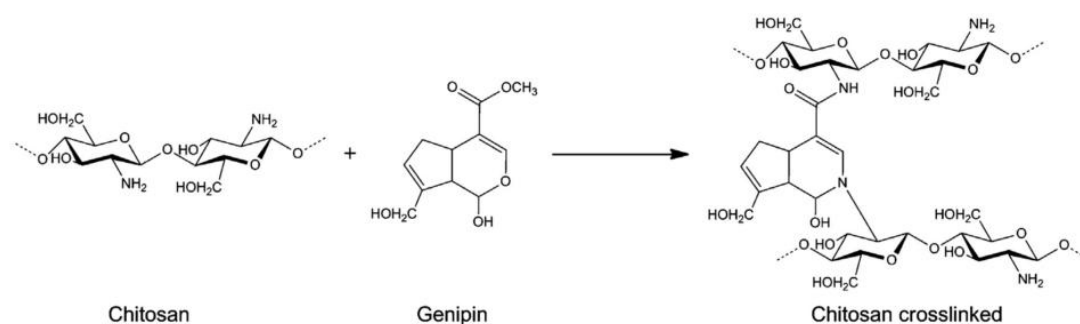


**Figure 7 -** Crosslinking reaction mechanism between chitosan and genipin [108].

## 3.4.1 Stability in acidic conditions

The acidic stomach conditions in the mucus layer near the epithelial cells were mimicked by phosphate-citrate buffer (citric acid 0.1 M and $Na_2HPO_4.2H_2O$ 0.2 M) at pH 6.0. Briefly, 20 µL of crosslinked chitosan microspheres were transferred to a 24-well plate and 500 µL of phosphate-citrate buffer were added. Chitosan microspheres were visualized by OM and images were taken every 5 min over an hour.

## 3.5 Chitosan microspheres adhesion to gastric mucosa

The efficiency of chitosan microspheres to adhere and penetrate the gastric mucosa was evaluated using stomach fresh samples. The model was first optimized using mice gastric mucosa, followed by further assessment using human gastric samples. Incubations were performed in phosphate-citrate buffer pH 6.0 at 37°C under 70 rpm.

## 3.5.1 Gastric mucosa labelling optimization

Gastric mucosa labelling optimization was performed using mice stomachs.

Stomachs from 6 to 10 week old wt C57BL/6 mice strain were obtained from Animal House at IBMC/INEB (Porto, Portugal) and used shortly after its sacrifice using carbon dioxide inhalation. Stomachs were opened through the great curvature from the duodenum to oesophagus using chirurgical scissors, obtaining a butterfly-like shape. The food contents were gently removed using 0.01 M PBS (pH 7.4) in order to preserve the stomach mucus layer. Then, a cut through the mice stomach smaller curvature was done in order to divide this organ in two halves. Each half was used separately corresponding to an individual stomach sample.

To better assess the penetration of chitosan microspheres, gastric mucosa was labelled recurring to nuclear and plasma membrane stains.

**Table 4** – Nuclear and plasma membrane stains evaluated.

| | Stains | Fluorescence excitation (nm) | Fluorescence emission (nm) | Concentration (µg/mL) | Incubation time (min) |
|---|---|---|---|---|---|
| **Nuclear** | **DAPI** | 350 | 470 | 1 (1:100) 10 (1:100) | 15 |
| | **Hoechst** | 350 | 461 | 1 (1:100) 10 (1:100) | 15 |
| **Plasma membrane** | **Wheat Germ Agglutinin (WGA), Alexa Fluor® 350 conjugate** | 346 | 442 | 5 | 15 |
| | **WGA, Alexa Fluor® 488 conjugate** | 495 | 519 | 1 | 15 30 |
| | **WGA, Alexa Fluor® 594 conjugate** | 590 | 617 | 5 20 | 15 |
| | **WGA, fluorescein conjugate** | 494 | 518 | 5 | 15 |
| | **CellMask™ Deep Red** | 649 | 666 | 1000X | - |

Regarding the nucleic acid stains, since DAPI is recommended for fixed or permeabilized cells, some samples were initially fixed with paraformaldehyde (PFA) 4% before staining. Moreover, both DAPI and Hoechst were mounted using two different mounting media, namely Vectashield and Fluoromount.

Samples concerning the plasma membrane staining, Wheat Germ Agglutinin conjugates (WGA, Invitrogen) and CellMask™ Deep Red (Molecular Probes), were kept fresh, and no fixation or mounting process was performed.

Samples were observed with IFM and a Leica SP2 and SP5 confocal laser scanning microscope (CLSM, Leica Microsystems).

### 3.5.2 Chitosan microspheres adhesion to mice gastric mucosa

Chitosan microspheres were firstly sonicated for 8 min, followed centrifugation (10000 rpm, 7 min) in order to transfer the microspheres (kept in ethanol 70%) to the pH 6.0 buffer. Afterwards, microspheres were counted using IN Cell Analyzer high-throughput microscopy and 500 microspheres in 60 µL of phosphate-citrate buffer pH 6.0 per sample were added to mice gastric mucosa for 2 h in 6-well plate covered with parafilm. Afterwards, samples were rinsed three times in 1 mL of 0.01 M PBS and mucosa labelling was performed. After that, samples were once again rinsed in 0.01 M PBS and visualized by IFM and CLSM.

### 3.5.3 Chitosan microspheres adhesion to human gastric mucosa

Human gastric mucosae were provided by Hospital São João (Porto, Portugal) and were obtained from stomach portions that were removed after a partial gastrectomy.

Chitosan microspheres adhesion to the mucosa was done similarly to the adhesion assay using mice gastric mucosa. CellMask™ Deep Red was used as stain.

## 3.6 *Helicobacter pylori* adhesion to chitosan microspheres

Apart from being able to penetrate gastric mucosa, chitosan microspheres must have the capability of adhering to *Helicobacter pylori (H. pylori)*, so that they can afterwards remove the bacteria from the gastric foveolae.

Since the *in vivo* adhesion of *H. pylori* to chitosan microspheres occurs with the bacteria alive, two independently adhesion assays were conducted with live and previously fixed J99 *H. pylori* strain, in order to understand whether the adhesion of *H. pylori* to chitosan microspheres might be influenced by the bacteria being alive.

### 3.6.1 *H. pylori* strain and culture conditions

*H. pylori* strain J99, obtained from human isolates, was obtained from the Department of Medical Biochemistry and Biophysics, Umeå University, Sweden [128]. Bacteria were cultured in OXOID Blood Agar base 2 (Probiológica) supplemented with 10% defibrinated horse blood (Probiológica) and antibiotic/antifungal cocktail at 37˚C, for 48 h, under microaerobic conditions. Bacteria were then spread and incubated for another 48 h. At the end of the incubation period, bacteria were harvested using 0.01 M PBS and their optical density at 600 nm ($OD_{600}$) was measured. Bacteria inoculum was adjusted to an optical density ($OD_{600}$) of 0.08 using pH 6.0 phosphate-citrate buffer.

*H. pylori* previously fixed and labelled with fluorescein isothiocyanate (FITC) and frozen according to the protocol described in [129] was also used ($OD_{600}$1.0).

### 3.6.2 Adhesion of *H. pylori* J99 strain to chitosan microspheres

Chitosan microspheres were incubated with live or FITC- labelled *H. pylori* at a final optical density ($OD_{600}$) of 0.04, corresponding to $1 \times 10^7$ colony forming units (CFU) per mL, for 2 h, under 120 rpm stirring with a final incubation volume of 60 µL of phosphate-citrate

buffer at pH 6.0. Adhesion assay with live bacteria was conducted at 37℃ while the assay with FITC-labelled bacteria was carried out at room temperature (RT). After incubation, in order to remove non-adherent bacteria, microspheres were rinsed five times using 500 µL of 0.01 M PBS by centrifugation at 10 000 rpm, for 7 min.

Regarding live bacteria assay, staining was performed after the adhesion, with DAPI (10 µg/mL) and Hoechst (10 µg/mL) as nucleic acid stains.

Microspheres were gently transferred to microscope slides. A drop of fluorescence mounting medium (Vectashield and Vectashield with DAPI) was added, a glass coverslip was placed on top of the preparation and observed under IFM and CLSM.

# Chapter 4

# Results and Discussion
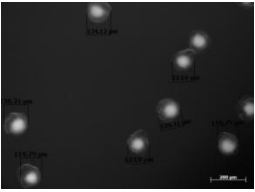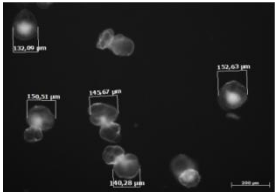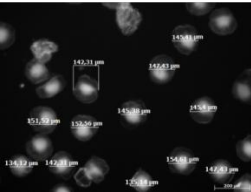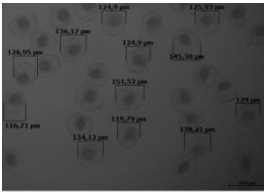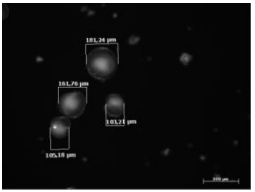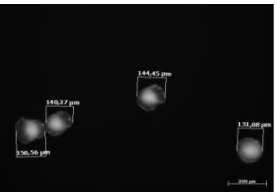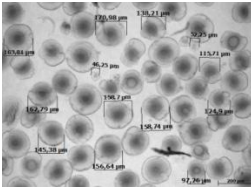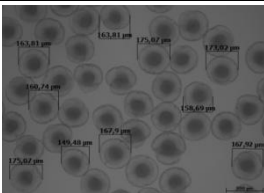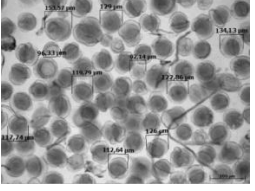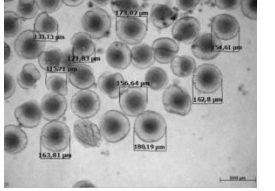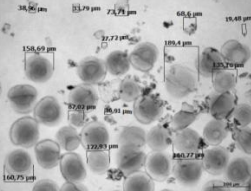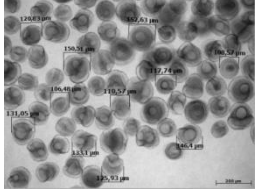
## 4.1 Chitosan microspheres production and characterization

Chitosan microspheres were produced using three different equipments, being the fundamental production process ionotropic gelation. However, since the formation of the microspheres occurred at pH 9.0, also coacervation of the chitosan chains occurs. Initially, a qualitative analysis was performed, followed by a quantitative analysis on those conditions apparently promising, until the condition presenting the 50 μm average diameter microspheres was selected. Chitosan microspheres characterization was performed recurring to microscopy and laser diffraction techniques.

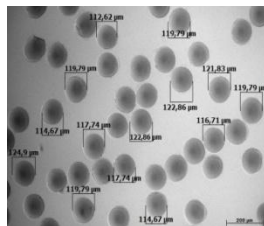### 4.1.1 High voltage electrostatic system
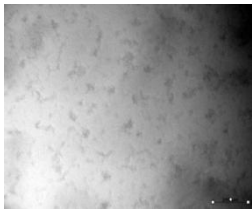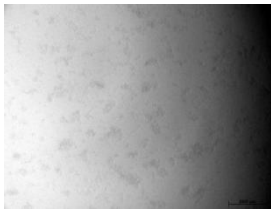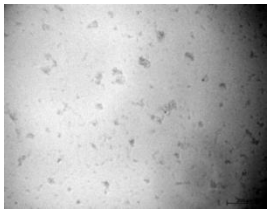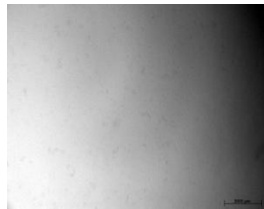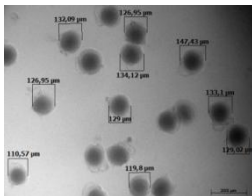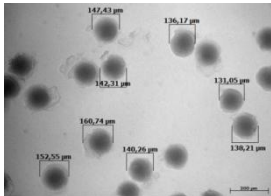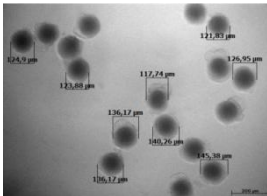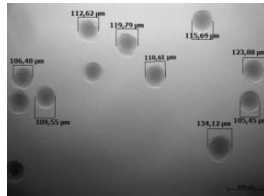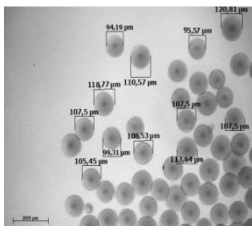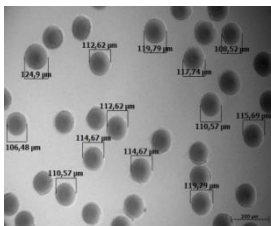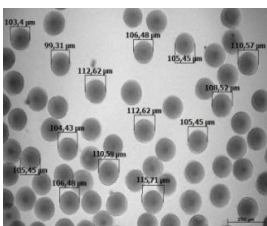
The effect of chitosan concentration and flow rate on the chitosan microspheres production was evaluated for both chitosan with DA of 6% (Table 5) and 16% (Table 6) using high voltage electrostatic system. A qualitative analysis was performed based on the average diameter and morphology.

**Table 5 -** Chitosan microspheres images obtained by optical microscopy (scale bar 200 µm). Different concentrations of chitosan solution (0.5%, 1% and 1.5% (w/v)) with DA of 6% and different flow rates (20, 10, 1 and 0.4 mL/h) are shown. Average diameter is indicated below each condition.

| | Flow rate | | | |
|---|---|---|---|---|
| | **20 mL/h** | **10 mL/h** | **1 mL/h** | **0.4 mL/h** |
| **0.5 % (w/v)** |  |  |  |  |
| | Mainly one population, ~130 µm | Mainly one population, ~150 µm | Mainly one population, ~145 µm | Mainly one population, ~131 µm |
| **1 % (w/v)** |  |  |  |  |
| | Several sizes, 105-180 µm | Mainly one population,~130 µm | Mainly two populations, ~50 µm and 115-160 µm | One population, 145-180 µm |
| **1.5 % (w/v)** |  |  |  |  |
| | Mainly one population, 90-150 µm | 115-180 µm | Two populations, 15-35 µm and 120-190 µm | One population, 100-150 µm |

*(Chitosan concentration — row label for the three concentration rows)*

Regarding chitosan with DA of 6% (Table 5), all chitosan microspheres present a uniform, spherical morphology, with what seems a denser region in the centre when comparing to the periphery (clearer and therefore less dense). Images from optical microscopy (OM) suggest that the production of chitosan microspheres is not affected by the variation of the chitosan concentration or flow rate, maintaining approximately similar sizes amongst all conditions (130-160 µm). Moreover, mostly one population is found in each condition, presenting a narrow size distribution.

**Table 6 -** Chitosan microspheres images obtained by optical microscopy (scale bar 200 µm). Different concentrations of chitosan solution (0.5%, 1% and 1.5% (w/v)) with DA of 16% and different flow rates (20, 10, 1 and 0.4 mL/h) are shown. Average diameter is indicated below each condition.



| | Flow rate | | | |
| --- | --- | --- | --- | --- |
| | **20 mL/h** | **10 mL/h** | **1 mL/h** | **0.4 mL/h** |
| **0.5 % (w/v)** | Aggregates, impossible to identify mics | Aggregates, impossible to identify mics | Aggregates, impossible to identify mics | Aggregates, impossible to identify mics |
| **1 % (w/v)** | One population, ~130 µm | One population, ~130-150 µm | One population, around 120-140 µm | One population, around 105-120 µm |
| **1.5 % (w/v)** | One population, 90-120 µm | One population, around ~115µm | One population around 100-110 µm | One population around 110 125 µm |

Regarding chitosan with a DA of 16% (Table 6), it can be seen that at in the lowest chitosan concentration (0.5% (w/v)) there is no identification of microspheres, only aggregates are seen. Nevertheless, when increasing the concentration to 1% and 1.5% (w/v), the formation of spherical and structural homogeneous microspheres is observed throughout the conditions (chitosan concentration of 1 % and 1.5 % (w/v)). Similar diameters are also found amongst all the conditions, suggesting once again that flow rate is not a differentiating variable in this process.

Over viewing the previous results, a brief comparison between DA denotes an evident difference regarding the morphology of the chitosan microspheres, though similarities regarding the spherical shape are observed. Microspheres produced with chitosan of DA 6% seem to present a heterogeneous internal density, with the centre being darker and therefore denser than the periphery, while when produced with chitosan with DA of 16%, a homogeneous structure was formed. This may be related to the number of free primary amine groups ($-NH_2$) that confer chitosan its almost unique properties of being positively charged. Moreover, the nature and extent of ionic reactions were found to be sensitive to variables such as charge density of both electrolytes [98], in this case chitosan and TPP, leading to different types of the chitosan-TPP complexes. When chitosan solutions are dropped into TPP solutions, gelled spheres are formed instantaneously: negative ions in TPP solution diffuse into chitosan droplets interacting with the positive amines on the chitosan

chain. If more amines are available to react, which is the case of chitosan with DA of 6%, for the same amount of negative ions, TPP may have difficulty to penetrate the droplet of chitosan, thus forming an external wall preventing the centre to proper reticulate. For DA of 16%, since less amines are available, a graduate formation of inter and intra molecular interactions occurs, leading to the formation of a compact structure [98]. However, in order to better understand whether this difference is actually due to the different density inside the microspheres or due to the passage of the light through different thicknesses, cryosections would have to be performed and analyzed.

Moreover, and regarding size, a slightly decrease on the average diameter is noticed when increasing the DA from 6% (around 150 μm) to 16% (around 115 μm), perhaps due to less repulsion between chitosan chains with DA of 16%.
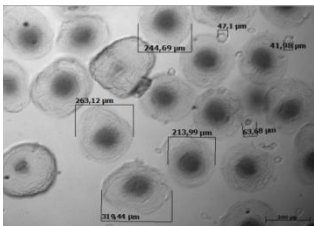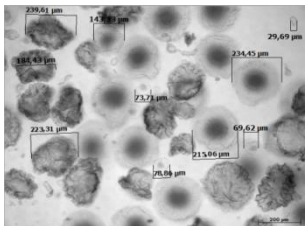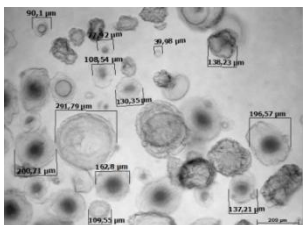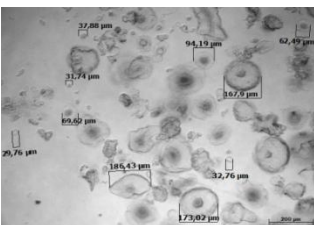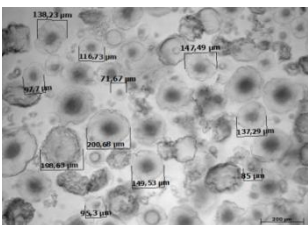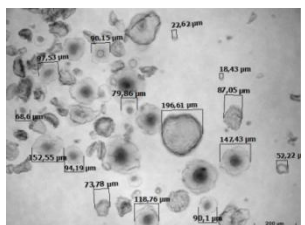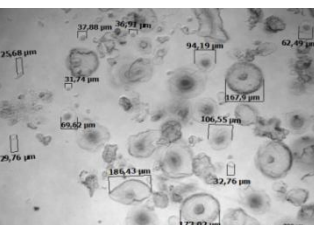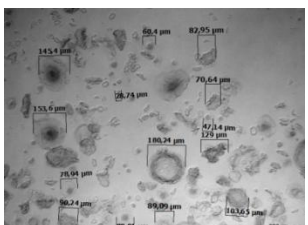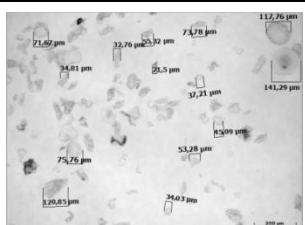
Overall, the chitosan concentration and the flow rate do not seem to have particularly influence on the production process using high voltage electrostatic system. However, chitosan DA appear to be an influent factor on the chitosan microspheres production process, changing their final characteristics. Since chitosan microspheres produced are bigger (115-150 μm) than desired, this system was considered not appropriate to continue the studies.

## 4.1.2  Co-axial air stream system

Regarding the droplet extrusion under co-axial air stream method, Tables 7, 8 and 9 gather the images obtained by optical microscopy for chitosan with DA of 6% at a concentration of 0.5%, 1% and 1.5% (w/v), respectively, for an increasing air stream pressure of 0.25, 0.4, 0.6 and 1 bar and flow rate of the syringe of 1, 10 and 20 mL/h. Tables 10, 11 and 12 represent the same analysis but for chitosan with DA of 16%.
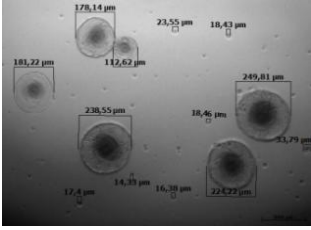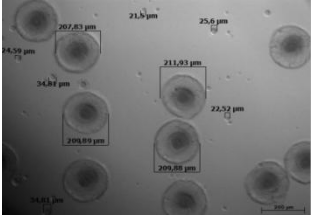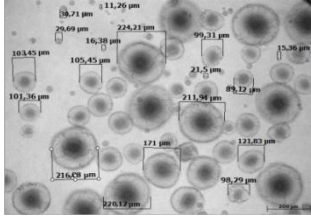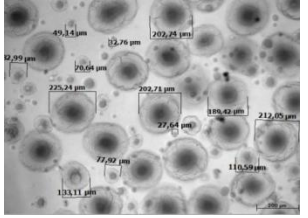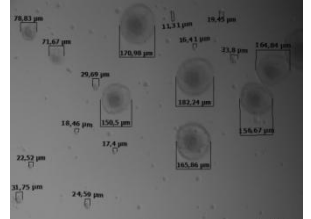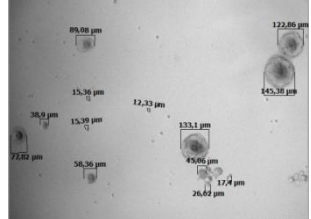
**Table 7 -** Chitosan microspheres images obtained by optical microscopy (scale bar 200 µm). Variation of the flow rate (20, 10, 1 mL/h) and air stream pressure (0.25, 0.4, 0.6 and 1 bar) regarding chitosan solution concentration of 0.5% (w/v)) and DA of 6% is shown. Average diameter is indicated below each condition.

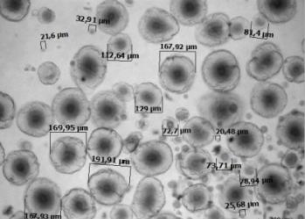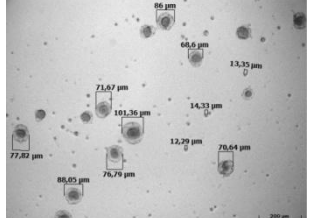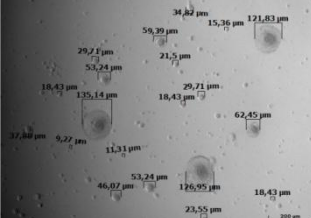| | | Flow rate | |
|---|---|---|---|
| 0.5% (w/v) | 1 mL/h | 10 mL/h | 20 mL/h |
| **0.25 bar** | ---- | Two populations: 50 µm and 260 µm | Three populations: 70 µm, 115 µm and 215 µm |
| **0.4 bar** | Several populations: 50, 150-200 and 300 µm | Several populations, mainly between 50 µm and 215 µm | Three populations: 20-60, 60-100 and 150-200 µm |
| **0.6 bar** | Several populations: 20-60, 100-150 and 200 µm | Several populations, mainly between 30 µm and 160 µm | Several populations, but few >150 µm |
| **1 bar** | Several sizes, 20-80 µm and few 120-140 µm | Several populations, mainly three: 15, 50 and 130 µm | ---- |

(Air stream pressure — row labels left margin)

Regarding chitosan solution concentration of 0.5% (w/v) (Table 7), microspheres with different morphologies and sizes can be observed throughout all the conditions evaluated. Chitosan microspheres present a more irregular shape, becoming less spherical when air stream pressure is increased. Moreover, different internal structures are observed even within the same condition, with microspheres presenting different roughness, shape and internal density and size.

Smaller chitosan microspheres are produced when increasing the air stream pressure, nevertheless a wide particle size distribution is observed even within the same condition. Despite obtaining particles with sizes closer to the 50 µm envisaged, at least another big population (>100 µm) is also observed.
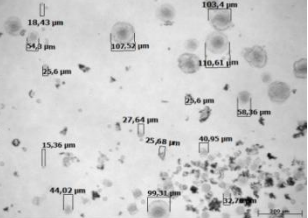
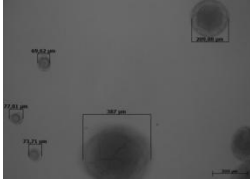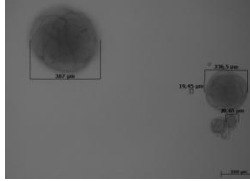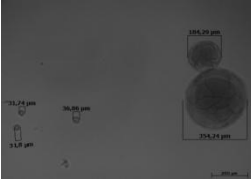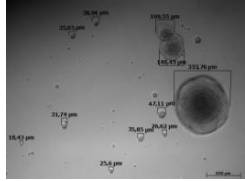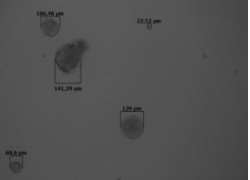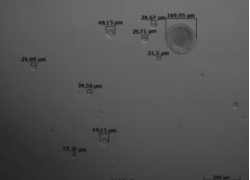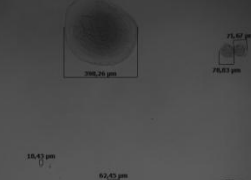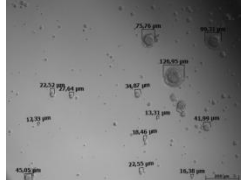**Table 8 -** Chitosan microspheres images obtained by optical microscopy (scale bar 200 μm). Variation of the flow rate (20, 10, 1 mL/h) and air stream pressure (0.25, 0.4, 0.6 and 1 bar) regarding chitosan solution concentration of 1 % (w/v)) and DA of 6% is shown. Average diameter is indicated below each condition.

| | Flow rate | | |
| --- | --- | --- | --- |
| 1 % (w/v) | 1 mL/h | 10 mL/h | 20 mL/h |
| **0.25 bar** | Several sizes, 10-30 μm (mainly) and 110-250 μm | ---- | ---- |
| **0.4 bar** | Two populations: 20-35 μm and ~200 μm | Three populations: 15-30, 100-150 and ~220 μm | Two populations: 30-70 μm and 210 μm |
| **0.6 bar** | Several sizes, 10-20 (higher amount), 70-100, 140-190 μm | Several sizes, 10-20 (higher amount),70-95 and 120-160 μm | Two populations: 20-75 μm and 130-170 μm |
| **1 bar** | Mainly two populations: 10-15 μm and 70-100 μm | Several sizes: higher amount of 10-20, some 35-60 and few 130 μm | Mainly small population of 13-25 μm, few 50-110 μm |

*Air stream pressure* (row label, left side)

Morphologically, 1% (w/v) chitosan microspheres are similar amongst conditions and within each particular condition, presenting a spherical shape with heterogeneous internal density, with the centre being darker, and therefore denser, than the periphery.

Regarding average diameter, a similar trend to the previous conditions can be observed: by increasing air stream pressure, smaller microspheres are produced. However, mainly one or two populations are identified, and despite a smaller population (10-30 μm) is observed throughout all the conditions, big microspheres are also observed.

**Table 9 -** Chitosan microspheres images obtained by optical microscopy (scale bar 200 µm). Variation of the flow rate (20, 10, 1 and 0.4 mL/h) and air stream pressure (0.25, 0.4, 0.6 and 1 bar) regarding chitosan solution concentration of 1.5% (w/v)) and DA of 6% is shown. Average diameter is indicated below each condition.

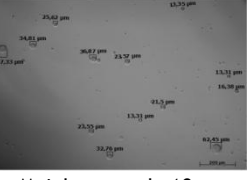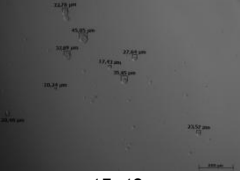| | Flow rate | | | |
|---|---|---|---|---|
| **1.5% (w/v)** | **0.4 mL/h** | **1 mL/h** | **10 mL/h** | **20 mL/h** |
| **0.25 bar** |  Several sizes, 20-90 (mainly), ~200 and 300-400 µm |  ~20 µm , 65-230 µm and 380-400 µm |  Several sizes, 30-50, ~170 and ~350 µm |  Several sizes, 18-50, 100-150 and ~330 µm |
| **0.4 bar** |  Several sizes: 20-70 µm, 120-140 µm and 200 µm (few) |  Mainly two populations: 20-50 µm and 160-200 µm |  Several sizes: 20-400 µm |  Several sizes, 10-30 and few, 60-120 and 200-290 µm |
| **0.6 bar** |  Mainly one population, 15-25 µm |  Several sizes, 15-40 µm and 90-230 µm |  20-40 µm and 80-115 µm. Some agglomerates were found |  Mainly three populations, 10-35, 70-120 and 220-280 µm |
| **1 bar** |  Mainly ~15 µm, with some linked microspheres |  Mainly around ~10 µm, some between 25-60 µm |  15-40 µm |  Mainly around 10-20 µm, with few ~130 µm |

*Air stream pressure*

When increasing the chitosan concentration to 1.5% (w/v), microspheres seem to present a homogeneous distribution of the chitosan, reducing the differences concerning their internal structure. A good sphericity is also observed throughout all the conditions.

Regarding size distribution, and despite the fact that the influence of the air stream pressure remains the same as in the previous set of conditions, smaller microspheres are produced. At 0.25 bar, though, bigger microspheres are found when comparing to the ones identified with chitosan of 0.5% and 1% (w/v).

Overall, though the air stream pressure seems to have the same effect regardless the chitosan concentration, leading to the production of smaller and less spherical microspheres, differences are observed when the chitosan concentration is altered, particularly from 0.5% to 1% and 1.5% (w/v). When increasing the latter variable, sphericity of microspheres is
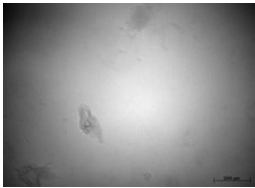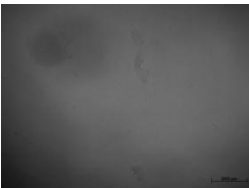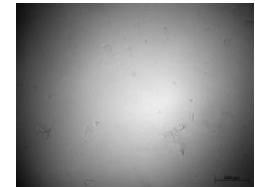
increased, presenting also a narrower size distribution, with some populations within the range aimed.

The irregularity of the particles may not be, however, a disadvantageous characteristic, since it is not mandatory that the particles wished to be obtained actually have a spherical shape. A rough surface may also be beneficial, since the surface contact area is increased.

Even though some conditions have chitosan microspheres within the aimed size ranged, the separation of those populations could reduce the production efficiency, since a high amount of chitosan would be lost.

As previously referred, chitosan with DA of 16% was also used to produce microspheres in this system.
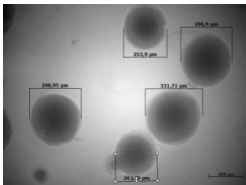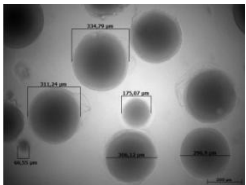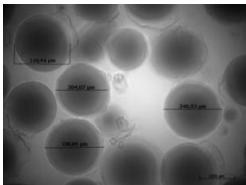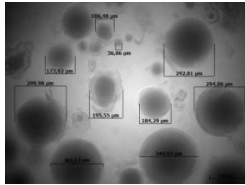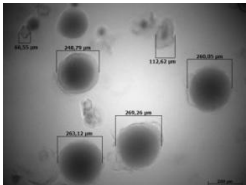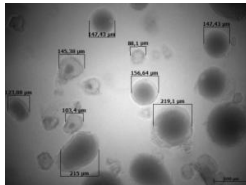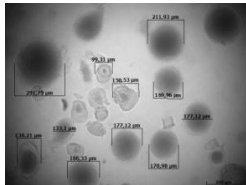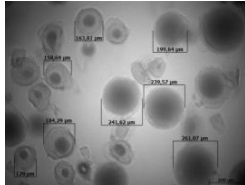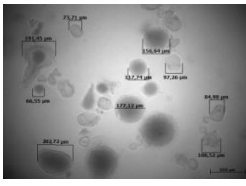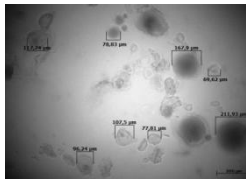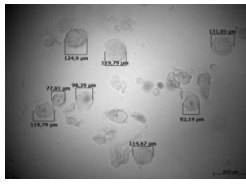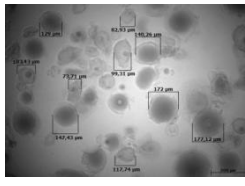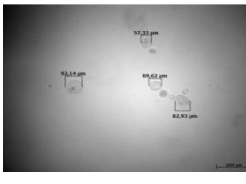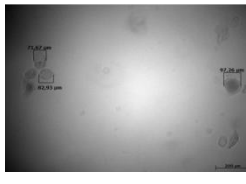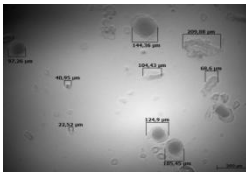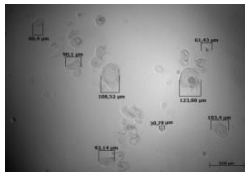
**Table 10 -** Chitosan microspheres images obtained by optical microscopy (scale bar 200 µm). Variation of the flow rate (20, 10, 1 and 0.4 mL/h) and air stream pressure (0.25, 0.4, 0.6 and 1 bar) regarding chitosan solution concentration of 0.5% (w/v)) and DA of 16% is shown. Average diameter is indicated below each condition.

| | | Flow rate | | |
|---|---|---|---|---|
| 0.5% (w/v) | 0.4 mL/h | 1 mL/h | 10 mL/h | 20 mL/h |
| 0.25 bar | | | | |
| 0.4 bar | | | | |
| 0.6 bar | | | | |
| 1 bar | | | | |



Regarding DA of 16%, at 0.5% (w/v) chitosan concentration (Table 10), the same outcome as obtained in the high voltage electrostatic system was obtained: no identifiable microspheres are seen, only aggregates. This may suggest that the conjugation of a low chitosan concentration and a smaller number of free amines seems to unable the formation of a microsphere.
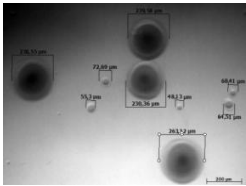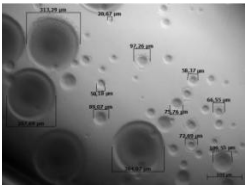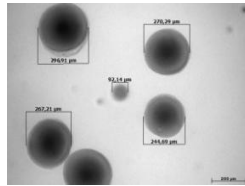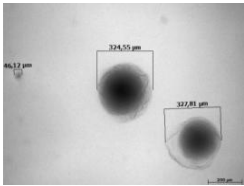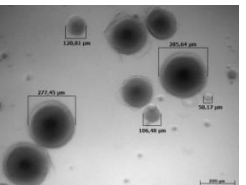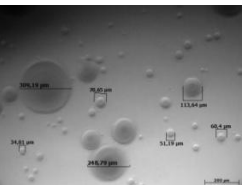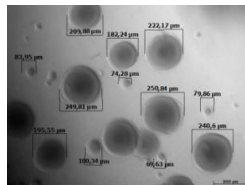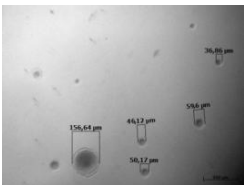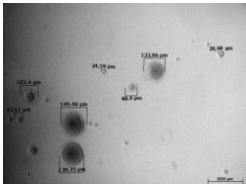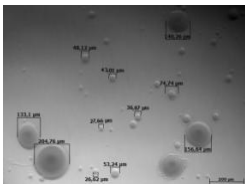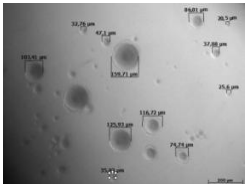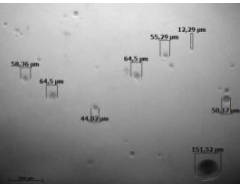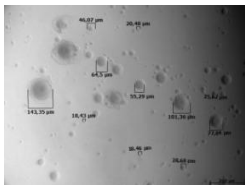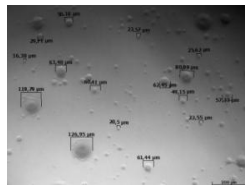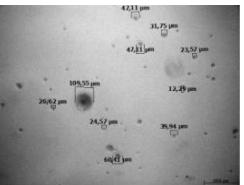
When increasing the concentration to 1% and 1.5% (w/v), individualized microspheres are produced (Table 11 and Table 12).

**Table 11 -** Chitosan microspheres images obtained by optical microscopy (scale bar 200 µm). Variation of the flow rate (20, 10, 1 and 0.4 mL/h) and air stream pressure (0.25, 0.4, 0.6 and 1 bar) regarding chitosan solution concentration of 1% (w/v)) and DA of 16% is shown. Average diameter is indicated below each condition.

| | Flow rate | | | |
|---|---|---|---|---|
| 1% (w/v) | 0.4 mL/h | 1 mL/h | 10 mL/h | 20 mL/h |
| 0.25 bar |  Mainly two populations, 250-300 µm (higher amount) and 90-150 µm |  Mainly two populations, higher amount of ~300 µm, fewer 120-190 µm |  Mainly ~300-340 µm, few small ones |  Mainly two populations: 250-320 and 100-180 µm |
| 0.4 bar |  Mainly two populations, 70-100 µm and 230-250 µm (higher amount) |  Several sizes, 90-160 µm and 200-250 µm |  Several sizes, 70-120 µm and 170-250 µm |  Two populations, 120-160 µm and 240-260 µm |
| 0.6 bar |  Several sizes, 150-200 µm and 60-100 µm |  Several sizes 160-210 µm and 70-100 µm |  Several sizes, few 70-160 µm |  Several sizes, 120-170 µm and agglomerated 50-100 µm |
| 1 bar |  Similar size, 55-90 µm |  One population, 70-100 µm with few ~170 µm |  Several sizes, 20-50 µm and 100-150 µm |  Several sizes: 50-130 µm |

(Air stream pressure — vertical axis label)

At 1% (w/v) chitosan concentration (Table 11), chitosan microspheres present a different distribution regarding size and shape between conditions. At 0.25 bar the microspheres are spherical and internally similar, however by increasing the air stream pressure the microspheres become smaller, more irregular and with different internal structures. The flow rate does not particularly seem to influence size or morphology.

**Table 12 -** Chitosan microspheres images obtained by optical microscopy (scale bar 200 μm). Variation of the flow rate (20, 10, 1 and 0.4 mL/h) and air stream pressure (0.25, 0.4, 0.6 and 1 bar) regarding chitosan solution concentration of 1.5% (w/v)) and DA of 16% is shown. Average diameter is indicated below each condition.

| | | Flow rate | | |
|---|---|---|---|---|
| 1.5% (w/v) | 0.4 mL/h | 1 mL/h | 10 mL/h | 20 mL/h |
| 0.25 bar | Several sizes: 40-75 μm, 230-260 μm and 300-350 μm | Two populations: 50-100 μm and 280-310 μm | Mainly 250-300 μm | Several populations, ~320 μm, ~100 μm and ~40 μm |
| 0.4 bar | Several sizes, 30-80 μm, 100-150 μm and 200-250 μm | Several sizes, mainly 35-80 μm, 100-150 μm and 200-250 μm | Several sizes, mainly 55-80 μm and 180-250 μm | Mainly small ones 35-65 μm with few 155-250 μm |
| 0.6 bar | 20-70 μm and 100-140 μm | Several sizes, mainly 20-75 μm and 100-190 μm | Two populations: 20-40 μm and 80-150 μm | Mainly small ones 20-70 μm, but few ~155 μm |
| 1 bar | Mainly 10-20 μm and 30-70 μm | 15-30 μm (higher amount), 50-80 μm and 100-140 μm | Two populations: 20-30 μm and 60-125 μm | Mainly small ones: 15-30 μm, 40-80 μm and 90-110 μm (few) |

*Air stream pressure* (row label spanning the table vertically on the left)

By increasing even more the chitosan concentration to 1.5% (w/v), smaller and spherical microspheres are produced throughout all the conditions. While the effect of flow rate is not so evident, the effect of the air stream pressure is relevant to the structure of the microspheres: at higher pressures smaller microspheres are formed, with spherical shape and similar internal structure. A wide distribution regarding sizes is still observed, with a smaller population present in all conditions.

Regarding the influence of chitosan DA, the same trend as observed with high voltage electrostatic system is observed: chitosan microspheres with DA of 16% present a consistent structure and generally are more spherical and structurally homogeneous than chitosan

microspheres produced with chitosan of 6% DA. The latter leads to more disrupted, heterogeneous microspheres, although the size does not vary significantly.

Air stream pressure is a variable that also seems to influence the characteristics of the chitosan microspheres produced by co-axial air stream system, where smaller particles are produced when air pressure is increased. This trend is observed in all chitosan concentrations evaluated and may be related to the unstable formation of the microspheres at higher air pressures, which also leads to the production of more irregular particles.

OM qualitative screening of chitosan microspheres produced by co-axial air stream system suggested some conditions with diameters within the aimed range of 50 μm. Since microspheres with lower DA are expected to be more mucoadhesive and bind more bacteria, preference was given to chitosan with DA of 6%. Therefore, a deeper analysis was conducted using the IN Cell Analyzer high-throughput imaging and high-content analysis system. Chitosan microspheres produced with chitosan concentration of 1% and 1.5% (w/v) and with DA of 6% were selected and their size distribution is shown in Table 13 and 14, respectively. Histograms shown are the result of the steps referred in section 3.

Image acquisition by IN Cell Analyzer high-throughput microscopy brings several advantages over OM, mainly due to the automated screening of the wells, therefore avoiding the manual arrangement of the plate. The autofocus option is also a valuable tool, fastening the acquisition process; however, it works better if a black plate is used. If using white plates, images on the periphery of the well are not collected correctly and a segmentation of the well needs to be done, applying the autofocus option to each area.

It is important to notice that although most of the microspheres are target as individualized ones, aggregates and overlapping microspheres are considered as one microsphere, thus wrongly contributing to the average diameter of the condition. Therefore, although this software allows a faster and more comprehensive analysis, it is difficult to assure that the created protocol targets each one and only microspheres. This problem could be overcome if a relative small amount of microspheres is assessed and if they are not aggregated, therefore detecting each microsphere as an individual. Indeed, despite the valuable imaging system, data analysis may be a time consuming process until de protocol is defined.

**Table 13** – Size distribution of chitosan microspheres produced with chitosan concentration of 1% (w/v) and DA of 6%. Data obtained by IN Cell Analyzer analysis software.

| 1% (w/v) | 1 mL/h | 10 mL/h | 20 mL/h |
|---|---|---|---|
| 0.25 bar |  | --- | --- |
| 0.4 bar |  |  |  |
| 0.6 bar |  |  |  |
| 1 bar |  |  |  |
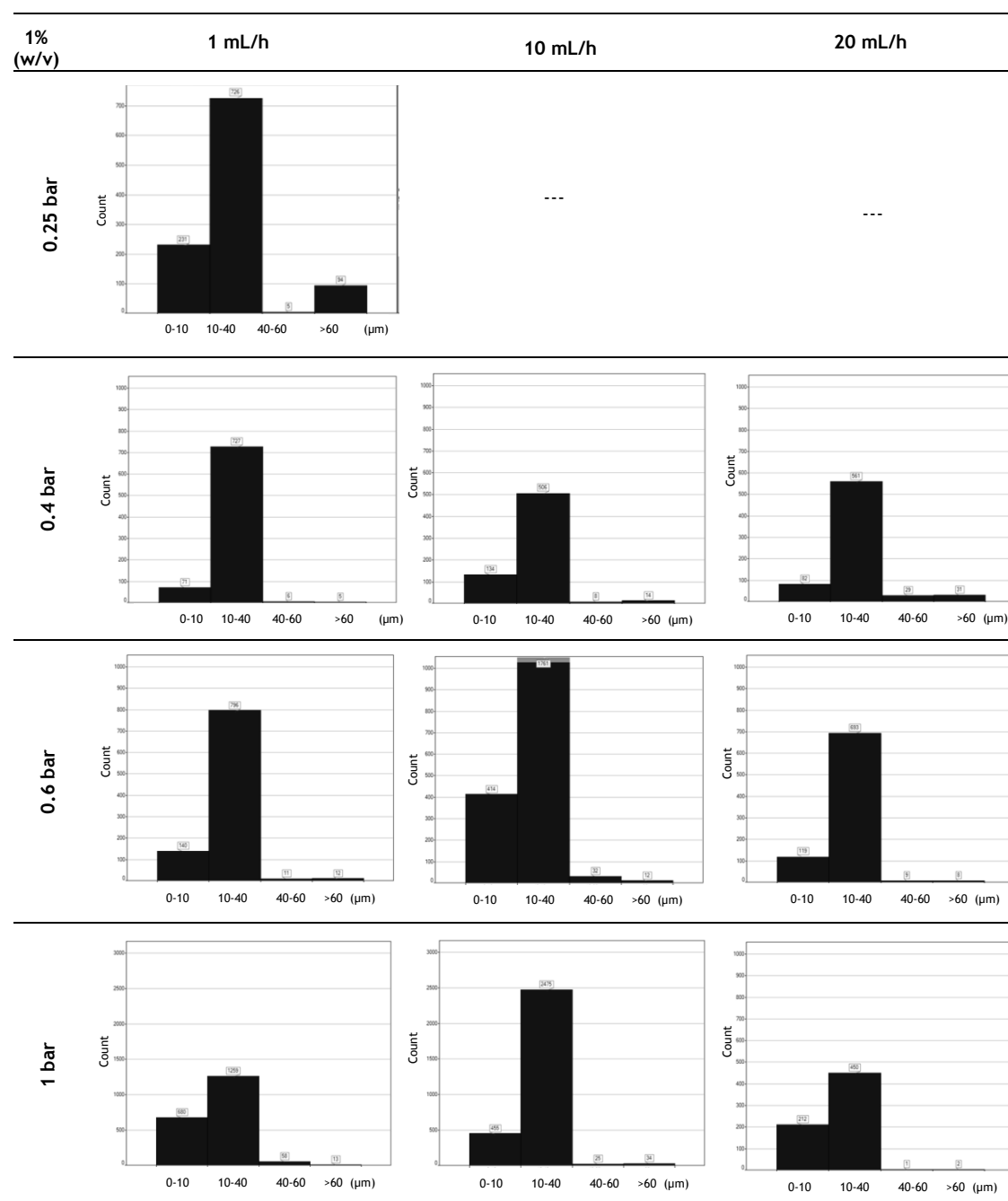
Despite not being very evident, IN Cell Analyzer results do correlate with the trend observed in OM images. By increasing the air stream pressure, the number of microspheres bigger than 60 µm seems to decrease while the number within the range 10-40 µm seems to increase. A population of 0-10 µm can be identified in all the evaluated conditions. Moreover, the amount of smaller microspheres, especially from 10-40 µm, is always higher than the remaining size ranges.

**Table 14 -** Size distribution of chitosan microspheres produced with chitosan concentration of 1.5% (w/v) and DA of 6%. Data obtained by IN Cell Analyzer analysis software.
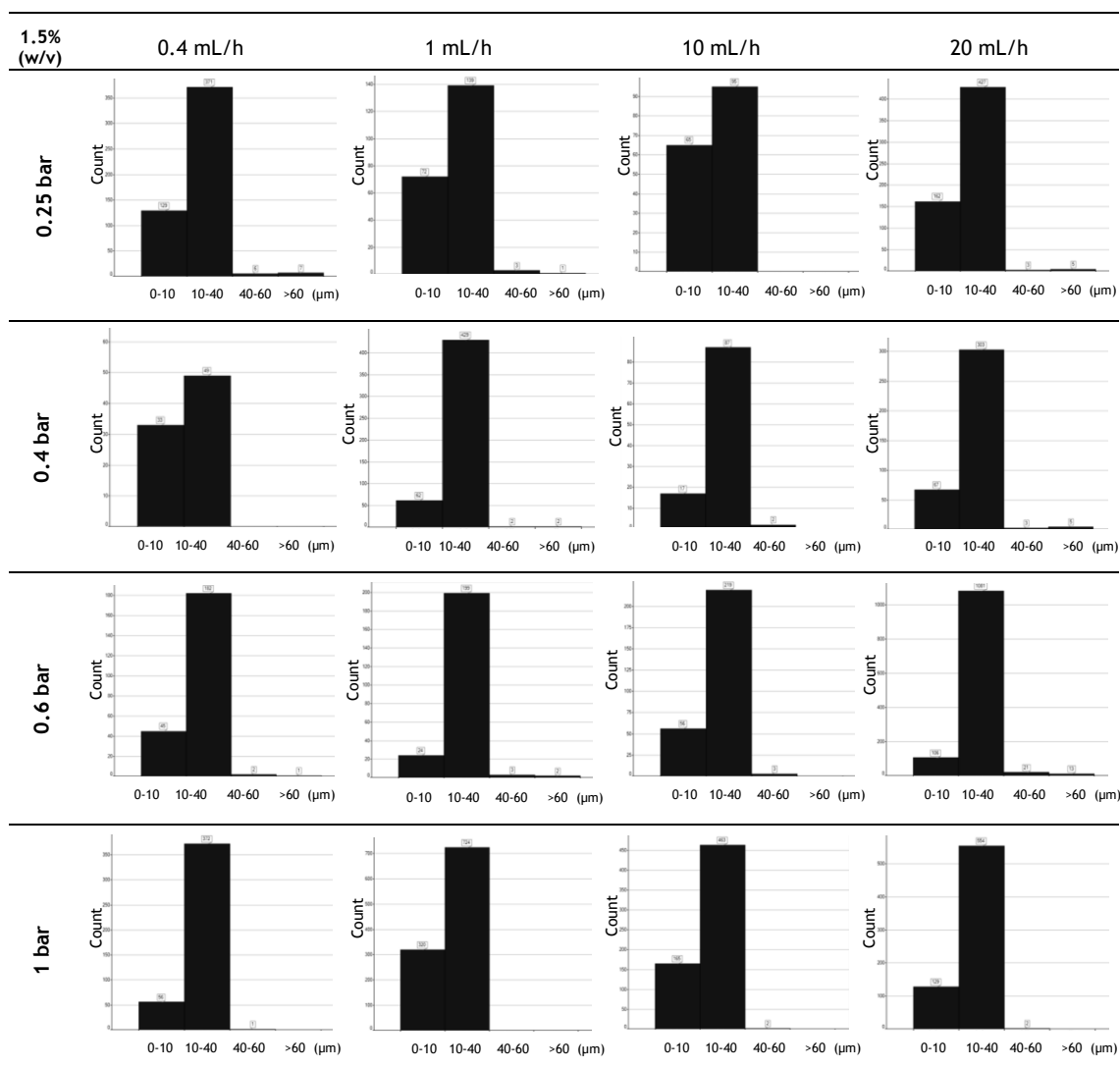


Regarding 1.5% (w/v) chitosan concentration, the size range described with OM presents some similarities with the data shown in Table 14. It can be seen that generally by increasing the air stream pressure, the amount of chitosan microspheres with relative bigger sizes are reduced, dominating the range size of 10-40 µm in all conditions. However not many microspheres bigger than 60 µm are found in the lowest air stream pressure, contrary to the OM results.
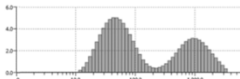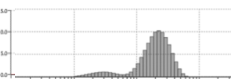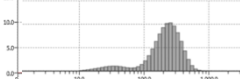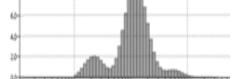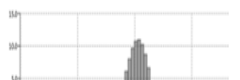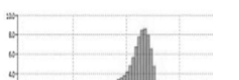
The fact that data obtained by the IN Cell Analyzer does not exactly correlate with the average diameter determined by OM is somehow expected. First, regarding the latter method, only few microspheres were assessed, and therefore the reduced number does not allow drawing statistically significant conclusions regarding size. Though it might indicate the average range of diameters, it is not an absolute data. Furthermore, the way average diameters are calculated in both methods is different. While in OM a straight line is manually draw horizontally from one point to the other of the microsphere, the IN Cell Analyzer software determines the average diameter as the mean of all internal diameters perpendicular to the maximum centre line through the microsphere, automatically.

Moreover, in the latter equipment microspheres on the border of each image are automatically excluded, although this may not have such influence, because the number of excluded microspheres may be distributed over the size range.

## 4.1.3 Aerodynamically driven system

Finally, results of microspheres produced using the aerodynamically driven system are reported. Focusing on the DA of 6%, a screening was performed to several conditions, varying the nozzle diameter of the equipment, air stream pressure and flow rate for two chitosan concentrations, 0.5% (Table 15) and 1% (w/v) (Table 16). OM analysis was not carried on since Mastersizer equipment presents particle size distributions in a faster and less time consuming way.

**Table 15** – Mastersizer analysis of size distribution of chitosan microspheres (DA 6%) produced by aerodynamically driven system with nozzle diameter of 0.25 mm. Histogram (relating size classes and volume (%)) and corresponding volume percentiles (Dv10, Dv50 and Dv90) are shown. XX axis represents the size classes (µm - 10, 100 and 1000 marks are shown).

| Nozzle 0.25 mm | | 0.25mL/min | 0.33mL/min | 0.5mL/min | 1mL/min |
|---|---|---|---|---|---|
| **0.5 % (w/v)** | 415 mBar | ---- | ---- |  Dv10 = 26 µm<br>Dv50 = 81.2 µm<br>Dv90 = 1390 µm | ---- |
| | 525 mBar | Agglomerates | ---- |  Dv10 = 20.4 µm<br>Dv50 = 55.2 µm<br>Dv90 = 331 µm |  Dv10 = 23.3 µm<br>Dv50 = 51.0 µm<br>Dv90 = 224 µm |
| **1 % (w/v)** | 255 mBar |  Dv10 = 66.8 µm<br>Dv50 = 203 µm<br>Dv90 = 361 µm | ---- |  Dv10 = 70.7 µm<br>Dv50 = 222 µm<br>Dv90 = 387 µm |  Dv10 = 26.7 µm<br>Dv50 = 115 µm<br>Dv90 = 239 µm |
| | 415 mBar | ---- | ---- |  Dv10 = 28.4 µm<br>Dv50 = 104 µm<br>Dv90 = 178 µm | ---- |
| | 525 mBar |  Dv10 = 41.2 µm<br>Dv50 = 159 µm<br>Dv90 = 305 µm |  Dv10 = 33.4 µm<br>Dv50 = 101 µm<br>Dv90 = 240 µm |  Dv10 = 23.9 µm<br>Dv50 = 79.6 µm<br>Dv90 = 145 µm |  Dv10 = 34.2 µm<br>Dv50 = 145 µm<br>Dv90 = 216 µm |

Data collected by the Mastersizer includes the histogram with the volume weighted particle size distributions and the percentiles regarding the maximum particle size for a given percentage volume of the sample (Dv10, Dv50 and Dv90). Overall, this information suggests that a wide size distribution (20-400 μm) can be obtained by aerodynamically driven system through variation of the different parameters. The percentage of particles smaller than 20 μm is small, and mostly two populations are found in each condition, with one generally in higher amount.

However, by increasing the air pressure (from 415 to 255 mBar and 525 mBar), a decrease in the Dv50 is observed for both concentrations, particularly at 1% (w/v) chitosan concentration (~200 μm), where a clear shift to the left is seen on the histogram. Regarding the effect of the flow rate, a pattern is not found between the conditions under the same pressure, suggesting that this parameter does not influence the chitosan microspheres production considerably.

When comparing chitosan concentrations, it can be observed that at 0.5% (w/v) chitosan particles present smaller sizes, with a Dv50 of around 50 μm at the highest air stream pressure. At 0.5 mL/min two clear and defined populations can be observed for both evaluated pressures. By increasing concentration to 1% (w/v), it can be seen an increase on the Dv50 values throughout all the samples.

**Table 16 -** Mastersizer analysis of size distribution of chitosan microspheres produced by aerodynamically driven system with nozzle diameter of 0.5 mm. Histogram (relating size classes and volume (%)) and corresponding volume percentiles (Dv10, Dv50 and Dv90) are shown. XX axis represents the size classes (μm - 10, 100 and 1000 marks are shown).

| Nozzle 0.5 mm | 0.25 mL/min | 0.33 mL/min | 0.5 mL/min | 1.5 mL/min |
|---|---|---|---|---|
| 255 mBar | ---- | ---- | ---- |  Dv10 = 41.7 μm<br>Dv50 = 167 μm<br>Dv90 = 369 μm |
| 525 mBar |  Dv10 = 52.2 μm<br>Dv50 = 208 μm<br>Dv90 = 495 μm |  Dv10 = 35.6 μm<br>Dv50 = 157 μm<br>Dv90 = 310 μm |  Dv10 = 36.1 μm<br>Dv50 = 157 μm<br>Dv90 = 322 μm | ---- |

(1 % (w/v))
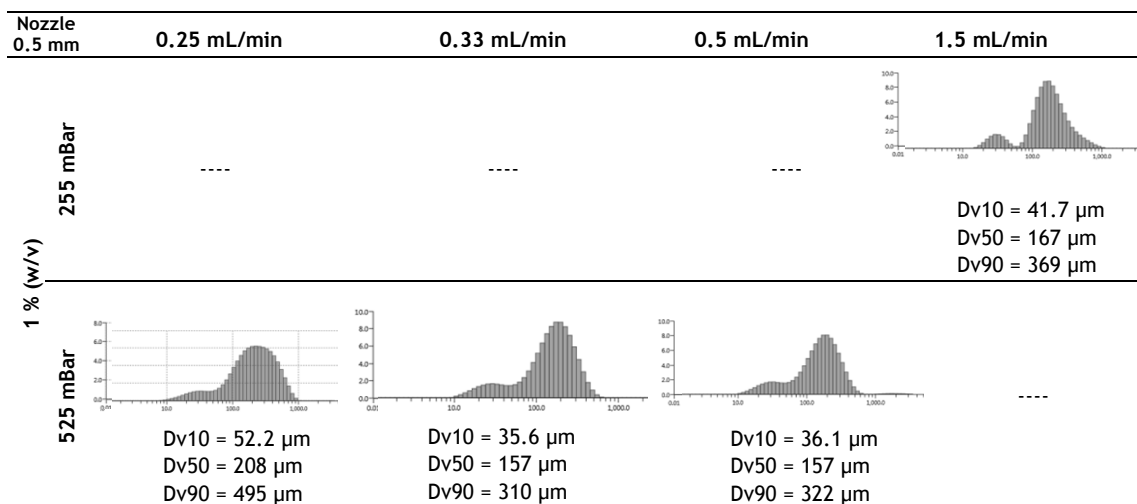
Altering the nozzle diameter of the equipment seems to be a preponderant factor, since at 1% (w/v) chitosan concentration is verified a significant increase on the particles diameter when comparing with the same concentration but with the smaller nozzle diameter (0.25 mm). A clear shift to the right on the histogram is observed, showing an increase in all the percentiles, for both low (255 mBar) and high (525 mBar) air pressures.

Microspheres produced with higher pressure (525 mBar) and nozzle diameter of 0.25 mm, and therefore smaller, were further used for size and morphology analysis in IN Cell Analyzer imaging system (Table 17 and 18).

**Table 17** – IN Cell Analyzer size distribution of chitosan microspheres (DA 6%) produced in the aerodynamically driven system with 0.25 mm nozzle under higher pressure (525 mBar).

| Nozzle 0.25mm | 0.25mL/min | 0.33mL/min | 0.5mL/min | 1mL/min |
|---|---|---|---|---|
| 0.5 % (w/v) 525 mBar | Agglomerates | ---- |  |  |
| 1 % (w/v) 525 mBar |  |  |  |  |
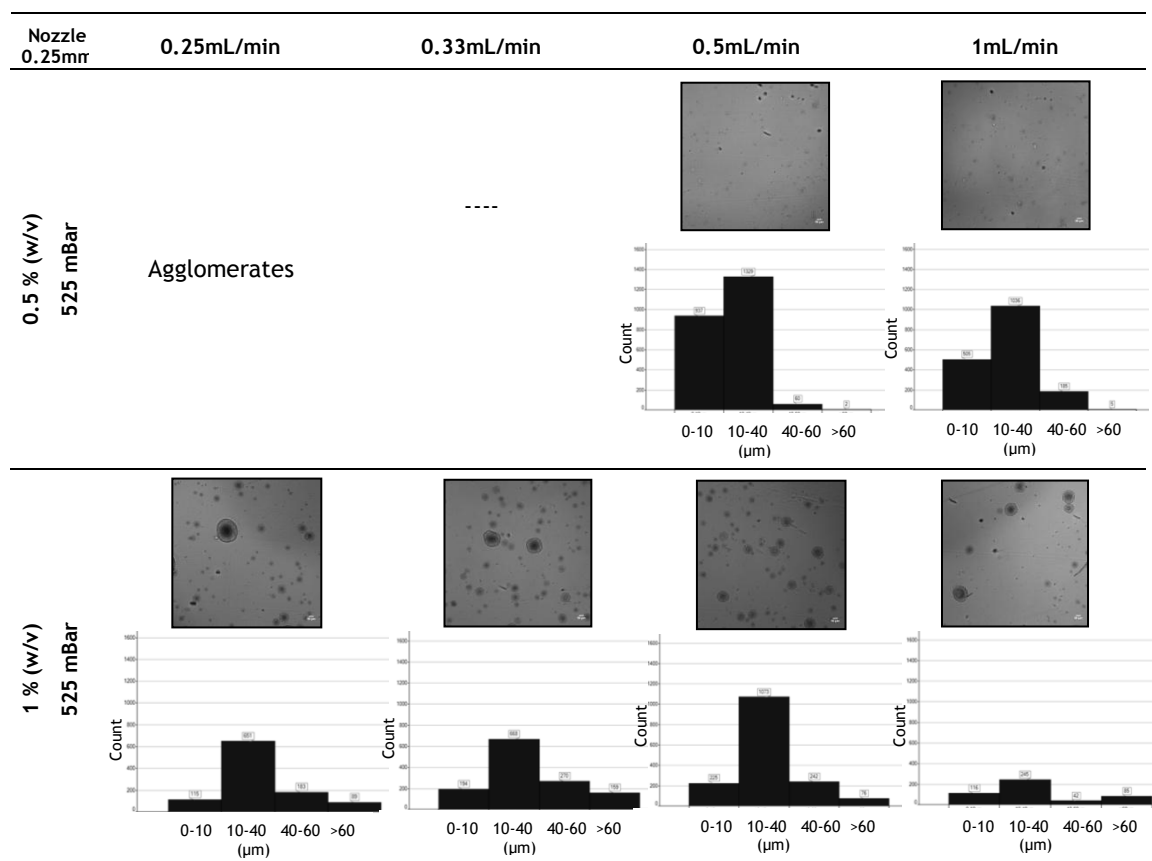
The effect of the chitosan concentration on the characteristics of the chitosan microspheres produced is once again observed with the IN Cell Analyzer high-throughput microscope. At the highest pressure (525 mBar) and with the 0.25 mm nozzle, chitosan particles present a bigger size when a higher chitosan concentration is used (1% (w/v)). It can be observed that with 0.5% (w/v) chitosan particles range mainly between 0-40 µm, with some amount between 40-60 µm. When increasing the concentration to 1% (w/v), the trend observed on the IN Cell Analyzer analysis is repeated and an increase on the average size of the particles is observed: the number of particles between 0-40 µm is reduced, increasing the number of particles within the range 40-60 µm and >60 µm. Flow rate 0.5 mL/min at 525 mBar represents the condition with the smaller Dv50, trend proven by this analysis as well.

Differences regarding chitosan microspheres morphology are also evident, being the microspheres produced with 1% (w/v) chitosan concentration more spherical and homogeneous than the ones produced using the low concentration.

When comparing the results from both IN Cell Analyzer and Mastersizer analysis, a correlation can be established. Concerning nozzle 0.25 mm and chitosan concentration of 1% (w/v), at 0.33 mL/min the Dv50 is 101 µm, meaning that 50% of the particles have a size below that value. This also means that more particles would be represented in the graph in the range 40-60 µm and > 60 µm than in the 0.5 mL/min condition, where the Dv50 is 79.6 µm, and therefore higher amount of particles are smaller. When comparing nozzle 0.5 mm condition for the same chitosan concentration and flow rate values, both graphs are similar as well as the percentiles. At 0.33 and 0.5 mL/min the Dv50 is 157 µm, with only 10% of the particles smaller than 35.6 µm and 36.1 µm, respectively. This average sizes would be within

the size range of 0-10 and 10-40 μm in the Mastersizer graphs, but in a smaller amount than it actually is. Differences regarding both analyses may be explained given the fact that though it is possible to convert particle size data from one type of distribution to another, this requires certain assumptions about the form of the particle and its physical properties. Therefore, a volume weighted particle size distribution measured using image analysis may not necessarily agree exactly with a particle size distribution measured by laser diffraction.

Nevertheless, the data collected by both methods is complementary, with the IN Cell Analyzer high-throughput imaging system having a particular relevance regarding assessment of chitosan microspheres morphology.

The optimization process of chitosan microspheres production narrowed the options and allowed identifying the aerodynamically driven system (Var J30), in conjugation with the parameters specified on Table 18, as the suitable one for the production of 50 μm diameter chitosan microspheres. This system was preferred over co-axial air stream system, mainly due to the speed of the production process.

**Table 18** – Set of parameters applied in encapsulation system Var J30 for production of 50 μm chitosan microspheres.

| | |
|---|---|
| **Degree of Acetylation** | 6% |
| **Chitosan concentration** | 0.5% (w/v) |
| **Nozzle** | 0.25 mm |
| **Flow rate** | 0.5 mL/min |
| **Air pressure** | 525 mBar |

The average size and the size distribution of the chitosan microspheres were determined by different methods, which results are shown in Figure 8.
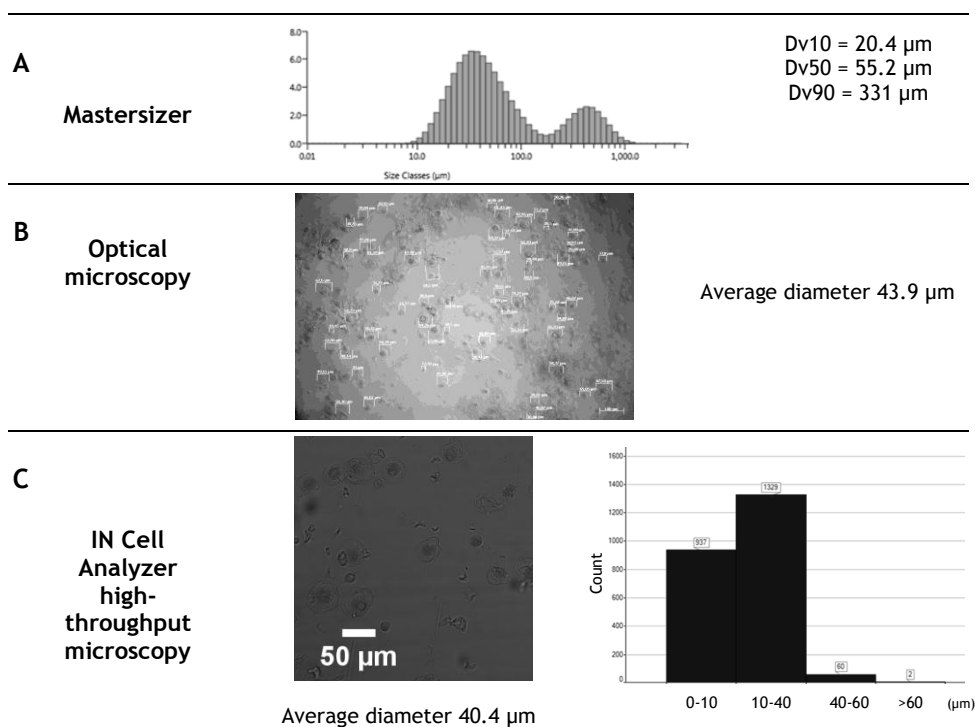


**Figure 8** – Size distribution of chitosan microspheres in TPP after ionotropic gelation evaluated by Mastersizer (A), optical microscopy (B, scale bar 100 μm) and IN Cell Analyzer high-throughput microscopy (C, scale bar 50 μm).

Particle size distribution was firstly collected based on a laser diffraction technique (Figure 8, A), where 50% of the particles were found to have a size below 55.2 μm. Optical microscopy was also used to assess chitosan microspheres morphology (Figure 8, B) and images were used to manually evaluate the average diameter of the microspheres (43.9 μm). Moreover, images obtained by IN Cell Analyzer high-throughput microscopy allowed a manual measurement of the average diameter of the microspheres (40.4 μm) (Figure 8, C); through an automatic analysis the majority of the microspheres were placed within the 10-40 μm range.

Despite the different characterization techniques, the average sizes obtained were similar.

## 4.2 Genipin crosslinking

Being a relevant and determinant factor for chitosan microspheres properties regarding stability in acidic conditions and mucoadhesion, the crosslinking degree of chitosan microspheres was evaluated by time-lapse using fluorescence microscopy.

Figure 9 shows the fluorescence behaviour of the first two hours of chitosan microspheres incubation with 10 mM genipin. Previous studies have determined 10 mM of genipin as the adequate concentration, since the reaction time required for crosslinking was shorter and with higher fluorescence levels when compared to 1 mM of genipin [108].
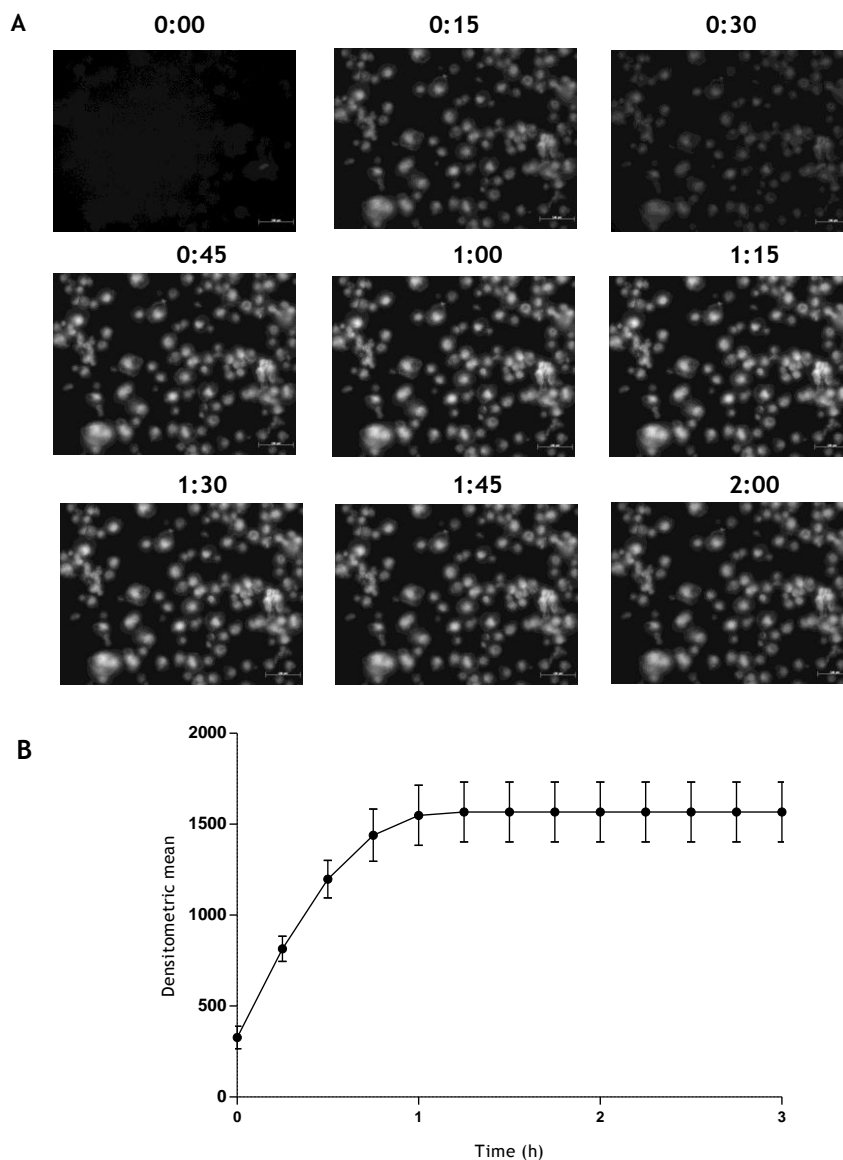
**Figure 9 -** Fluorescence microscopy images of chitosan microspheres crosslinked with 10 mM genipin (A). The time of crosslinking (h) is represented on the top of each image, scale bar 100 μm. Crosslinking kinetic of chitosan microspheres in the presence of 10 mM genipin (B)

Results have shown an increase of fluorescence intensity with crosslinking time for the genipin concentration tested (10 mM), reaching a plateau after approximately 1h15min of reaction.

Since chitosan mucoadhesive properties are dependent of the amount of primary amines available in the chitosan chain, the crosslinking process must be controlled. For that reason, 45 min was established as enough time to assure that the microspheres do not dissolve in acidic conditions, while maintain their mucoadhesive properties conferred by the free amines. As such, after crosslinking of chitosan microspheres genipin 10 mM for 45 min, they were submitted to lyophilisation.

Figure 10 shows the morphology of the microspheres before (A) and after (B) the crosslinking and lyophilisation (followed by hydration).
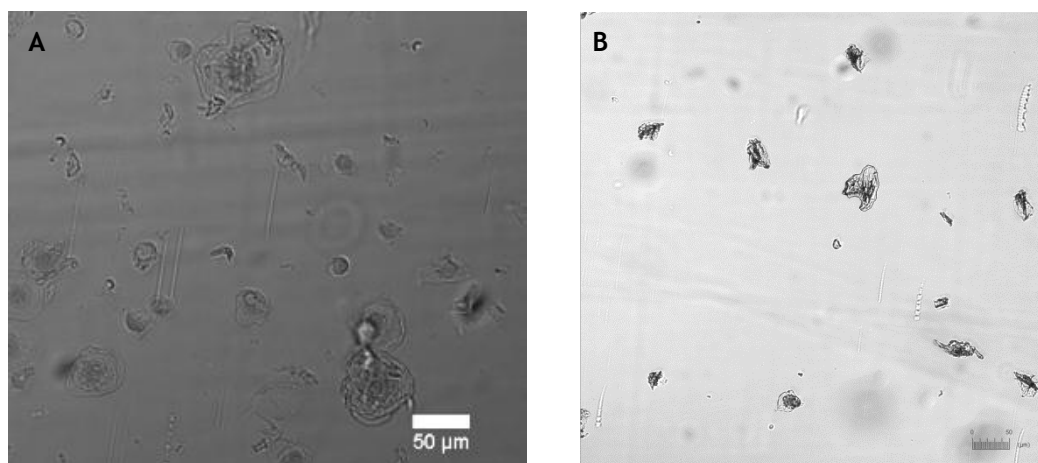
**Figure 10 -** IN Cell Analyzer images of chitosan microspheres before (A) and after (B) crosslinking and lyophilisation and hydration. Scale bar 50 µm.

Images obtained by IN Cell Analyzer high-throughput microscopy revealed an evident change in chitosan microspheres morphology, with lyophilised microspheres presenting a rather irregular, rough structure, with reduced sphericity.

An intensive characterization was performed by IN Cell Analyzer, with a strict analysis on the Spotfire™ DecisionSite™. Average diameter, maximum chord, form factor and area are some of the parameters measured, graphically represented below.
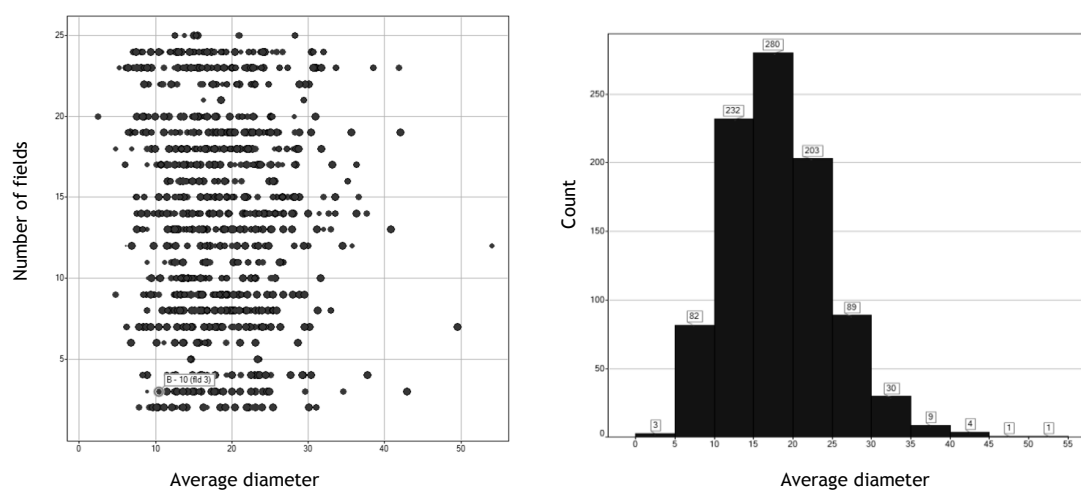


**Figure 11** – Average diameter distribution of the individualized chitosan microspheres, after lyophilisation.

Both graphs on Figure 11 represent similar data concerning size distribution of chitosan microspheres, although the left graph shows the distribution throughout the 25 fields of the well and the right graph the amount of microspheres within each range of sizes. Average diameter is calculated as the mean internal distance perpendicular to the maximum curved chord, which is the maximum centre line through a target. It can be acknowledged in both graphs that size varies from approximately 5 to 60 µm, with the higher amount being concentrated around 10-30 µm. Once again, the size of the black dots corresponds to the form factor associated to each microspheres. When comparing the average size before and after liophilisation, a decrease is observed from 50 µm to around 20 µm.
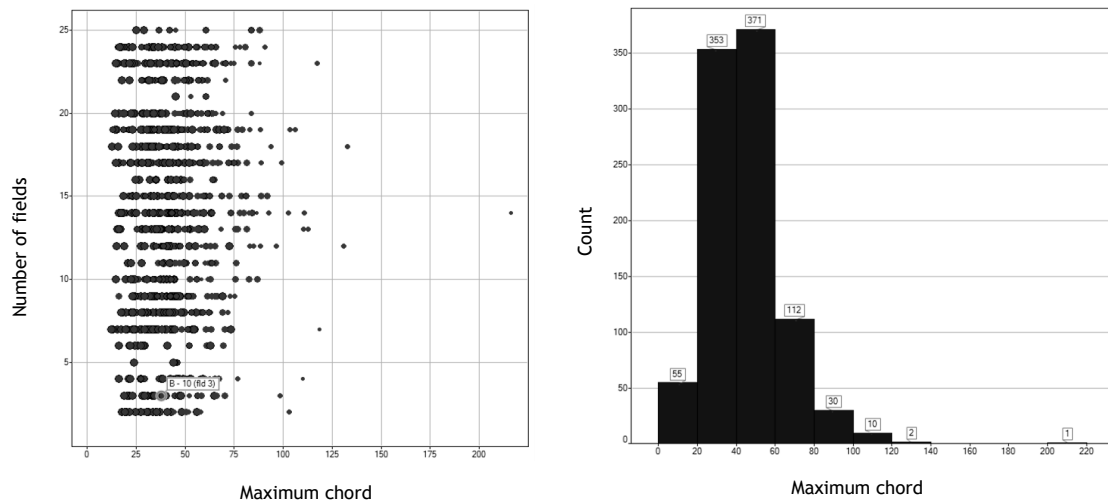
**Figure 12** – Maximum chord of chitosan microspheres, after lyophilisation.

Regarding the morphology, it was observed that the liophilisation process led to a change in the shape of the spheres, turning them more irregular and similar to particles. Because the particles are not spherical, average diameter may not provide all information regarding microsphrees size, and therefore maximum chord may be a valuable information as well. Based on Figure 12, most particles present a maximum chord of 50 µm despite ranging between 40 and 60 µm, which corresponds to the expected average diameter.
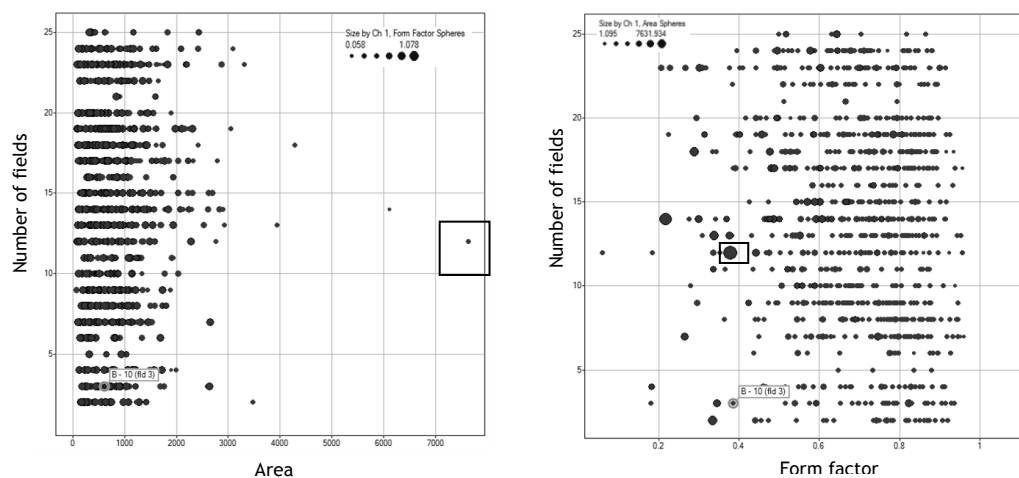


**Figure 13** – Area (left graph) and form factor (right graph) of each chitosan microsphere, after lyophilisation.

Each black dot corresponds to a single chitosan microsphere, throughout the 25 fields taken of each well. Regarding the graph on the left, the area of each microsphere is represented on the XX axis, revealing that most of chitosan microspheres present an area inferior to 1000 µm$^2$. However, the size of each black dot also correlates to its form factor: smaller black dots possess a smaller value regarding form factor, and therefore are more irregular, while bigger dots correspond to rounder microspheres. This can be also correlated to the graph on the right, which shows the distribution of the chitosan microspheres regarding their form factor. In this case, the size of the black dots correlates to the area of the actual microspheres. The selected dot on both graphs corresponds to the same microsphere.

As such, chitosan microspheres present not only a different morphology but also a decrease in the average diameter when comparing to microspheres before lyophilisation. Chitosan microspheres present a more irregular structure, with an average diameter around 20 μm, but with a maximum chord around 50 μm.

## 4.2.1  Stability in acidic conditions

In order to validate the chitosan microspheres for application in the stomach without dissolution, their stability under acidic conditions must be evaluated. Given the pH range found in the gastric mucosa (from pH 1.2-2.5 in the lumen to neutral at the epithelial surface pH ~7.4), a compromise had to be made and pH 6.0 was chosen to conduct the experiments.

Chitosan microspheres were therefore incubated in pH 6.0 phosphate-citrate buffer and their behaviour was followed over 1-h period (Figure 14).
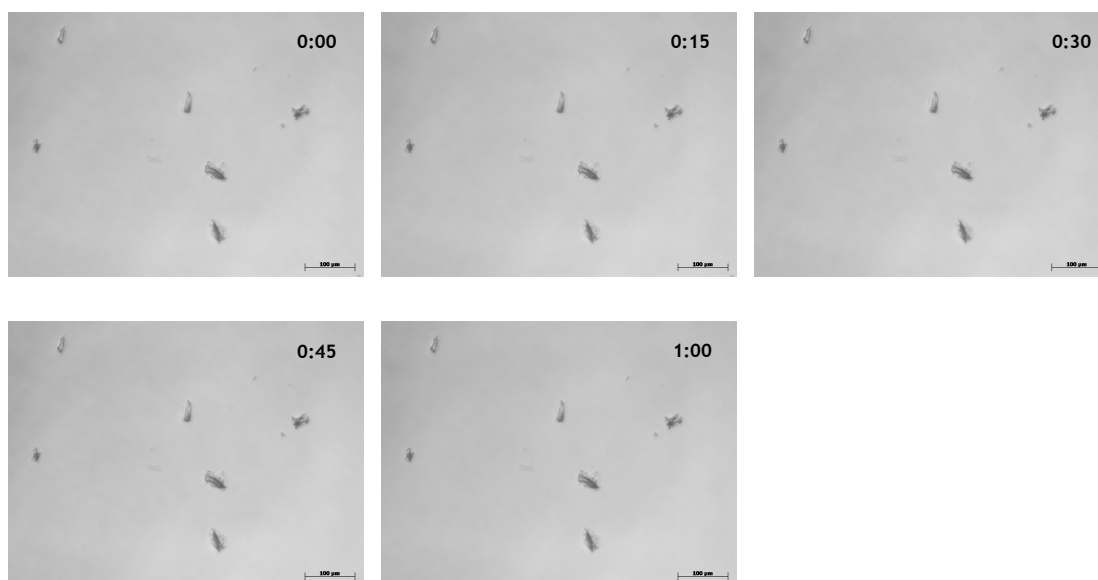


**Figure 14** – Optical microscopy images of chitosan microspheres in acidic conditions over 1 h. Scale bar 100 μm.

As can be seen in Figure 14, no major differences are observed regarding the morphology of chitosan microspheres, suggesting their stability under pH 6.0.

## 4.3  Chitosan microspheres emission spectrum

Fluorescence is probably the best technique to evaluate microspheres capacity to penetrate gastric foveolae and to bind *H. pylori*. As such, understanding chitosan microspheres fluorescence properties is fundamental. Microspheres spectrum was evaluated by exciting microspheres with different lasers: 405 nm, 488 nm and 561 nm. The spectrum corresponding to the excitation of 405 nm is presented below (Figure 15).
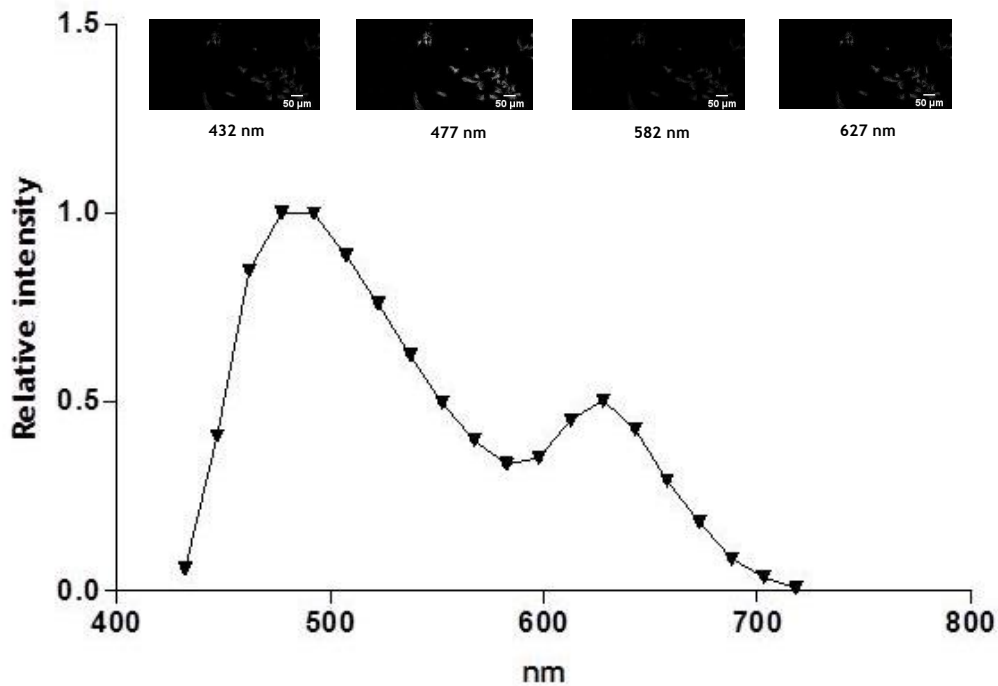
**Figure 15 -** Chitosan microspheres emission spectrum obtained by CLSM when excited by 405 nm laser.

By exciting the chitosan microspheres with a 405 nm laser, two peaks can be identified in their emission spectrum: a maximum value at 477 nm, followed by a slow decrease in relative fluorescence, and an increase again at 627 nm, approximately, though less intense than the first peak. This behaviour can be followed on the fluorescence images shown.

When chitosan microspheres are excited with different lasers (488 nm and 561 nm, data not shown), the exact same behaviour can be observed, although only the second peak is observed since excitation is made in a wavelength higher than the first emission peak (677 nm).

Therefore, these results indicate that independently of the excitation laser, the emission spectrum of the chitosan microspheres will be always the same. The microspheres were not previously labelled, and consequently this spectrum can also reveal chitosan microspheres auto-fluorescence throughout a wide range of wavelength (450 nm to 650 nm, approximately).

## 4.4 Chitosan microspheres adhesion to gastric mucosa

Evaluation of the chitosan microspheres capacity of penetrate the gastric mucosa, in order to reach deeper *H. pylori* living inside the gastric foveolae, is one of the main aims initially established. Microspheres adhesion studies to gastric mucosa were performed and evaluated by Inverted Fluorescence Microscopy and Confocal Laser Scanning Microscopy.

## 4.4.1  Optimization of gastric mucosa labelling

The direct observation of ex-vivo samples of gastric mucosa would ease the process of evaluating the penetration of the chitosan microspheres into the gastric foveolae. Therefore, fresh mice stomach samples were used to optimize the fluorescence labelling of gastric mucosa.

Initially, fresh mice gastric mucosas were mounted only with different mounting media (Figure 16).
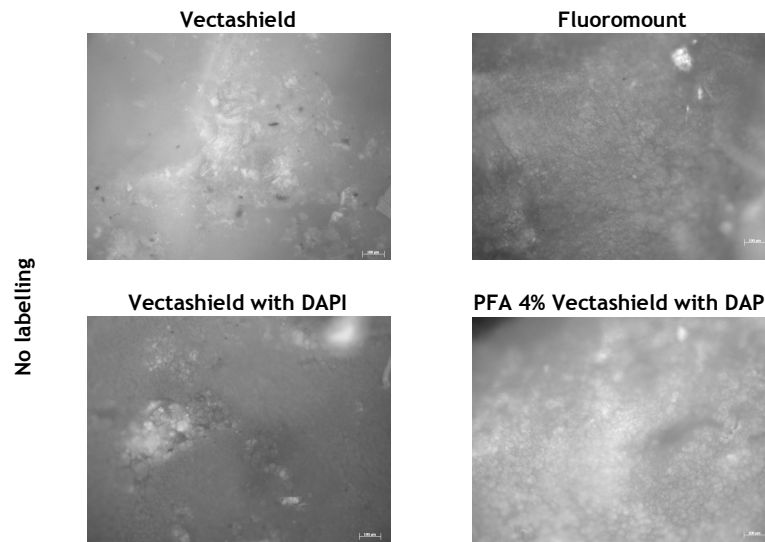


**Figure 16** – Fluorescence microscopy images of mice gastric mucosa mounted with different mounting media. Scale bar 100 µm.

Figure 16 allows the observation of the tissue, although not in a very clear way. No gastric structures are identified, suggesting that auto-fluorescence of the tissue is residual. This auto-fluorescence is apparently improved by the usage of Fluoromount as mounting medium, although the difference is not evident. Regarding the application of Vectashield with DAPI, previous fixation of the tissue with PFA 4% seems to improve its observation when comparing to the sample when only Vectashield with DAPI was applied.

DAPI and Hoechst were then tested as nucleic acid stains (Figure 17), while several Wheat Germ Agglutinin conjugates and a CellMask™ Deep Red stain were used as plasma membrane stains (Figure 18).
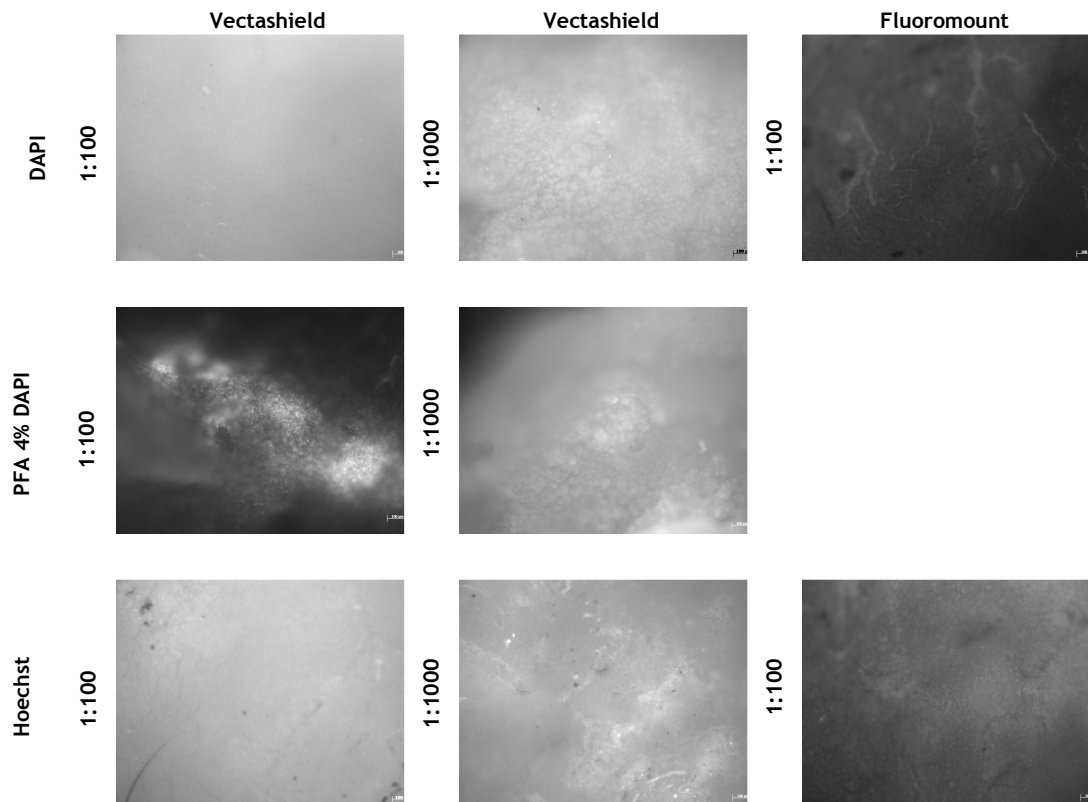
**Figure 17** – Fluorescence microscopy images of mice gastric mucosa stained with nucleic acid dyes (with two different concentrations, 1:100 and 1:1000), using two different mounting media. Scale bar 100 μm.

The blurred image of gastric mucosa labelled with DAPI 1:100 suggests that this staining is not strong enough to adequately label the DNA of the mucosa allowing its visualization. The same is observed when Hoechst 1:100 is used. However, DAPI is a stain recommended for fixed or permeabilized cells. As such, when analysing the fixed mucosa with PFA 4% followed labelling with DAPI, bright spots are observed, identifying what seems to be the nucleus of the gastric cells of the surface of the mucosa. Comparing the two concentrations of DAPI, a clear and brighter image is obtained when the higher concentration (1:100) is used.

Figure 18 shows the fluorescence labelling of gastric mucosa by different plasma membrane stains. As previously referred, these samples were kept fresh without adding mounting media. Fluorescently labelled lectins, such as WGA, were exploited as plasma membrane stains as well as CellMask™ Deep Red.

**5 µg/mL, 15 min incubation**

WGA, Alexa Fluor® 350

**1 µg/mL, 15 min incubation**   **1 µg/mL, 30 min incubation**

WGA - Alexa Fluor® 488

**5 µg/mL, 15 min incubation**   **20 µg/mL, 15 min incubation**

WGA, Alexa Fluor® 594

**5 µg/mL, 15 min incubation**

WGA, FITC

**1000x, no period of incubation**

CellMask™ Deep Red
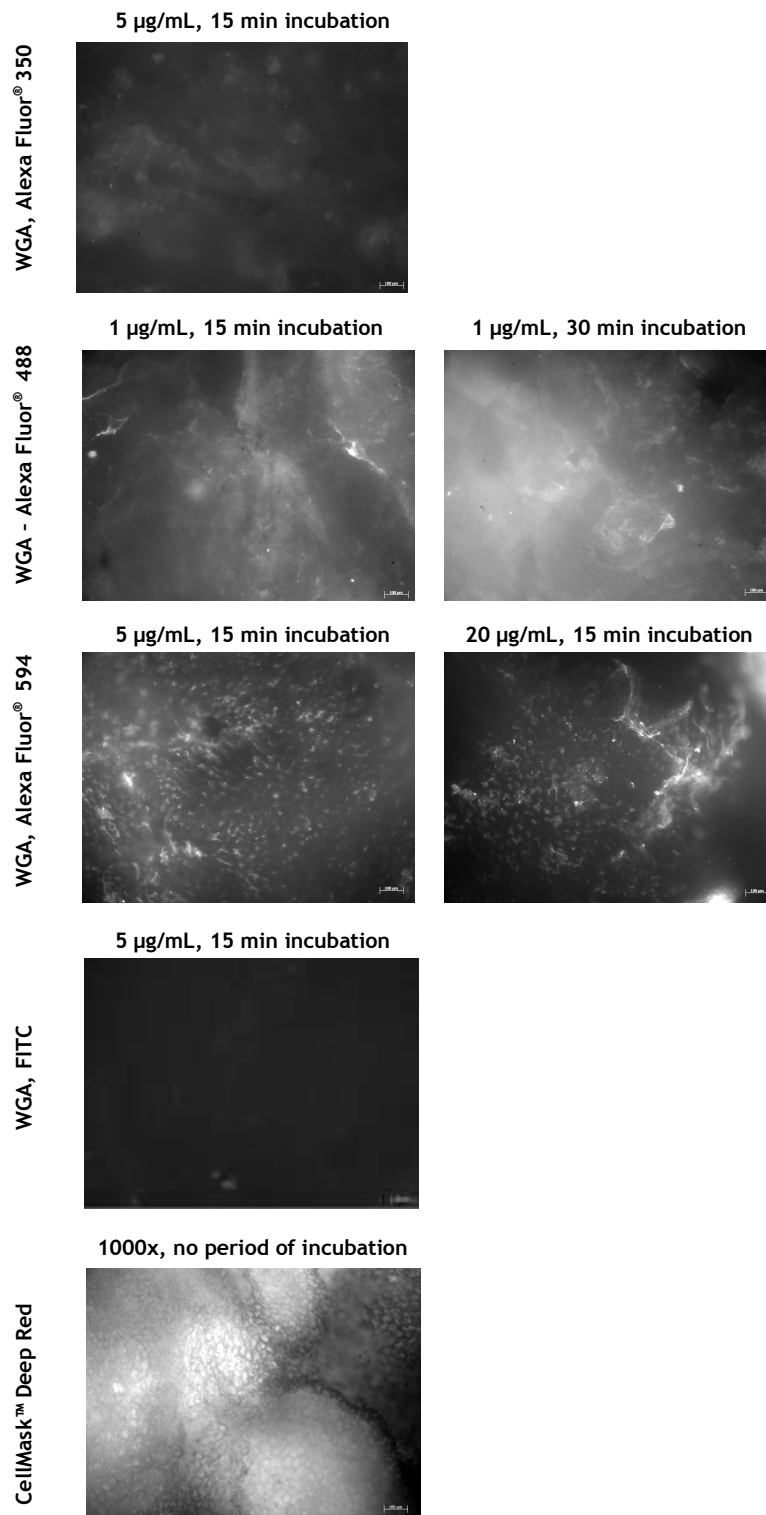
**Figure 18 -** Fluorescence microscopy images of mice gastric mucosa labelled with different plasma membrane staining, at different concentrations and time of incubation (indicated above each image). Scale bar 100 µm.

Over viewing the different WGA conjugates, none successfully labelled the mucosa. However, CellMask™ Deep Red stain performs a stronger staining of the plasma membrane of the cells from the gastric mucosa. According to the manufacturer, when comparing to labelled WGA, CellMask™ Deep Red plasma membrane stain takes more time to be internalized, thus maintaining the staining or a longer period. Therefore, this plasma

membrane stain has proved to perform an excellent and rapid plasma membrane staining, excluding the need of previous fixation and incubation periods.

Based on this first screening, DAPI (fixed sample) and CellMask™ Deep Red plasma membrane (fresh) stain were determined as good gastric mucosa markers. In order to better assess its feasibility for further adhesion studies, gastric mucosa without labelling (Figure 19), and stained with DAPI 1:100 after fixation with PFA 4% (Figure 20) were observed under CLSM as well as CellMask™ Deep Red labelled mucosa (Figure 21). Different Z-plans of the mucosa were acquired and are represented below.
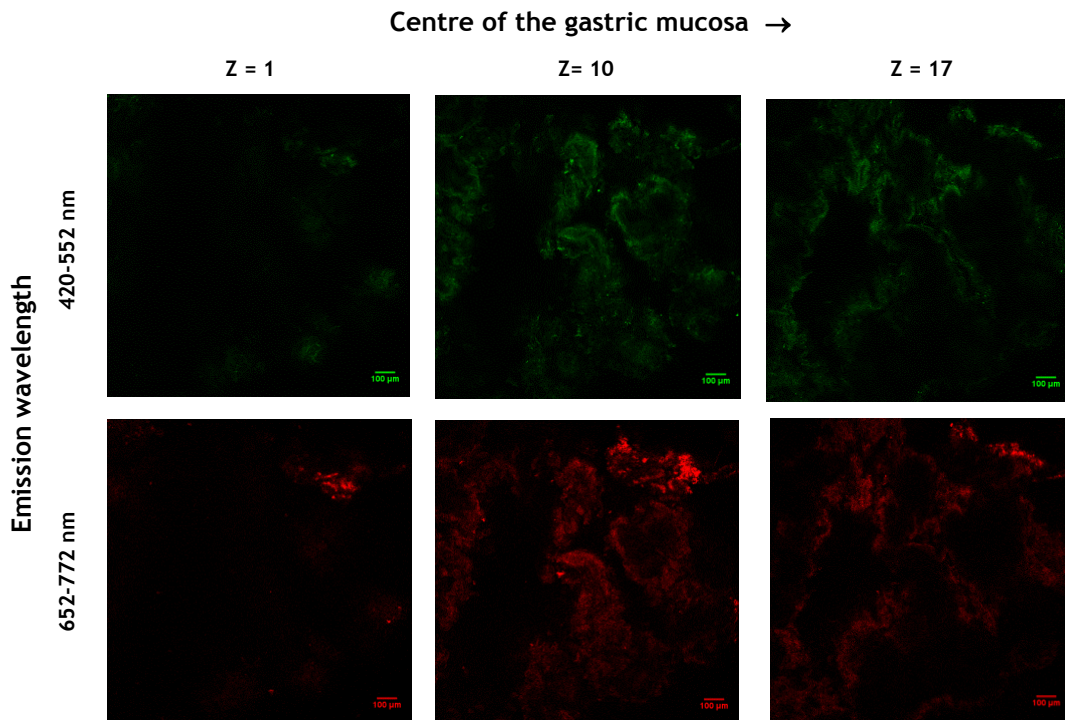


**Figure 19** – Auto-fluorescence of mice gastric mucosa in two ranges of emission wavelength. CLSM images of the outer layer (Z=1) and deeper layers (Z=10 and Z=17) of mice gastric mucosa (ScanMode xyz; step size 2.9 µm). Scale bar 100 µm.

CLSM images confirm a residual auto-fluorescence of the gastric mucosa, which emits fluorescence between 420-552 nm (green) and between 652-772 nm (red). However, the emission is not strong enough to properly observe the physical characteristics of the gastric mucosa.

Figure 20 illustrates the difference in the gastric mucosa morphology when going deeper inside the tissue of the sample fixed with PFA 4% followed labelling with DAPI 1:100. Apart from the horizontal section of the tissue, two orthogonal views of two stacks are shown as well. The vertical and horizontal images correspond to a perpendicular plan to the one visualized from above on the area of the white crosshair.

**Centre of the gastric mucosa →**

Z = 5          Z = 7          Z = 9



Z = 11          Z = 13          Z = 15
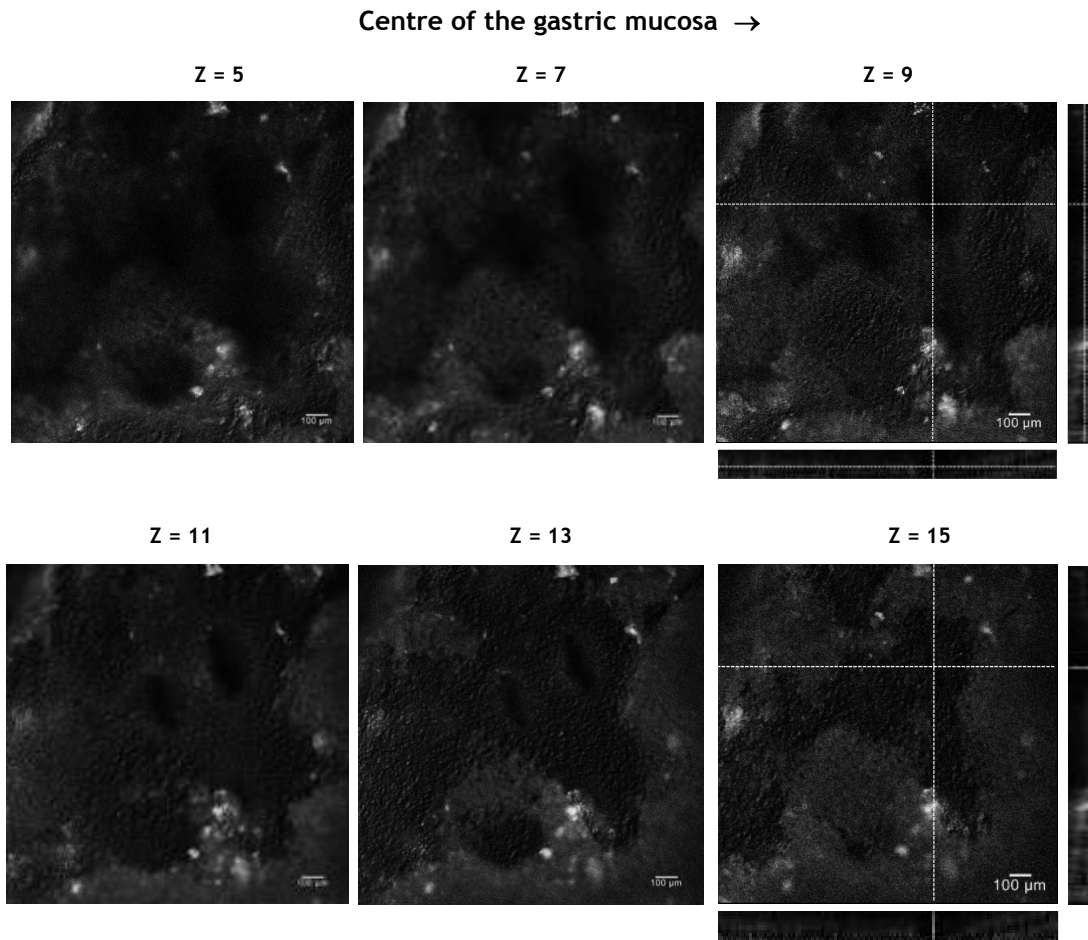


**Figure 20** – Mice gastric mucosa fixed with PFA 4% and labelled with DAPI 1:100. CLSM images of the outer layer (Z=5) and deeper layers (Z=7 to Z=15) of mice gastric mucosa (ScanMode xyz; step size 9.99 µm). Orthogonal views of two stacks (Z=9 and Z=15) are shown (ScanMode xzy). Scale bar 100 µm.

Evaluation of the different stacks at different depths suggests the combination of PFA 4% with DAPI 1:100 labelling as a good procedure to observe gastric foveolae. Different stacks from the same area allow the identification of three gastric foveolae, whose diameter is decreased when going deeper into the tissue (from Z=5 to Z=15). On the orthogonal views the curvature of the foveolae is also seen (darker region).

CLSM images of different stacks from the CellMask™ Deep Red labelled mucosa are gathered on Figure 21.

**Centre of the gastric mucosa** →
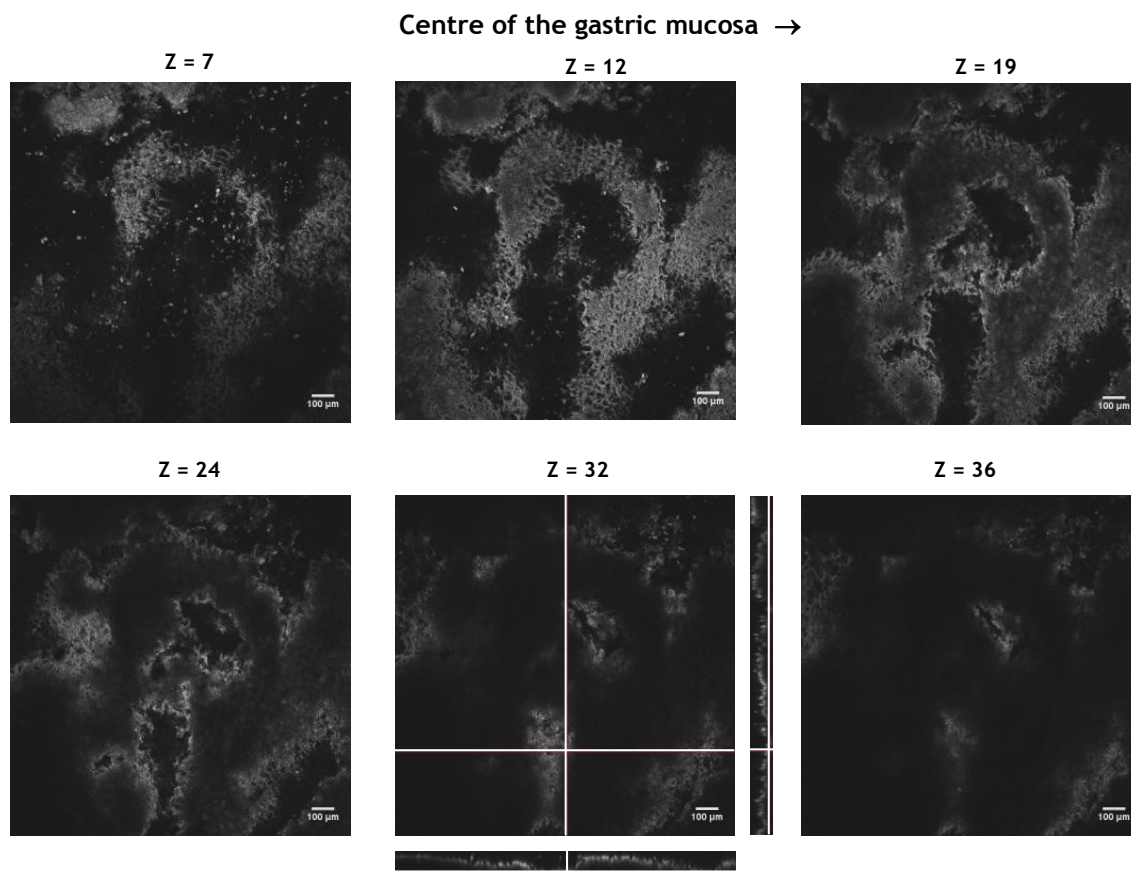


**Figure 21** – Mice gastric mucosa cells labelled with CellMask™ Deep Red stain. CLSM images of the outer layer (Z=7) and deeper layers (Z=12 to Z=36) of mice gastric mucosa (ScanMode xyz; step size 2.6 μm). Orthogonal views of stack Z=32 is shown (ScanMode xzy). Scale bar 100 μm.

Labelling with CellMask™ Deep Red seems strong enough to clearly observe the mucosa and the foveolae. By going deeper inside the tissue, a change in the morphology of the mucosa is seen; the structures become darker and the diameter of the dark areas smaller. By going inside the tissue, the mucosa ends up with only dark areas, due to a decrease on the fluorescence. The orthogonal view shows the corresponding curvature of the foveolae.

Combination of PFA 4% fixation and DAPI 1:100 labelling as well as the CellMask™ Deep Red plasma membrane stain allowed a good observation of the gastric mucosa, both by fluorescence and confocal microscopy. Therefore, these staining were applied for the following studies.

## 4.4.2 Chitosan microspheres adhesion to mice gastric mucosa

Chitosan microspheres adhesion studies to mice gastric mucosa were performed at 37°C, at pH 6.0 and under stirring, in order to mimic the *in vivo* conditions. Staining was afterwards employed considering the results from the last section.

Figure 22 shows the gastric mucosa labelled with DAPI 1:100 after fixation with PFA 4%, both without (control) and with chitosan microspheres adhered. Figure 23 gathers the same information although regarding CellMask™ Deep Red staining.
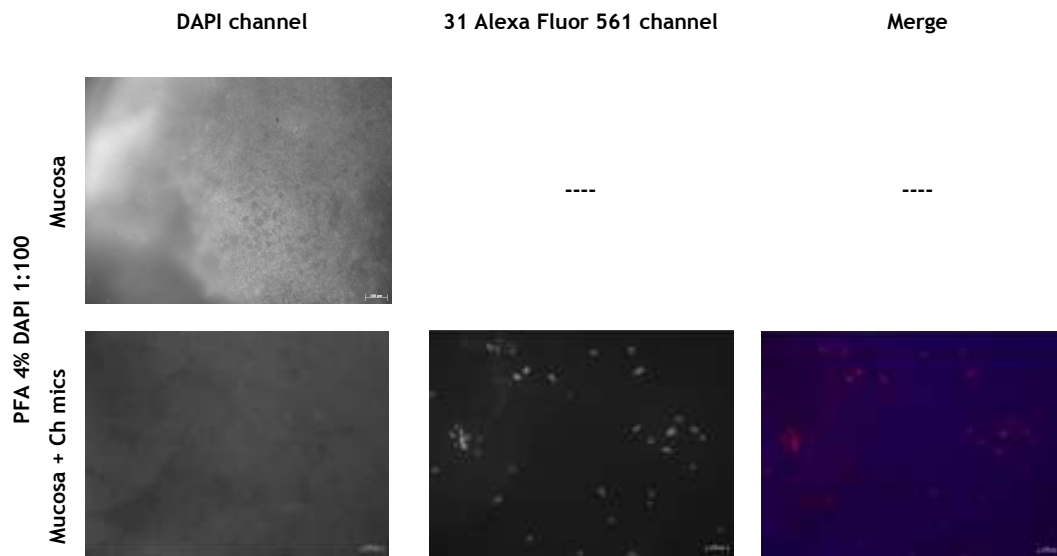


**Figure 22 -** Fluorescence microscopy images of mice gastric mucosa alone and with chitosan microspheres. Mucosa was fixed with PFA 4% followed labelling with DAPI 1:100 in both conditions. Scale bar 100 µm.
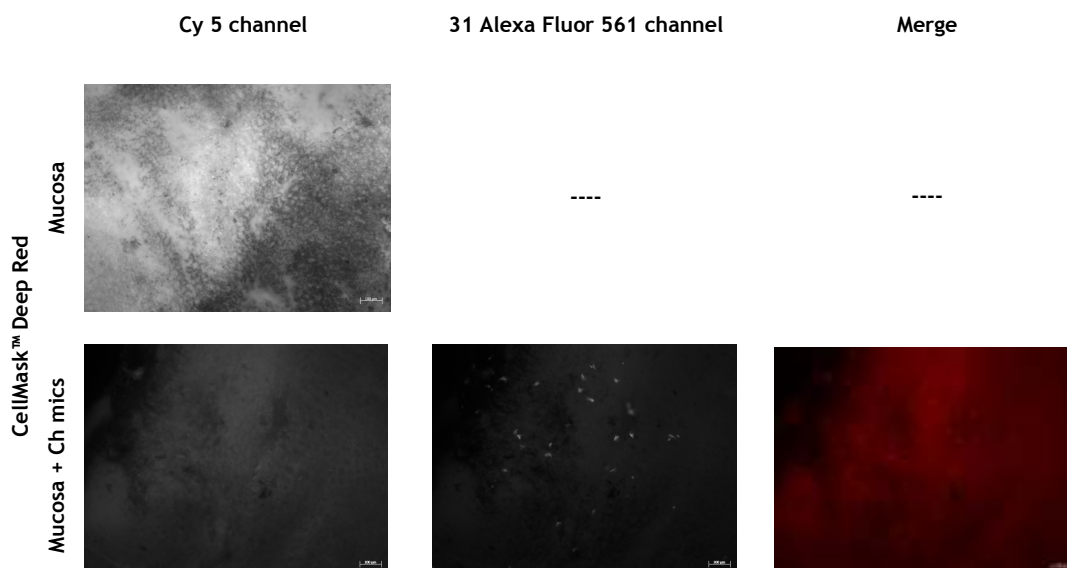


**Figure 23 -** Fluorescence microscopy images of mice gastric mucosa alone and with chitosan microspheres. Mucosa was labelled with CellMask™ Deep Red in both conditions. Scale bar 100 µm.

Both conditions allow the observation of adhered chitosan microspheres, confirming their ability to adhere to the gastric mucosa.

In order to evaluate whether chitosan microspheres are able to penetrate the gastric mucosa, 3D images are required. Confocal images for both conditions are presented below.

Figure 24 concerns the gastric mucosa labelled with PFA 4% DAPI 1:100. DNA of gastric cells of the mucosa is labelled in blue, while the microsphere is seen in red. A single microsphere was selected and observed closely. Different stacks were taken in order to understand the position of the microsphere in relation to the gastric mucosa.
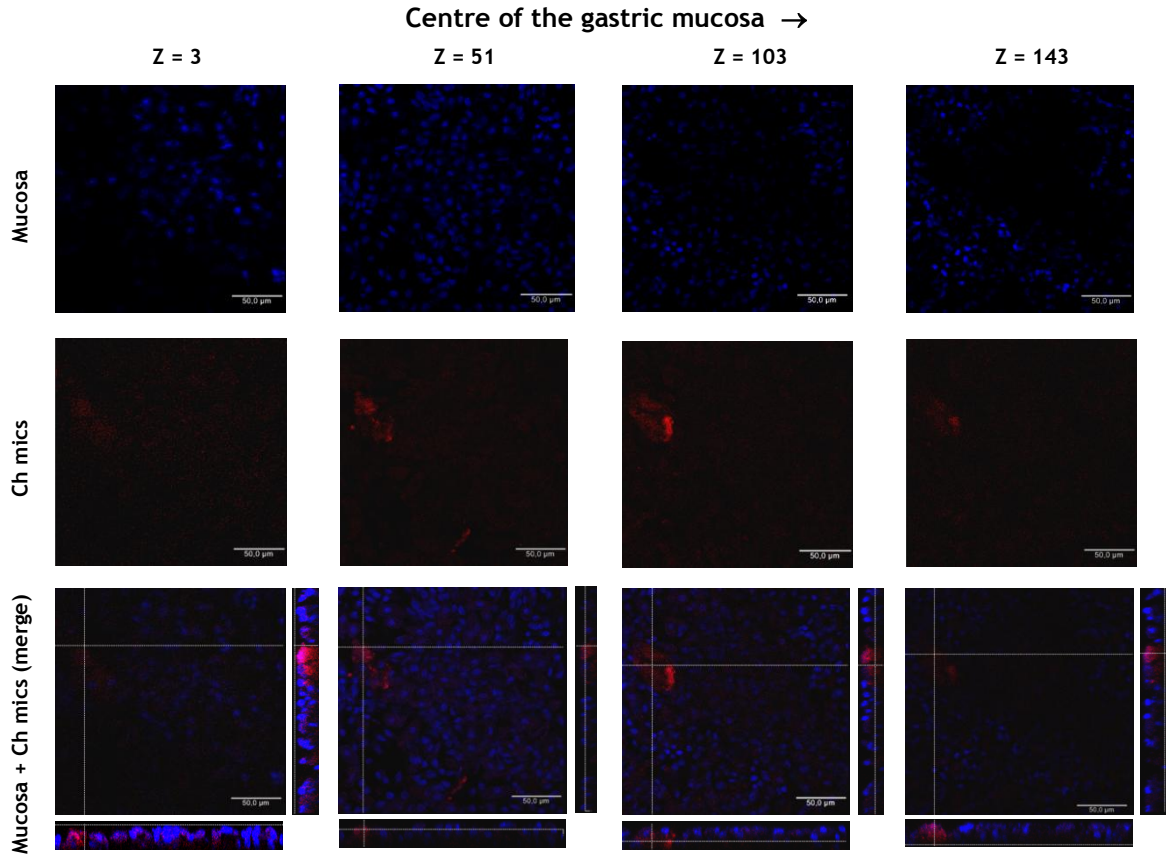


**Figure 24** – Chitosan microspheres (red) adhered to mice gastric mucosa fixed with PFA 4% and labelled with DAPI 1:100 (blue). CLSM images of the outer layer (Z=3) and deeper layers (Z=51 to Z=143) of mice gastric mucosa (ScanMode xyz; step size 0.17 μm). Orthogonal views of merged images are shown (ScanMode xzy). Scale bar 50 μm.

Different stacks of the mucosa allow a 3D perpective of the latter, in order to understand whether the microsphere is inside the mucosa and consequently between the cells (blue). Going through deeper stacks it can be seen that in fact the chitosan microsphere (red) penetrated the mucosa. At stack Z=3 the presence of  the microsphere is almost imperceptible, however when at Z=51 it starts to appear, being some cells visible above the microsphere. At Z=103 a complete plan of the microsphere is seen, however at Z=143 it disappears, suggesting that the imaging section is already in an area with only cells.

Figure 25 presents an orthogonal view of a single chitosan microsphere (red), which is clearly inserted on the mucosa (blue).

| Mucosa | Ch mics | Merge |
|--------|---------|-------|
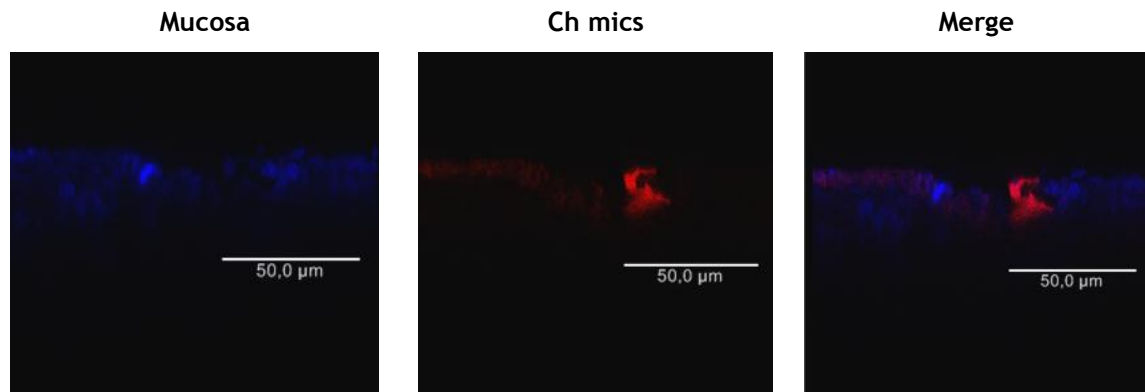


**Figure 25** – Orthogonal view of chitosan microsphere (red) inserted into mice gastric mucosa fixed with PFA 4% and labelled with DAPI 1:100 (blue) (ScanMode xzy). Scale bar 50 µm.

Gastric mucosa labelled with CellMask™ Deep Red is seen in Figure 26, showing several stacks taken at different depths.

**Centre of the gastric mucosa →**

| | Z = 20 | Z = 28 | Z = 35 | Z = 59 |
|--|--------|--------|--------|--------|
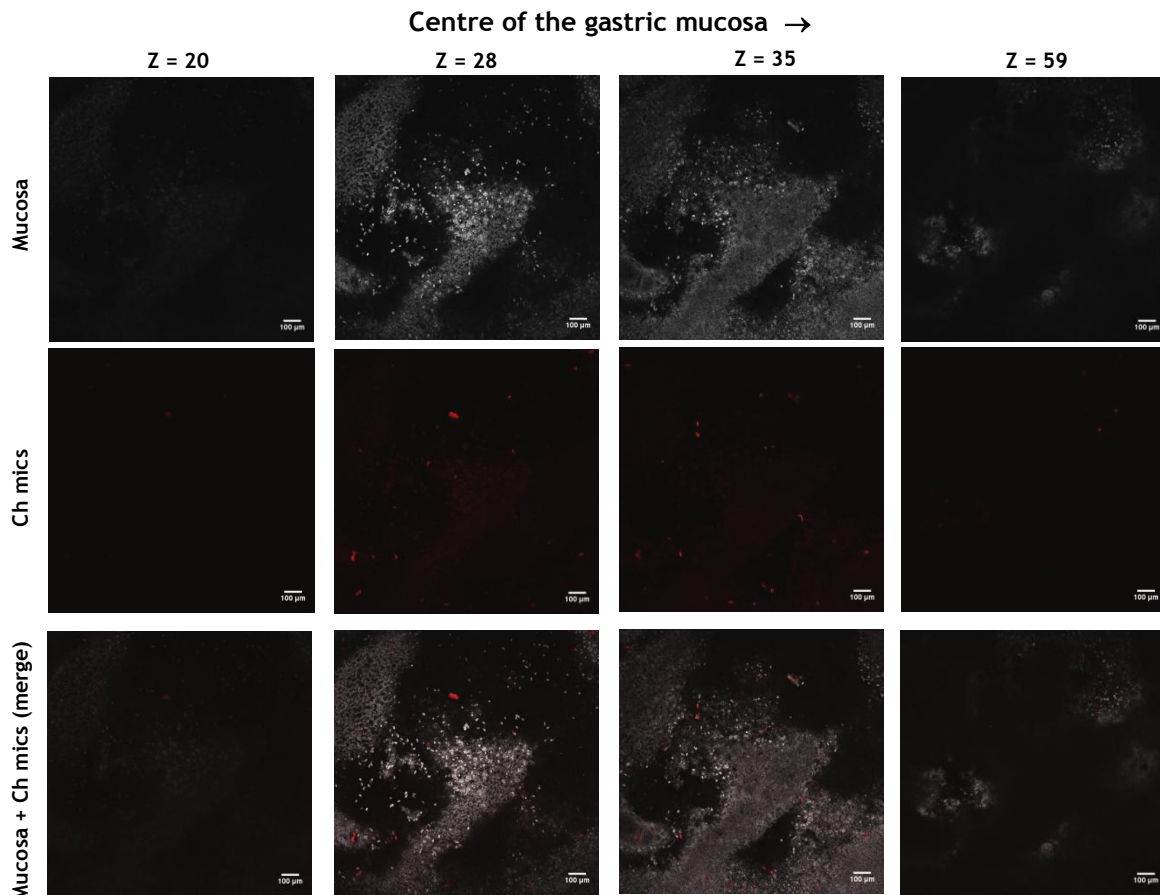


**Figure 26 -** Mice gastric mucosa cells labelled with CellMask™ Deep Red stain with chitosan microspheres adhered (red). CLSM images of the outer layer (Z=20) and deeper layers (Z=28 to Z=59) of mice gastric mucosa (ScanMode xyz; step size 2.6 µm). Scale bar 100 µm.

Observation of the latter set of images allows identifying the presence of chitosan microspheres in different plans. At Z=20, a superficial image taken, an imperceptible visualization of the mucosa as well as the microsphere indicates the microspheres ability to

penetrate. The following stacks confirm that ability, since when going in the direction of the muscle, some microspheres are no longer observed while fluorescence of other microspheres is detected. This suggests that microspheres are indeed in different plans of the mucosa, being able to cross the remaining mucus layer.

Both stainings allow the identification of 3D depressions corresponding to gastric foveolae and chitosan microspheres, revealing the presence of the microspheres not only on the superficial plans, but deeper inside the tissue. These images were taken after the rinsing step, suggesting the chitosan microspheres as highly mucoadhesive, since they are able to remain attached to the fresh mucosa.

However, in order to mimic the natural conditions closely, fresh samples (without fixation) may be preferable as a study model.

## 4.4.3 Chitosan microspheres adhesion to human gastric mucosa

Ultimately, human gastric mucosa was used to evaluate the ability of chitosan microspheres to penetrate the tissue.

Given the good performance as mice gastric mucosa labelling, and since it does not require fixation of the tissue or an incubation period, CellMask™ Deep Red plasma membrane stain was selected to label the human gastric mucosa previously to observation by CLSM.

Figure 27 shows the labelling of the human gastric mucosa with CellMask™ Deep Red stain.
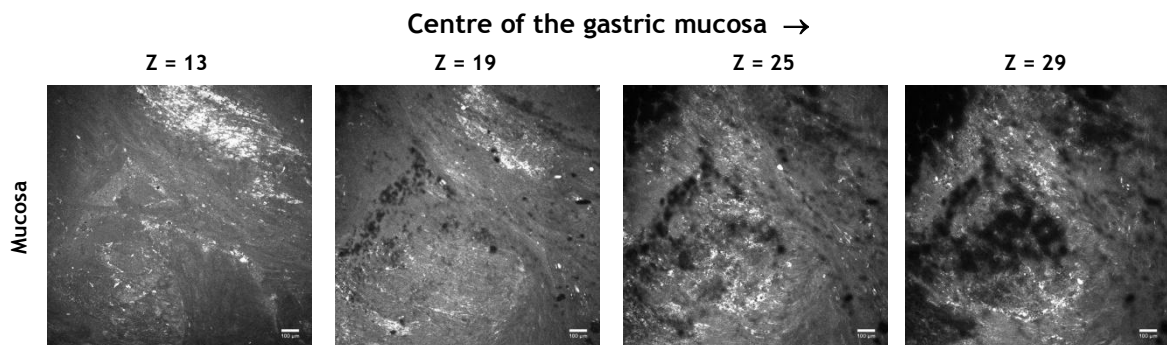


**Figure 27 -** Human gastric mucosa labelled with CellMask™ Deep Red stain. CLSM images of the outer layer (Z=13) and deeper layers (Z=19, Z=25 and Z=29) of human gastric mucosa (ScanMode xyz; step size 3.9 µm). Scale bar 100 µm.

Firstly, a different morphology of the tissue can be observed when comparing to the mice gastric mucosa previously evaluated. Nevertheless, the marker seems to stain the tissue properly, since a clear change is seen when going deeper. A thick layer of mucus was observed, shown at Z=13, which starts to disappear when stacks from a higher depth are taken. At Z=29 it is observed the presence of a darker area, which may resemble the gastric foveolae seen in the mice stomach. However the physiology is different and difficult to compare.

Chitosan microspheres adhesion studies were also performed using human gastric mucosa, at 37ºC, at pH 6.0 and under stirring. Figure 28 shows the same area at different depths.

**Centre of the gastric mucosa  →**
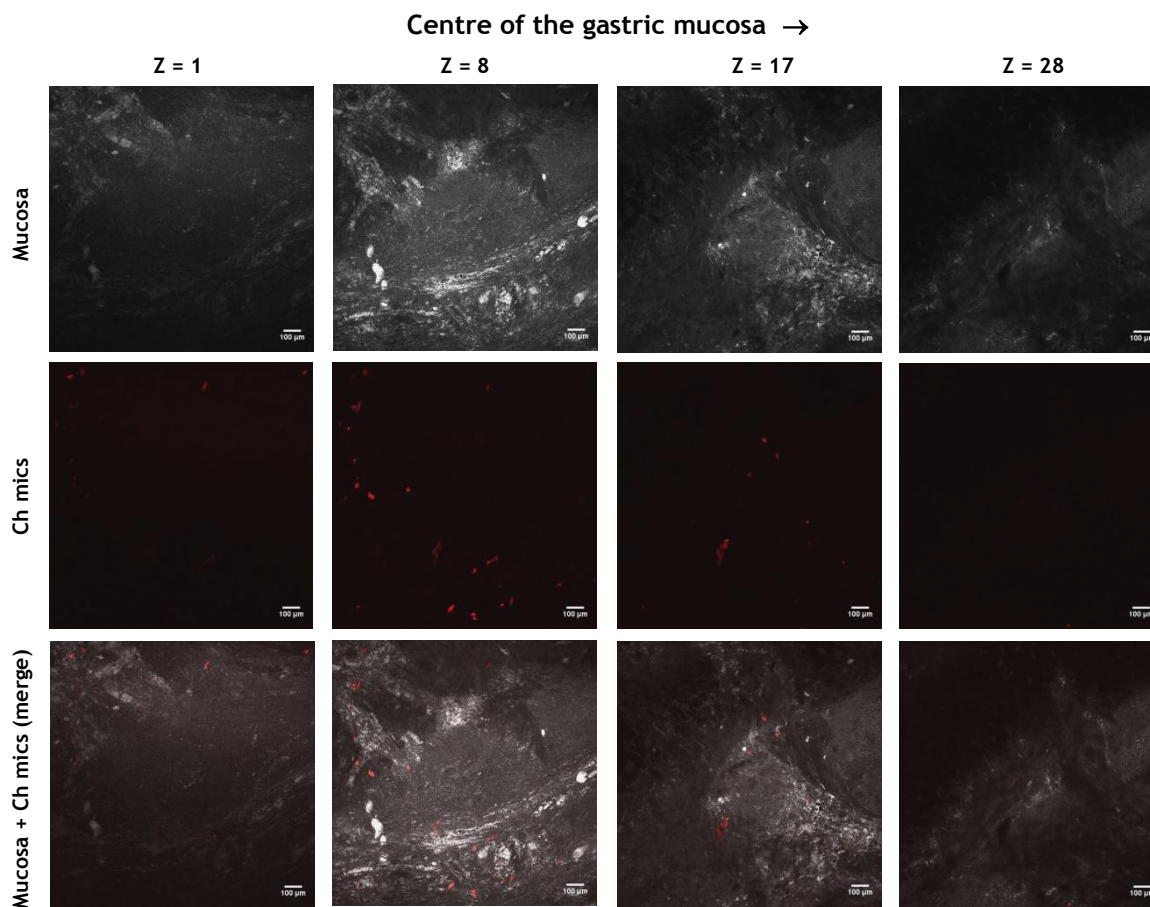


**Figure 28 -** Human gastric mucosa labelled with CellMask™ Deep Red stain. CLSM images of the outer layer (Z=1) and deeper layers (Z=8, Z=17 and Z=28) of human gastric mucosa (ScanMode xyz; step size 3.01 µm). Scale bar 100 µm.

Regarding the evaluation of the ability of chitosan microspheres to penetrate the human foveolae, it can be observed that most of the particles remain in superficial plans: though a depth of around 140 µm was evaluated, chitosan microspheres are no longer observed at a depth higher than 84.3 µm (Z=28). In addition, it is important to consider the thickness of the mucus layer, which may reduce even more the actual depth penetrated by the chitosan microspheres. Nevertheless, it is not known whether the microspheres do not actually penetrate or if deeper plans cannot be obtained, because lack of fluorescence, thus revealing their presence. When comparing to mice gastric mucosa, around 250 µm depth can be observed through CLSM, therefore microspheres in deeper plans can be observed.

## 4.5 *Helicobacter pylori* adhesion to chitosan microspheres

The ability of chitosan microspheres to adhere to *Helicobacter pylori (H. pylori)* is also important considering the final aim of using chitosan microspheres to remove the bacteria from the stomach. Therefore, a study was conducted *in vitro* using J99 strain of *H. pylori* alive and previously fixed and labelled with FITC, at a pH of 6.0.

## 4.5.1 Adhesion of live *H. pylori* J99 strain to chitosan microspheres

Because the *in vivo* adhesion process between the microspheres and the bacteria occurs with the bacteria alive, in this study labelling of the bacteria was performed only after the 2h-period of adhesion. Inverted fluorescence microscopy results are shown in Figure 29.
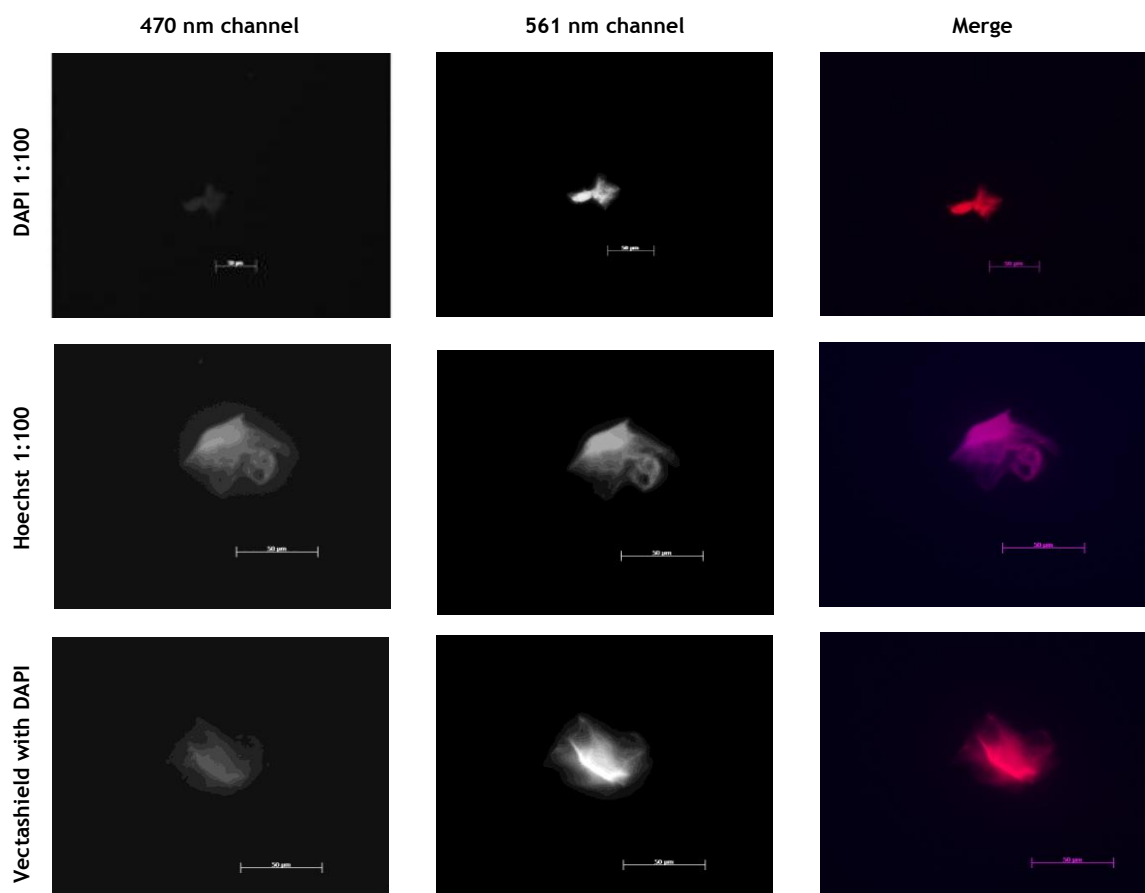


**Figure 29** – Fluorescence microscopy images of DAPI, Hoechst and Vectashield with DAPI -labelled *H. pylori* adhered to chitosan microspheres. Scale bar 50 μm.

Apparently, only small dots corresponding to bacteria are seen when Vectashield with DAPI is used. When DAPI or Hoechst 1:100 are used no evident differences are found between the samples, and the chitosan microspheres are still able to be observed in both channels.

Figure 30 shows confocal images of a chitosan microsphere with adhered bacteria labelled with Vectashield with DAPI.

**470 channel**        **561 nm channel**
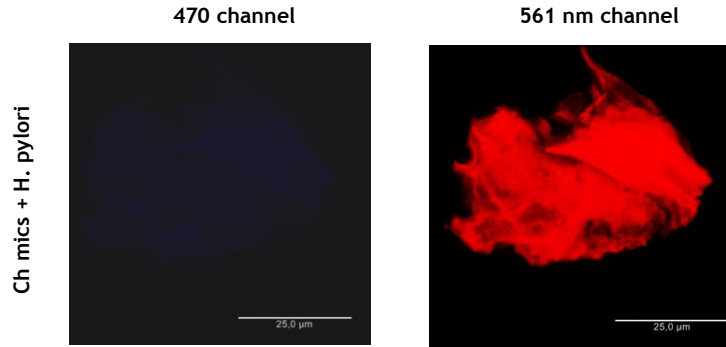
**Figure 30 –** Maximum projection of a chitosan microsphere with Vectashield with DAPI-labelled bacteria. Images were obtained by CLSM. Scale bar 25 μm.

As it can be seen, no dots representing the bacteria are observed. This can mean that bacteria did not adhere to the chitosan microsphere, or it can also mean that the auto-fluorescence of the chitosan particle in the blue wavelength is too intense to detected bacteria DNA labelling.

In order to try to eliminate/reduce the factor of auto-fluorescence, a microsphere labelled with Vectashield with DAPI should be used as a control. The minimum blue fluorescence would be initially determined, so that when the same settings were applied to the labelled sample, the auto-fluorescence was subtracted and the labelled bacteria detected. For this, similar microspheres should be used: since they are heterogeneous among them, microspheres with different density would contribute differently to the auto-fluorescence.

Given this results, it can be said that visualization of live DNA labelled-bacteria is difficult by both fluorescence and confocal microscopy, being required a different label method.

## 4.5.2 Adhesion of fixed *H. pylori* J99 strain to chitosan microspheres

The adhesion of FITC-labelled *H. pylori* to chitosan microspheres at pH 6.0 was evaluated by CLSM (Figure 31).
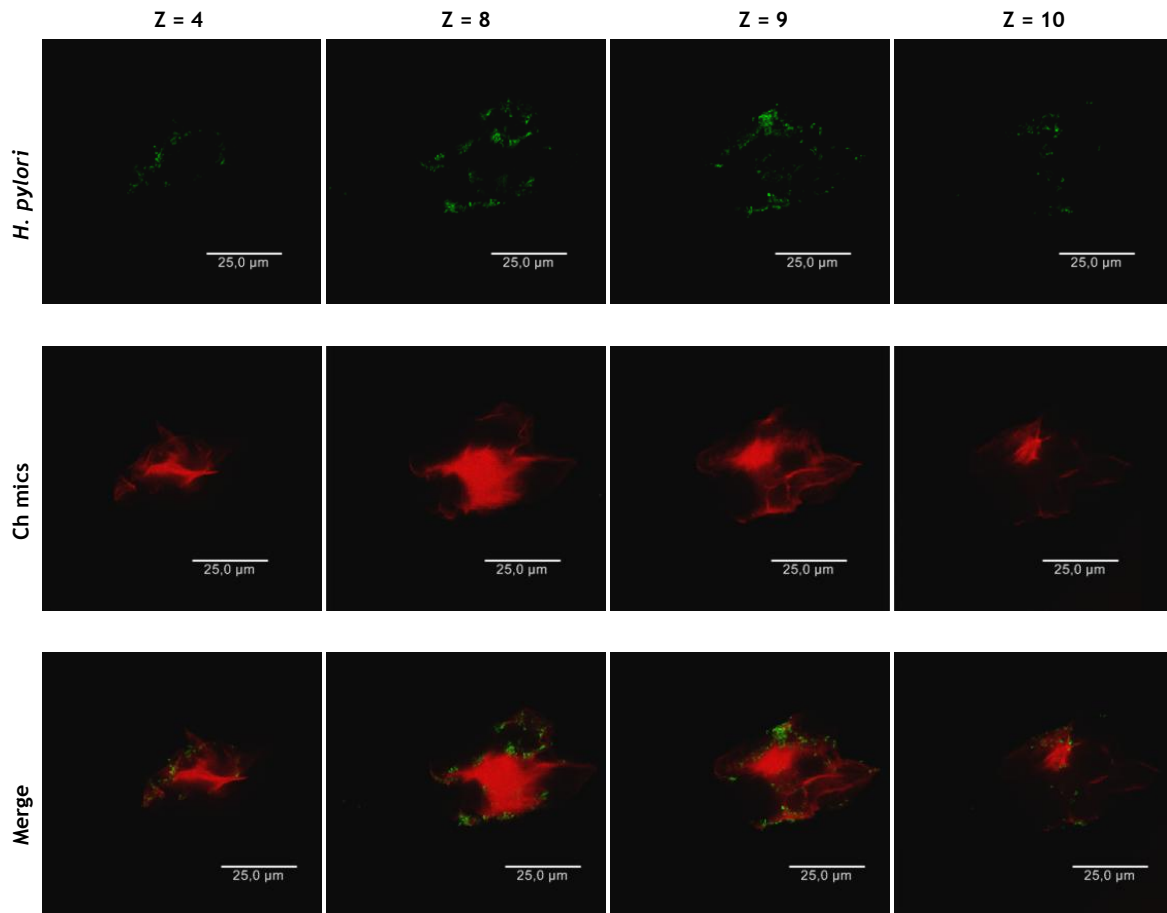
**Figure 31 -** FITC-labelled J99 strain (green) adhered to chitosan microspheres (red) under pH 6.0 for five z-stacks (Z, step size of 2.98 µm). Images were obtained by CLSM. Scale bar 25 µm.

In this case, a brighter and stronger signal was detected from FITC-labelled bacteria, allowing an easy and clear assessment of the adhesion to the chitosan microspheres. CLSM allowed the visualization of stacks of the whole microsphere, revealing that bacteria were well distributed all over the surface of the microspheres, though no bacteria were found inside the microsphere. The fact that the microsphere presents an irregular and heterogeneous surface increases the surface contact area and therefore the number of adhered bacteria.

It is herein demonstrated that chitosan microspheres crosslinked with genipin and lyophilised have the capacity to adhere to J99 *H. pylori* strain under pH 6.0.

# Chapter 5

# Conclusions and future considerations

## Conclusions

Chitosan microspheres were produced by three different equipments, in order to evaluate the influence of different parameters on microspheres features. Overall, when using the high voltage electrostatic system the chitosan concentration and the flow rate do not seem to influence the production process. However, chitosan DA appears to be an influent factor on the chitosan microspheres production process, with chitosan microspheres with DA of 16% presenting a consistent structure and generally being more spherical and structurally homogeneous than chitosan microspheres produced with chitosan of 6% DA. Since chitosan microspheres produced are bigger (115-150 µm) than desired, this system was considered not appropriate. The same trend regarding the influence of chitosan DA on microspheres morphology was observed with co-axial air stream system. Moreover, the air stream pressure is a preponderant factor in this system, with smaller particles being produced when air pressure is increased. Regarding aerodynamically driven system, the increase in the nozzle diameter of the equipment seems to lead to an increase in particles diameter. Moreover, by increasing the pressure smaller microspheres are produced. Flow rate was accordingly to the previous system not a relevant factor. Though co-axial air stream system presented some conditions within the diameter range expected, aerodynamically driven system was selected mainly due to its speed regarding particles production.

Chitosan microspheres with an average diameter of 40 µm were successfully produced by ionotropic gelation with TPP coupled with coacervation using the aerodynamically driven system and chitosan of DA 6% and 0.5% (w/v) concentration under optimized conditions of 0.5mL/min flow rate, 525 mBar air pressure and 0.25 mm nozzle.

Throughout the production process, microspheres were characterized by different equipments based on optical microscopy and laser diffraction. Optical microscopy was initially used to perform a qualitative analysis, giving information related with size and morphology of chitosan particles. IN Cell Analyzer equipment provided an automated approach to acquire high quality images and assess morphological parameters concerning each microsphere. In this equipment, an advanced analysis tool is coupled to the acquisition software allowing a thorough analysis of parameters as average diameter, maximum chord, area and form factor. Mastersizer particle sizing instrument uses the laser diffraction to measure particle size distribution. In this case, no images are provided, and thus, in order to assess morphology, one of the other techniques must be used. In conclusion, all three techniques provide complementary information, however depending on the purpose, a specific technique might be selected.

Minimal genipin crosslinking was performed with a genipin concentration of 10 mM during 45 minutes, only enough to avoid microspheres dissolution in acidic pH without losing their mucoadhesiveness. Following crosslinking, chitosan microspheres were lyophilised, presenting not only a different morphology but also a decrease in the average diameter when comparing to microspheres before lyophilisation. Chitosan microspheres present a more irregular structure, with an average diameter around 20 μm, but with a maximum chord around 50 μm.

Optimization of the gastric mucosa labelling was performed using C57BL/6 mice fresh stomachs. Both nucleic acid and plasma membrane stains were employed with a better outcome associated with CellMask™ Deep Red stain, which can be applied to fresh stomachs without the need of previous fixation. Fixation of the mucosa followed by staining with DAPI also showed good results, though the use of fresh samples is preferable. Adhesion studies using the same models demonstrated that the developed chitosan microspheres have the ability to penetrate the gastric mucosa, which can be promising for future *H. pylori* removing assays. Regarding human gastric mucosa, few microspheres can be seen in deeper plans, suggesting that the microspheres have difficulty in penetrating, perhaps due to the thick layer of mucus observed over the surface of the mucosa.

*H. pylori* adhesion to developed microspheres was evaluated at pH 6.0, and confirmed by incubation of previously fixed J99 *H. pylori* strain, labelled with FITC. When observed by CLSM, a spread adhesion of the bacteria to the chitosan microspheres is observed. The irregularity of the surface may indeed beneficiate the adhesion, since a higher surface area is available. Adhesion assays with live bacteria (only labelled with nucleic acid stains after adhesion to microspheres) did not allow drawing any conclusions, due to the auto-fluorescence capability of chitosan microspheres. Therefore, further improvements need to be addressed regarding the labelling of the live bacteria, since it might be interesting to understand and evaluate the influence of bacteria being alive or fixed on the adhesion assay.

In conclusion, the results suggest that chitosan microspheres have the potential to be used as binding system, demonstrating their ability to penetrate the gastric mucosa and adhere to J99 *H. pylori* strain.

# Future work

*Mucoadhesive effect of microspheres produced with chitosan with DA of 16%*

Because microparticles have more difficulty to penetrate through viscoelastic mucus layer than nanoparticles, an elevated number of positive charges (lower DA) could make the particles too mucoadhesive avoiding their penetration through the mucus layer.

The production of microspheres with chitosan with DA of 16% in the VarJ30 could be therefore relevant to assure the benefits of using chitosan with a high or low DA.

*Live bacteria staining and bacteria adhesion quantification*

An alternative to the difficult observation of DNA staining would be to transform the bacteria with green GFP. While the amount of DNA of the bacteria remains the same, the GFP is replicated and therefore the signal becomes stronger. Also, and because of its higher amount, the contribution of the auto-fluorescence of the chitosan on the green range would be smaller, since the laser would not need to be so intense.

Even regarding the quantification of the adhered bacteria this option could be interesting to assess. Image Stream is an imaging flow cytometer, combining the speed, sensitivity, and phenotyping abilities of flow cytometry with the detailed imagery and functional insights of microscopy. Since the equipment available at INEB only excites with the 488 nm laser, the detection of this protein would be facilitated when comparing to the DNA staining. Comparisons between fixed and live bacteria adhered to the chitosan microspheres could be performed.

*Study of chitosan microspheres ability to remove H. pylori from stomach fresh samples*

After evaluating the capability of chitosan microspheres to adhere to gastric mucosa and to *H. pylori* J99 strain, a system where all components interact should also be studied. Stomach samples should be infected with H. pylori, followed by incubation with developed chitosan microspheres.

*Immobilization of glycosylated receptors on chitosan microspheres surface*

Chitosan microspheres have shown to adhere to *H. pylori* due to only their mucoadhesive capacity. However, evaluating the influence on *H. pylori* adhesion of immobilized glycosylated receptors (Gly-R), such as Le$^b$ and sLe$^x$, on chitosan microspheres surface could be interesting.

# References

[1] Wroblewski LE, Peek RM, Wilson KT. Helicobacter pylori and gastric cancer: factors that modulate disease risk. Clin Microbiol Rev 2010;23:713–39.

[2] Graham DY, El-Omar EM. Helicobacter pylori. Nat Rev Gastroenterol Hepatol 2013:2013.

[3] Logan RPH, Walker MM. ABC of the upper gastrointestinal tract: Epidemiology and diagnosis of Helicobacter pylori infection. BMJ 2001;323:920–2.

[4] Kim N, Marcus E, Wen Y. Genes of Helicobacter pylori regulated by attachment to AGS cells. Infect Immun 2004.

[5] Arora S, Bisen G, Budhiraja R. Mucoadhesive and muco-penetrating delivery systems for eradication of helicobacter pylori. Asian J Pharm 2012;6:18.

[6] Kobayashi M, Lee H, Nakayama J, Fukuda M. Carbohydrate-dependent defense mechanisms against Helicobacter pylori infection. Curr Drug Metab 2009;10:29–40.

[7] Schreiber S, Konradt M, Groll C, Scheid P, Hanauer G, Werling H-O, et al. The spatial orientation of Helicobacter pylori in the gastric mucus. Proc Natl Acad Sci U S A 2004;101:5024–9.

[8] Farthing MJ. Helicobacter pylori infection: an overview. Br Med Bull 1998;54:1–6.

[9] Leunk RD, Johnson PT, David BC, Kraft WG, Mrgan DR. Cytotoxic activity in broth-culture filtrates of Camp ylobacter p ylori 1988;26:93–9.

[10] Cover T. The vacuolating cytotoxin of Helicobacter pylori. Mol Microbiol 1996;20:241–6.

[11] Papini E, Bernard M De, Milia E, Bugnoli M, Zerial M, Rappuoli R, et al. Cellular vacuoles induced by Helicobacter pylori originate from late endosomal compartments. Proc … 1994;91:9720–4.

[12] Szabò I, Brutsche S, Tombola F, Moschioni M, Satin B, Telford JL, et al. Formation of anion-selective channels in the cell plasma membrane by the toxin VacA of Helicobacter pylori is required for its biological activity. EMBO J 1999;18:5517–27.

[13] Cover T, Krishna U, Israel D, Peek R. Induction of gastric epithelial cell apoptosis by Helicobacter pylori vacuolating cytotoxin. Cancer Res 2003:951–7.

[14]   Polk DB, Peek RM. Helicobacter pylori: gastric cancer and beyond. Nat Rev Cancer 2010;10:403–14.

[15]   Aspholm-Hurtig M, Dailide G, Lahmann M, Kalia A, Ilver D, Roche N, et al. Functional adaptation of BabA, the H. pylori ABO blood group antigen binding adhesin. Science 2004;305:519–22.

[16]   Ilver D, Arnqvist a, Ogren J, Frick IM, Kersulyte D, Incecik ET, et al. Helicobacter pylori adhesin binding fucosylated histo-blood group antigens revealed by retagging. Science 1998;279:373–7.

[17]   Bisignano C, Filocamo A, La Camera E, Zummo S, Fera MT, Mandalari G. Antibacterial activities of almond skins on cagA-positive and-negative clinical isolates of Helicobacter pylori. BMC Microbiol 2013;13:103.

[18]   Blaser MJ, Perez-perez GI, Kleanthous H, Cover TL, Peek RM, Chyou PH, et al. Infection with Helicobacter pylori strains possessing cagA is associated with an increased risk of developing adenocarcinoma of the stomach. Cancer Res 1995;55:2111–5.

[19]   Odenbreit S, Püls J, Sedlmaier B, Gerland E, Fischer W, Haas R. Translocation of Helicobacter pylori CagA into gastric epithelial cells by type IV secretion. Science 2000;287:1497–500.

[20]   Kwok T, Zabler D, Urman S, Rohde M, Hartig R, Wessler S, et al. Helicobacter exploits integrin for type IV secretion and kinase activation. Nature 2007;449:862–6.

[21]   Cover TL, Blaser MJ. Helicobacter pylori in health and disease. Gastroenterology 2009;136:1863–73.

[22]   Atherton J, Cao P, Peek R, Tummuru M, Blaser M, Cover T. Mosaicism in vacuolating cytotoxin alleles of Helicobacter pylori. J Biol Chem 1995;270:17771–7.

[23]   Enroth H, Kraaz W, Engstrand L. Helicobacter pylori Strain Types and Risk of Gastric Cancer : A Case-Control Study Helicobacter pylori Strain Types and Risk of Gastric Cancer : 2000:981–5.

[24]   Malfertheiner P, Megraud F, O'Morain C a, Atherton J, Axon ATR, Bazzoli F, et al. Management of Helicobacter pylori infection--the Maastricht IV/ Florence Consensus Report. Gut 2012;61:646–64.

[25]   Malfertheiner P, Megraud F, O'Morain C, Bazzoli F, El-Omar E, Graham D, et al. Current concepts in the management of Helicobacter pylori infection: the Maastricht III Consensus Report. Gut 2007;56:772–81.

[26]   Malfertheiner P, Megraud F, O'Morain C, Bazzoli F, El-Omar E, Graham D, et al. Current European concepts in the management of Helicobacter pylori infection. The Maastricht Consensus Report. European Helicobacter Pylori Study Group. Gut 1997;41:8–13.

[27]   Graham DY, Fischbach L. Helicobacter pylori treatment in the era of increasing antibiotic resistance. Gut 2010;59:1143–53.

[28]   Gisbert JP, Calvet X. Review article: non-bismuth quadruple (concomitant) therapy for eradication of Helicobater pylori. Aliment Pharmacol Ther 2011;34:604–17.

[29]    O'Morain C, Borody T, Farley A, De Boer WA, Dallaire C, Schuman R, et al. Efficacy and safety of single-triple capsules of bismuth biskalcitrate, metronidazole and tetracycline, given with omeprazole, for the eradication of Helicobacter pylori: an international multicentre study. Aliment Pharmacol Ther 2003;17:415–20.

[30]    Conway BR. Drug delivery strategies for the treatment of Helicobacter pylori infections. Curr Pharm Des 2005;11:775–90.

[31]    Hejazi R, Amiji M. Stomach-specific anti-H. pylori therapy. I: Preparation and characterization of tetracyline-loaded chitosan microspheres. Int J Pharm 2002;235:87–94.

[32]    Shah S, Qaqish R, Patel V, Amiji M. Evaluation of the factors influencing stomach-specific delivery of antibacterial agents for Helicobacter pylori infection. J Pharm Pharmacol 1999;51:667–72.

[33]    Ramteke S, Ganesh N, Bhattacharya S, Jain NK. Amoxicillin, clarithromycin, and omeprazole based targeted nanoparticles for the treatment of H. pylori. J Drug Target 2009;17:225–34.

[34]    Erah P, Goddard A, Barrett D, Shaw P, Spiller R. The stability of amoxycillin, clarithromycin and metronidazole in gastric juice: relevance to the treatment of Helicobacter pylori infection. J Antimicrob Chemother 1997:5–12.

[35]    Fontana G, Licciardi M, Mansueto S, Schillaci D, Giammona G. Amoxicillin-loaded polyethylcyanoacrylate nanoparticles: influence of PEG coating on the particle size, drug release rate and phagocytic uptake. Biomaterials 2001;22:2857–65.

[36]    Thijs JC, van Zwet AA, Moolenaar W, Wolfhagen MJ, ten Bokkel Huinink J. Triple therapy vs. amoxicillin plus omeprazole for treatment of Helicobacter pylori infection: a multicenter, prospective, randomized, controlled study of efficacy and side effects. Am J Gastroenterol 1996;91:93–7.

[37]    Parsons HK, Carter MJ, Sanders DS, Winstanley T, Lobo a J. Helicobacter pylori antimicrobial resistance in the United Kingdom: the effect of age, sex and socio-economic status. Aliment Pharmacol Ther 2001;15:1473-8.

[38]    Glupczynski Y, Mégraud F, Lopez-Brea M, Andersen LP. European multicentre survey of in vitro antimicrobial resistance in Helicobacter pylori. Eur J Clin Microbiol Infect Dis 2001;20:820–3.

[39]    Megraud F, Kist M, Lopez Brea M, Hirschl A, Andersen LP, Glupczynski Y. Surveillance of Helicobacter pylori Resistance to Antibiotics in Europe 2008-2009. Gastroenterology 2011;140:S–312.

[40]    Niv Y, Hazazi R. Helicobacter pylori recurrence in developed and developing countries: meta-analysis of 13C-urea breath test follow-up after eradication. Helicobacter 2008;13:56–61.

[41]    Laine L, Hunt R, El-Zimaity H, Nguyen B, Osato M, Spénard J. Bismuth-based quadruple therapy using a single capsule of bismuth biskalcitrate, metronidazole, and tetracycline given with omeprazole versus omeprazole, amoxicillin, and clarithromycin for eradication of Helicobacter pylori in duodenal ulcer patients: a . Am J Gastroenterol 2003;98:562-7.

[42]    Vakil N. Helicobacter pylori treatment: a practical approach. Am J Gastroenterol 2006;101:497-9.

[43]   Gonçalves IC, Magalhães A, Fernandes M, Rodrigues I V, Reis C a, Martins MCL. Bacterial-binding chitosan microspheres for gastric infection treatment and prevention. Acta Biomater 2013;9:9370–8.

[44]   Correia M, Michel V, Osório H, El Ghachi M, Bonis M, Boneca IG, et al. Crosstalk between Helicobacter pylori and gastric epithelial cells is impaired by docosahexaenoic acid. PLoS One 2013;8:e60657.

[45]   Del Giudice G, Malfertheiner P, Rappuoli R. Development of vaccines against Helicobacter pylori. Expert Rev Vaccines 2009;8:1037–49.

[46]   El Nujumi a M, Dorrian C a, Chittajallu RS, Neithercut WD, McColl KE. Effect of inhibition of Helicobacter pylori urease activity by acetohydroxamic acid on serum gastrin in duodenal ulcer subjects. Gut 1991;32:866–70.

[47]   Díaz-Gómez R, López-Solís R, Obreque-Slier E, Toledo-Araya H. Comparative antibacterial effect of gallic acid and catechin against Helicobacter pylori. LWT - Food Sci Technol 2013;54:331–5.

[48]   Correia M, Michel V, Matos A a, Carvalho P, Oliveira MJ, Ferreira RM, et al. Docosahexaenoic acid inhibits Helicobacter pylori growth in vitro and mice gastric mucosa colonization. PLoS One 2012;7:e35072.

[49]   Ramteke S, Jain NK. Clarithromycin- and omeprazole-containing gliadin nanoparticles for the treatment of Helicobacter pylori. J Drug Target 2008;16:65–72.

[50]   Thompson L, Cockayne a, Spiller RC. Inhibitory effect of polyunsaturated fatty acids on the growth of Helicobacter pylori: a possible explanation of the effect of diet on peptic ulceration. Gut 1994;35:1557-61.

[51]   Ford AC, Axon ATR. Epidemiology of Helicobacter pylori infection and public health implications. Helicobacter 2010;15 Suppl 1:1–6.

[52]   Rupnow MFT, Chang AH, Shachter RD, Owens DK, Parsonnet J. Cost-effectiveness of a potential prophylactic Helicobacter pylori vaccine in the United States. J Infect Dis 2009;200:1311–7.

[53]   Aebischer T, Bumann D, Epple HJ, Metzger W, Schneider T, Cherepnev G, et al. Correlation of T cell response and bacterial clearance in human volunteers challenged with Helicobacter pylori revealed by randomised controlled vaccination with Ty21a-based Salmonella vaccines. Gut 2008;57:1065–72.

[54]   Nakamura H, Yoshiyama H, Takeuchi H, Mizote T, Okita K, Nakazawa T. Urease plays an important role in the chemotactic motility of Helicobacter pylori in a viscous environment. Infect Immun 1998;66:4832–7.

[55]   Mabe K, Yamada M, Oguni I. In Vitro and In Vivo Activities of Tea Catechins against Helicobacter pylori In Vitro and In Vivo Activities of Tea Catechins against Helicobacter pylori 1999;43.

[56]   Yahiro K, Shirasaka D, Tagashira M. Inhibitory effects of polyphenols on gastric injury by Helicobacter pylori VacA toxin. Helicobacter 2005;10.

[57]   Obreque-Slier E, Peña-Neira A, López-Solís R, Zamora-Marín F, Ricardo-da Silva JM, Laureano O. Comparative study of the phenolic composition of seeds and skins from Carménère and Cabernet Sauvignon grape varieties (Vitis vinifera L.) during ripening. J Agric Food Chem 2010;58:3591–9.

[58]    Petros R a, DeSimone JM. Strategies in the design of nanoparticles for therapeutic applications. Nat Rev Drug Discov 2010;9:615–27.

[59]    Wilczewska AZ, Niemirowicz K, Markiewicz KH, Car H. Nanoparticles as drug delivery systems. Pharmacol Rep 2012;64:1020–37.

[60]    Dhawan S, Singla AK, Sinha VR. Evaluation of mucoadhesive properties of chitosan microspheres prepared by different methods. AAPS PharmSciTech 2004;5:e67.

[61]    Cooreman M. Local gastric and serum amoxicillin concentrations after different oral application forms. Antimicrob Agents … 1993;37.

[62]    Jain S, Jangdey M. Lectin conjugated gastroretentive multiparticulate delivery system of clarithromycin for the effective treatment of Helicobacter pylori. Mol Pharm 2008;6:295–304.

[63]    Peppas N a, Sahlin JJ. Hydrogels as mucoadhesive and bioadhesive materials: a review. Biomaterials 1996;17:1553–61.

[64]    Tur KM, Ch'ng H. Evaluation of possible mechanism (s) of bioadhesion. Int J Pharm 1998;160:61–74.

[65]    Nagahara N, Akiyama Y, Nakao M, Tada M, Kitano M, Ogawa Y. Mucoadhesive microspheres containing amoxicillin for clearance of Helicobacter pylori. Antimicrob Agents Chemother 1998.

[66]    Patel J, Patil P. Preparation and characterization of amoxicillin mucoadhesive microparticles using solution-enhanced dispersion by supercritical $CO_2$. J Microencapsul 2012;29:398–408.

[67]    Ishak R a H, Awad G a S, Mortada ND, Nour S a K. Preparation, in vitro and in vivo evaluation of stomach-specific metronidazole-loaded alginate beads as local anti-Helicobacter pylori therapy. J Control Release 2007;119:207–14.

[68]    Akiyama Y, Nagahara N, Nara E, Kitano M, Iwasa S, Yamamoto I, et al. Evaluation of oral mucoadhesive microspheres in man on the basis of the pharmacokinetics of furosemide and riboflavin, compounds with limited gastrointestinal absorption sites. J Pharm Pharmacol 1998;50:159–66.

[69]    Woodley J. Bioadhesion. New Possibilities for Drug Administration? Clin Pharmacokinet 2001;40:77–84.

[70]    Park K, Robinson JR. Bioadhesive polymers as platforms for oral-controlled drug delivery: method to study bioadhesion. Int J Pharm 1984;19:107–27.

[71]    Lehr C-M, Bouwstra JA, Schacht EH, Junginger HE. In vitro evaluation of mucoadhesive properties of chitosan and some other natural polymers. 1992.

[72]    Lehr C-M, Boddé HE, Bouwstra JA, Junginger HE. A surface energy analysis of mucoadhesion II. Prediction of mucoadhesive performance by spreading coefficients. Eur J Pharm Sci 1993;1:19–30.

[73]    Hejazi R, Amiji M. Stomach-specific anti-H. pylori therapy; part III: effect of chitosan microspheres crosslinking on the gastric residence and local tetracycline concentrations in fasted gerbils. Int J Pharm 2004;272:99–108.

[74] Gonçalves IC, Henriques PC, Seabra CL, Martins MCL. The potential utility of chitosan micro/nanoparticles in the treatment of gastric infection. Expert Rev Anti Infect Ther 2014.

[75] Mi F-L, Sung H-W, Shyu S-S. Synthesis and characterization of a novel chitosan-based network prepared using naturally occurring crosslinker. J Polym Sci Part A Polym Chem 2000;38:2804–14.

[76] Muzzarelli RAA. Natural chelating polymers: alginic acid, chitin, and chitosan. 1973.

[77] Chandy T, Sharma CP. Chitosan--as a biomaterial. Biomater Artif Cells Artif Organs 1990;18:1–24.

[78] Kato Y, Onishi H, Machida Y. Application of chitin and chitosan derivatives in the pharmaceutical field. Curr Pharm Biotechnol 2003;4:303–9.

[79] Dash M, Chiellini F, Ottenbrite RM, Chiellini E. Chitosan—A versatile semi-synthetic polymer in biomedical applications. Prog Polym Sci 2011;36:981–1014.

[80] Giri TK, Thakur A, Alexander A, Badwaik H, Tripathi DK. Modified chitosan hydrogels as drug delivery and tissue engineering systems: present status and applications. Acta Pharm Sin B 2012;2:439–49.

[81] Mi F-L, Sung H-W, Shyu S-S, Su C-C, Peng C-K. Synthesis and characterization of biodegradable TPP/genipin co-crosslinked chitosan gel beads. Polymer (Guildf) 2003;44:6521–30.

[82] Kean T, Thanou M. Biodegradation, biodistribution and toxicity of chitosan. Adv Drug Deliv Rev 2010;62:3–11.

[83] He P, Davis SS, Illum L. In vitro evaluation of the mucoadhesive properties of chitosan microspheres. Int J Pharm 1998;166:75–88.

[84] Felt O, Buri P, Gurny R. Chitosan: a unique polysaccharide for drug delivery. Drug Dev Ind Pharm 1998;24:979–93.

[85] Hejazi R, Amiji M. Chitosan-based gastrointestinal delivery systems. J Control Release 2003;89:151–65.

[86] Giunchedi P, Genta I, Conti B, Muzzarelli R a, Conte U. Preparation and characterization of ampicillin loaded methylpyrrolidinone chitosan and chitosan microspheres. Biomaterials 1998;19:157–61.

[87] Park BK, Kim M-M. Applications of chitin and its derivatives in biological medicine. Int J Mol Sci 2010;11:5152–64.

[88] Strand SP, Vandvik MS, Vårum KM, Østgaard K. Screening of chitosans and conditions for bacterial flocculation. Biomacromolecules 2001;2:126–33.

[89] Mao HQ, Roy K, Troung-Le VL, Janes K a, Lin KY, Wang Y, et al. Chitosan-DNA nanoparticles as gene carriers: synthesis, characterization and transfection efficiency. J Control Release 2001;70:399–421.

[90] Patel JK, Patel MM. Stomach specific anti-helicobacter pylori therapy: preparation and evaluation of amoxicillin-loaded chitosan mucoadhesive microspheres. Curr Drug Deliv 2007;4:41–50.

[91]    Xu Y, Du Y. Effect of molecular structure of chitosan on protein delivery properties of chitosan nanoparticles. Int J Pharm 2003;250:215–26.

[92]    Mitra S, Gaur U, Ghosh PC, Maitra a N. Tumour targeted delivery of encapsulated dextran-doxorubicin conjugate using chitosan nanoparticles as carrier. J Control Release 2001;74:317–23.

[93]    Nihant N, Schugens C, Grandfils C, Jérôme R, Teyssié P. Polylactide microparticles prepared by double emusion/evaporation technique. I. Effect of primary emulsion stability. Pharm Res 1994.

[94]    Hombreiro-Pérez M, Siepmann J, Zinutti C, Lamprecht a, Ubrich N, Hoffman M, et al. Non-degradable microparticles containing a hydrophilic and/or a lipophilic drug: preparation, characterization and drug release modeling. J Control Release 2003;88:413–28.

[95]    Crini G, Badot P-M. Application of chitosan, a natural aminopolysaccharide, for dye removal from aqueous solutions by adsorption processes using batch studies: A review of recent literature. Prog Polym Sci 2008;33:399–447.

[96]    Shu XZ, Zhu KJ. Chitosan/gelatin microspheres prepared by modified emulsification and ionotropic gelation. J Microencapsul 2001;18:237–45.

[97]    Wang L-Y, Ma G-H, Su Z-G. Preparation of uniform sized chitosan microspheres by membrane emulsification technique and application as a carrier of protein drug. J Control Release 2005;106:62–75.

[98]    Mi F-L, Shyu S-S, Lee S-T, Wong T-B. Kinetic study of chitosan-tripolyphosphate complex reaction and acid-resistive properties of the chitosan-tripolyphosphate gel beads prepared by in-liquid curing method. J Polym Sci Part B Polym Phys 1999;37:1551–64.

[99]    Thanoo BC, Sunny MC, Jayakrishnan A. Cross-linked chitosan microspheres: Preparation and evaluation as a matrix for the controlled release of pharmaceuticals. J Pharm Pharmacol 1992;44:283–6.

[100]   Sung HW, Huang RN, Huang LL, Tsai CC, Chiu CT. Feasibility study of a natural crosslinking reagent for biological tissue fixation. J Biomed Mater Res 1998;42:560–7.

[101]   Mi F-L, Sung H-W, Shyu S-S. Release of indomethacin from a novel chitosan microsphere prepared by a naturally occurring crosslinker: Examination of crosslinking and polycation-anionic drug interaction. J Appl Polym Sci 2001;81:1700–11.

[102]   Sung HW, Liang IL, Chen CN, Huang RN, Liang HF. Stability of a biological tissue fixed with a naturally occurring crosslinking agent (genipin). J Biomed Mater Res 2001;55:538–46.

[103]   Sung HW, Huang RN, Huang LL, Tsai CC. In vitro evaluation of cytotoxicity of a naturally occurring cross-linking reagent for biological tissue fixation. J Biomater Sci Polym Ed 1999;10:63–78.

[104]   Tsai CC, Huang RN, Sung HW, Liang HC. In vitro evaluation of the genotoxicity of a naturally occurring crosslinking agent (genipin) for biologic tissue fixation. J Biomed Mater Res 2000;52:58–65.

[105]  Mi FL, Tan YC, Liang HC, Huang RN, Sung HW. In vitro evaluation of a chitosan membrane cross-linked with genipin. J Biomater Sci Polym Ed 2001;12:835–50.

[106]  Sinha VR, Singla a K, Wadhawan S, Kaushik R, Kumria R, Bansal K, et al. Chitosan microspheres as a potential carrier for drugs. Int J Pharm 2004;274:1–33.

[107]  Portero A, Remuñán-López C, Criado MT, Alonso MJ. Reacetylated chitosan microspheres for controlled delivery of anti-microbial agents to the gastric mucosa. J Microencapsul 2002;19:797–809.

[108]  Fernandes M, Gonçalves IC, Nardecchia S, Amaral IF, Barbosa M a, Martins MCL. Modulation of stability and mucoadhesive properties of chitosan microspheres for therapeutic gastric application. Int J Pharm 2013;454:116–24.

[109]  Mi F-L, Shyu S-S, Peng C-K. Characterization of ring-opening polymerization of genipin and pH-dependent cross-linking reactions between chitosan and genipin. J Polym Sci Part A Polym Chem 2005;43:1985–2000.

[110]  Yamada T, Onishi H, Machida Y. In vitro and in vivo evaluation of sustained release chitosan-coated ketoprofen microparticles. Yakugaku Zasshi 2001;121:239–45.

[111]  Lim ST, Martin GP, Berry DJ, Brown MB. Preparation and evaluation of the in vitro drug release properties and mucoadhesion of novel microspheres of hyaluronic acid and chitosan. J Control Release 2000;66:281–92.

[112]  Berger J, Reist M, Mayer JM, Felt O, Peppas N a., Gurny R. Structure and interactions in covalently and ionically crosslinked chitosan hydrogels for biomedical applications. Eur J Pharm Biopharm 2004;57:19–34.

[113]  Huang Y-C, Chiang C-H, Yeh M-K. Optimizing formulation factors in preparing chitosan microparticles by spray-drying method. J Microencapsul 2003;20:247–60.

[114]  Luo D, Guo J, Wang F, Sun J, Li G, Cheng X, et al. Preparation and evaluation of anti-Helicobacter pylori efficacy of chitosan nanoparticles in vitro and in vivo. J Biomater Sci Polym Ed 2009;20:1587–96.

[115]  Raval J a, Patel JK, Patel MM. Formulation and in vitro characterization of spray dried microspheres of amoxicillin. Acta Pharm 2010;60:455–65.

[116]  Jumaa M, Furkert FH, Müller BW. A new lipid emulsion formulation with high antimicrobial efficacy using chitosan. Eur J Pharm Biopharm 2002;53:115–23.

[117]  Muzzarelli R, Tarsi R, Filippini O, Giovanetti E, Biagini G, Varaldo PE. Antimicrobial properties of N-carboxybutyl chitosan. Antimicrob Agents Chemother 1990;34:2019–23.

[118]  Guo Z, Chen R, Xing R, Liu S, Yu H, Wang P, et al. Novel derivatives of chitosan and their antifungal activities in vitro. Carbohydr Res 2006;341:351–4.

[119]  Pujals G, Suñé-Negre JM, Pérez P, García E, Portus M, Tico JR, et al. In vitro evaluation of the effectiveness and cytotoxicity of meglumine antimoniate microspheres produced by spray drying against Leishmania infantum. Parasitol Res 2008;102:1243–7.

[120]  Darmadji P, Izumimoto M. Effect of chitosan in meat preservation. Meat Sci 1994;38:243–54.

[121] Chen M-C, Yeh GH-C, Chiang B-H. Antimicrobial and Physicochemcal properties of methylcellulose and chitosan films containing a preservative. J Food Process Preserv 1996;20:379–90.

[122] Coma V, Martial-Gros A, Garreu S, Copinet A, Salin F, Deschamps A. Edible antimicrobial films based on chitosan matrix. J Food … 2002;67.

[123] Leceta I, Guerrero P, Ibarburu I, Dueñas MT, de la Caba K. Characterization and antimicrobial analysis of chitosan-based films. J Food Eng 2013;116:889–99.

[124] Nogueira F, Gonçalves IC, Martins MCL. Effect of gastric environment on Helicobacter pylori adhesion to a mucoadhesive polymer. Acta Biomater 2013;9:5208–15.

[125] Martins MCL, Gonçalves IC, Gomes P, Oliveira JR, Reis CA, Magalhães A. Microspheres. PCT/GB2013/051181, 2013.

[126] Lee JW, Park JH, Robinson JR. Bioadhesive-based dosage forms: the next generation. J Pharm Sci 2000;89:850–66.

[127] Ascencio F, Guruge JL, Ljungh Å, Mégraud F, Wei S, Wadström T. Lectin Typing of Helicobacter pylori. Berlin, Heidelberg: Springer Berlin Heidelberg; 1990.

[128] Mahdavi J, Sondén B, Hurtig M, Olfat F. Helicobacter pylori SabA adhesin in persistent infection and chronic inflammation. Science (80- ) 2002;297:573–8.

[129] Falk P, Roth K a, Borén T, Westblom TU, Gordon JI, Normark S. An in vitro adherence assay reveals that Helicobacter pylori exhibits cell lineage-specific tropism in the human gastric epithelium. Proc Natl Acad Sci U S A 1993;90:2035–9.